A Passive Night-Sky Radiation Cooling System

by
Gideon Daniël Joubert

Thesis presented in fulfilment of the requirements for the degree of Masters in Mechanical Engineering in the Faculty of Engineering at Stellenbosch University

Supervisor: RT Dobson

Department of Mechanical and Mechatronic Engineering

December 2014

Declaration

By submitting this thesis electronically, I declare that the entirety of the work contained therein is my own, original work, that I am the sole author thereof (save to the extent explicitly otherwise stated), that reproduction and publication thereof by Stellenbosch University will not infringe any third party rights and that I have not previously in its entirety or in part submitted it for obtaining any qualification.

Date: December 2014 .....

Abstract

A Passive Night-Sky Radiation Cooling System

G.D. Joubert

Thesis: MEng (Mec)

November 2014

A passive night-sky radiation cooling system consists of a radiation panel and a cold water storage tank. The stored cold water may be used to cool a room during the day time, particularly in summer. In this thesis a theoretical and mathematically sound simulation model is developed. An experimental set-up was constructed and subsequently used to show that the theoretical model effectively simulates the transient heating or cooling response of the system.

It is shown that under South African conditions the typical heat emitting rate during the night is 55 W/m^2. After the heat has been removed from the water, it is stored in a cold water tank from where it is circulated through a natural convector during the day time to absorb heat from the room. The experiment extracted a minimum of 102 W/m^3 of heat from a 1.87 m^3 galvanized steel room while a brick room with a volume of 120 m^3 requires 22.7 W/m^3. Additional to cooling, the system during the day, absorbed an average of 362 W of energy and heated 68 l of water from 24 °C to 62 °C within an 8-hour period. The system achieved similar results during winter conditions and the experiment confirms that the system is capable of operating without a control system. Therefore it is recommended that renewable energy-conscious designers pay more attention to the use of night-sky radiation cooling in future.

Uittreksel

'n Passiewe Ruimte Stralins Verkoelings Stelsel

('A Passive Night-Sky Radiation Cooling System")

G.D. Joubert

Tesis: MIng (Meg)

November 2014

'n Passiewe ruimte stralings verkoelings sisteem bestaan uit 'n stralings paneel en 'n koue water tenk. Die sisteem kan gebruik word om 'n vertrek gedurende die dag te verkoel, veral in die somer, deur gebruik te maak van die gestoorde verkoelde water. In hierdie tesis word 'n teoretiese en sinvolle wiskundige simulasie model ontwikkel. 'n Eksperimentele stelsel is gebou en vervolgens gebruik om te bewys dat die teoretiese model die veranderende verkoeling en verwarming van die stelsel effektief simuleer.

Die tesis dui aan dat onder Suid Afrikaanse toestande daar 'n hitte vrystellings tempo van 55 W/m^2 is gedurende die nag. Nadat die water verkoel is, word dit gestoor in die koue water tenk vanwaar dit deur 'n natuurlike konvektor sirkuleer en gedurende die dag warmte vanuit die vertrek onttrek. Die eksperiment het 'n minimum van 102 W/m^3 warmte vanuit die galvaniseerde 1.87 m^3 vertrek geabsorbeer, terwyl 'n baksteen vertrek van 120 m^3, 22.7 W/m^3 verkoeling benodig. Bykomstig tot die verkoelingstelsel verhit die sisteem 68 l water vanaf 24 °C to 62 °C gedurende 'n 8-uur periode in die dag, dus word 362 W energie geabsorbeer. Die sisteem is ook getoets tydens winter toestande, die resultate was dieselfde as wat in die somer verkry is. Verder is daar ook bewys dat die sisteem sonder enige beheerstelsel kan funksioneer. Verder word daar aanbeveel dat hernubare energie bewuste ontwerpers in die toekoms meer aandag aan ruimte straling verkoeling skenk.

Acknowledgements

Thanks to our heavenly Father for the blessing of endless love, grace and opportunities.

I would like to thank Mr. Robert Dobson for his contribution toward the project, always being there to help and explaining hours without end. Without Mr Dobson the completion of the project would not have been possible.

Dedications

I would like to dedicate the thesis to my mother and father. Without their love and their faith in me this thesis would not have been possible. They gave me the opportunity to study.

Contents

List of Figures

List of Tables

Nomenclature

A	Area	$[\mathrm{m}^2]$
A_x	Crossectional area	$[\mathrm{m}^2]$
A_z	Surface area	$[\mathrm{m}^2]$
c_p	Constant pressure specific heat	$[\mathrm{J/kg\,K}]$
C_f	Friction coefficient	$[\ ]$
D	Diameter	$[\mathrm{m}]$
EOT	Equation of time	$[\mathrm{min}]$
G	Volumetric flow rate	$[\mathrm{m}^3/\mathrm{s}]$
Gr	Grashoff number, $Gr = \beta \Delta T g \rho^2 L^3/\mu$	$[\ ]$
H	Height	$[\mathrm{m}]$
h	Convection heat transfer coefficient	$[\mathrm{W/m^2\,K}]$
h	Enthalpy	$[\mathrm{J/kg}]$
I	Solar irradiation	$[\mathrm{W/m^2}]$
k	Thermal conductivity	$[\mathrm{W/m\,K}]$
L	Length	$[\mathrm{m}]$
m	Mass	$[\mathrm{kg}]$
$\dot{m}$	Mass flow rate	$[\mathrm{kg/s}]$
N	Number of	$[\ ]$
Nu	Nusselt number, $Nu = hL/k$	$[\ ]$
P	Pressure	$[\mathrm{Pa}]$

P_L	Pitch	[m]
Pr	Pradtl Number	[ ]
$\dot{Q}$	Heat transfer rate	[W]
R	Resistance	[K/W]
Ra	Raleigh number, $Ra = Gr\ Pr$	[ ]
Re	Reynolds number, $Re = \rho v D/\mu$	[ ]
RH	Relative humidity	[ ]
r	Radius	[m]
S_L	Distance between rows of tubes	[m]
T	Temperature	[°C or K]
TOT	Total	[ ]
t	Time	[s]
t	Thickness	[m]
U	Internal energy	[J/kg]
V	Volume	[m^3, l]
v	Velocity	[m/s]
W	Width	[m]

Greek Symbols

α	Absorbtivity	[ ]
α_{sol}	Solar azimuth	[Degrees]
Δ	Difference	[ ]
δ	Declination	[Degrees]
β	Coeficient of volumetric expansion	[1/K]
ϵ	Emissivity	[ ]
η	Efficiency	[ ]
θ_z	Zenith	[Degrees]

μ	Dynamic viscosity	$[\mathrm{kg\,m/s}]$
ρ	Density	$[\mathrm{kg/m^3}]$
σ	Stephan Boltzmann Constant, $\sigma = 5.67e^{-8}$	$[\mathrm{W/m^2K^4}]$
τ	Shear stress	$[\mathrm{N/m^2}]$
Φ	Correction factor	[ ]
ϕ	Latitude	[Degrees]
ω	Hour angle	[Degrees]

Subscripts

amb	Ambient
a	Air
b	Bottom
$Cold$	Cold
c	Control
$cond$	Conduction
con	Convector
$conv$	Convection
CW	Cold water
D	Diameter
dp	Dew point
E	East
fin	Fin
Hot	Hot
HW	Hot water
h	Hydraulic
Ins	Insulation
in	In

M Manifold

$minor$ Minor losses

N North

out Out

p Pipe

R Radiator

ref Reference

rad Radiation

$room$ Room

S South

s Surface

sky Sky

sol Solar

T Tank

t Top

W Water

W West

z Length of control volume

Abbreviations

DAQ Data acquisition

GHG Green house gas

ID Inner diameter

RH Relative humidity

RTD Resistance temperature detector

1 Introduction

Air conditioning is an energy greedy operation that is mostly accomplished by the use of vapour compression refrigeration systems (Okoronkwo *et al.*, 2014). The conventional energy sources in South Africa cause pollution and lead to an increase in environmental air and water temperatures, which is ascribed to the increased emission of greenhouse gas (GHG)(Winkler, 2007). South Africa, compared to other developing countries, is the highest emitter of GHG per person. Coal fired power stations which provide 93% of South Africa's electricity are largely responsible for the immense emissions of GHG, with Sasol's Secunda plant being the largest point source of coal pollution in the world (Botha *et al.*, 2013).

It is accepted internationally that buildings are responsible for 33% of the total energy use. A building consumes far more energy during its productive lifespan to meet demands for heating, cooling and lighting than the energy demanded during its construction (Milford, 2009). Decreasing the demand for energy required for air conditioning in buildings is therefore part of the quest for a more-sustainable future.

Renewable energy is the key to reducing the current dependency on conventional energy sources (fossil fuels) for energy. Renewable energy resources make use of the natural flow of energy through the earth's ecosystem (Winkler, 2005). Night-sky radiation is one of these natural flow of energy phenomena, whereby some of the energy collected by the earth's surface during the day radiates back into the cold night-sky.

Night-sky radiation is a sustainable environmentally friendly natural phenomenon that could be used for the air conditioning of buildings. According to Robinson *et al.* (2013) night-sky radiation has the best cooling potential compared to other cooling techniques such as evaporative cooling and dry bulb cooling. Dry bulb cooling circulates ambient air at dry bulb temperature through breeze ways to cool the air surrounding the building. At night the sky acts as a heat sink and all objects emit energy through long wave radiation to the cold sky causing the objects to cool. Incorporating night-sky radiation and other natural phenomena such as thermosyphoning, where a fluid flows due to a temperature induced density gradient, a system could be designed

for the natural cooling of buildings. In this way the cooling may be effected without the use of a pump and active controls.

A night-sky radiation system cools water at night, this water is then used during the day to cool a building or a room in a building. Since a night-sky radiation system has the same properties as a solar water heater it could also be implemented to heat water during the day and act as a pre-heater for the geyser. The night sky radiation system then transforms into a dual system increasing its utility and return on investment.

1.1 Objectives

The objectives of the researcher with this project are to study the cooling potential of a night-sky radiation system by:

- Designing, constructing and testing an experimental night-sky radiation system that has no electrically operated parts.
- Developing a theoretical simulation model of the system
- Comparing the results obtained theoretically and experimentally and thereby validating the developed theoretical model.

further investigating the solar heating capabilities of the system.

1.2 Thesis Layout

In this thesis the process followed to design and test a night-sky radiation system is discussed. A computer program is developed to theoretically predict the performance of the specific night-sky radiation system. This theoretical model is validated by comparing its results to results obtained through experimentation.

The thesis starts with an introduction (Chapter 1), and moves on to a literature study given in Chapter 2. In the literature study natural phenomena such as thermosyphoning and night-sky radiation are discussed. Environmental conditions influencing a night-sky radiator are discussed in Section 2.2 as well as radiator design options (Section 2.3). Previous studies and in particular the cause and effect of stratification are also discussed. In Section 2.6 the three heat transfer mechanisms used in the theoretical model are discussed. This section is followed by the equations of change section where the conservation of mass, energy and momentum are discussed. The chapter ends with Section 2.8 where the procedure followed to determine the fluid properties is described.

With the knowledge gained from the literature study an experimental set-up was designed. In Chapter 3 the design criteria for the experimental set-up are described. The design layout with a description of the main components is presented.

This is followed by Chapter 4 in where the experimental set-up is described. In addition the measurements of flow and temperature, calibration of thermocouples and the start-up of the experimental set-up are discussed.

Chapter 5 presents the theoretical modelling of the system. The theoretical model is developed by implementing the three heat transfer mechanisms and the conservation of mass, energy and momentum.

Chapter 6 shows the results obtained experimentally and theoretically. The results are compared and discussed. This comparison together with the sensitivity analysis presented in Section 6.6 serve as a validation of the theoretical model.

In Chapter 7 the discussion and conclusion of the thesis are presented. This chapter provides a review of the important conclusions made throughout the report. The validity of the theoretical model is established and whether a night-sky radiation system could be used for the cooling of a room in a building.

In the final chapter are recommendations and ideas for future work. Alternative designs are presented.

2 Literature Survey

2.1 Introduction

Decreasing the amount of energy consumed by buildings is of utmost importance. By tapping into nature's sustainable resources unnecessary energy consumption can be eliminated. One of these sustainable resources is night-sky radiation. Night-sky radiation is a natural phenomena that occurs at night. Farmers are familiar with this natural cooling effect occurring at night. An object will radiate energy to the sky which acts as a heat sink, causing the temperature of the body to decrease. This thermal radiation is also known as long wave radiation and specified between 8 to 13 μm and 13.5 to 16 μm (Wang *et al.*, 2008). The phenomenon is visible when dew forms on an object. The object's temperature drops below the dew point temperature of the surroundings causing the water vapour in the air to condense on the surface of the object. The rate at which an object is cooled by radiation is affected by environmental conditions such as relative humidity, ambient temperature and cloud cover.

Night-sky radiation implemented in a closed loop system induces another natural phenomena called thermosyphoning. Thermosyphoning occurs due to a temperature induced density gradient. Consider a closed loop system filled with a working fluid as shown in Figure 2.1. Temperature differences cause a change in density, the cold left side of the loop is denser than the hot right hand side. The difference in density causes the pressure on the cold left hand side to be higher than that of the right hand side ($\rho g H_{cold} > \rho g H_{hot}$). This pressure difference will cause the working fluid to flow in an anticlockwise direction, as indicated.

Systems implementing night-sky radiation and thermosyphoning or just night-sky radiation have been investigated for the last three decades. In studies water cooled systems are more popular than the air cooled systems. During a study Givoni (1977) cooled air in a roof cavity via night-sky radiation. The cooled air was pumped into a thermal storage unit and was recovered when needed. With some adjustments it could also be used to heat air during the day.

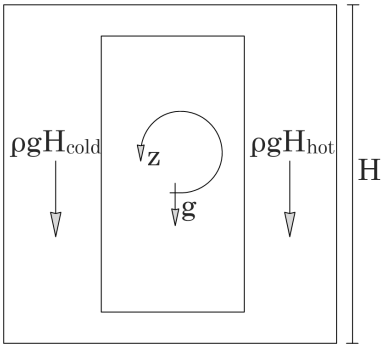

Figure 2.1 Illustration of thermo-siphoning

More recent studies are those involving the cooling of water via night sky radiation. Water is stored either in a solar pond or storage tank. The solar pond allows the water to thermally radiate energy extracted from the building and solar energy absorbed by the solar pond, while the storage tank system circulates water through a radiator which radiates the thermal energy extracted from the building. The radiator used for radiation is very similar to that of conventional solar water heaters. For the design of a night sky radiation system, environmental conditions affecting the performance of the system such as ambient temperatures, air relative humidities and cloud cover need to be considered.

2.2 Environmental Conditions

Natural forces such as ambient and sky temperatures, wind speeds and clear skies affect the cooling capabilities of a night-sky radiation system. These environmental conditions will be discussed qualitatively in this section; in section 2.3, a more quantitative approach is adopted.

Ambient temperature influences the cooling capacity of the system by adding or removing energy. Thermal energy is added to the system if the ambient temperature is higher than the fluid's temperature, causing a decrease in the cooling capacity of the system. The opposite is also possible, energy is removed from the system when the ambient temperature is below the temperature of the fluid causing an increase in the cooling capacity. The cooling capacity is also influenced by the rate at which thermal energy is removed or added. The rate at which this energy is removed or added is a function of the heat transfer coefficient which is affected by wind speeds.

A large convection heat transfer coefficient indicates a higher rate of heat transfer. The convection heat transfer coefficient is dependent on the velocity of the wind. The correlation between wind speeds and the convection heat transfer coefficient is presented in a study done by Loveday and Taki (1996).

The correlation is given in Chapter 5 Section 5.1.2. Heat transfer rates are also dependent on another heat transfer mechanism known as radiation.

Radiation heat transfer rates are affected by sky temperatures. A low sky temperature results in a higher heat transfer rate than a high sky temperature. The higher heat transfer rate is ascribed to an increase in temperature difference between the radiating surface and the sky temperature which acts as a heat sink. The sky temperature is defined as the equivalent temperature of water vapour and other atmospheric elements that make up the sky or atmosphere to which a surface radiates heat.

The greatest influence on the sky temperature is water vapour. The presence of water vapour in the air is indicated by the relative humidity (RH) ratio. Saturated air has a relative humidity of one, while drier air has lower RH values. High RH results in warmer sky temperatures. According to Lawrence (2005) RH and dew point temperature are related. The dew point temperature is used to calculate the temperature of the sky. The relationship between the sky temperature and dew point temperature is given by Erell and Etzion (2000).

Clouds are a visible mass of condensed water vapour, which form a body to which the radiating panel has to radiate thermal energy. The capability of the radiator to radiate energy to the sky is limited by the presence of clouds. Figure 2.2 illustrates the difference between clear and cloudy skies, the radiator is forced to radiate energy to the clouds instead of the clear sky. The clouds are at a much higher temperature than the sky. Therefore, a decrease in the rate of heat transfer and cooling capacity are expected. The heat transfer rate is reduced by the clouds due to a decrease in the temperature difference between the radiating surface and the body it is radiating to.

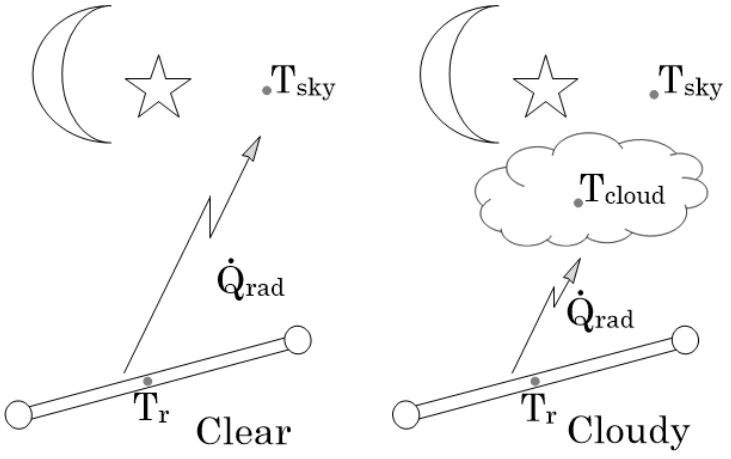

Figure 2.2 Illustration of the system's behaviour with cloudy and clear skies

2.3 Radiator Designs

To design a night-sky radiation system, different radiator designs need to be considered. Radiator design factors such as geometry and positioning need consideration. Other system design factors such as the ratio between radiator aperture to tank volume and mass flow rates also influence the cooling capacity.

The first aspect of radiator design to be discussed is the absence or presence of fins on a radiator. Fins increase the efficiency of conventional solar water heaters, but night-sky radiators operate in different conditions. If the ambient temperature is higher than that of the fluid inside the radiator, the fin efficiency will be reduced due to energy gains caused by convection. Erell and Etzion (2000) studied the effect of fins on a night-sky radiator and concluded that convection heat gains could be reduced by decreasing the number of fins. A configuration consisting only of pipes is suggested for the best operating night-sky radiation system.

Apart from the elimination of fins, convection heat gains could be reduced by creating a stagnant air gap above the radiator. This was done by Al-Nimr *et al.* (1998) who placed a polyethylene cover over the radiator. Polyethylene allows long wave thermal energy to pass through, reducing heat gains or losses to or from the surroundings due to convection. Selecting the right cover is crucial. The cover has to allow long wave radiation to pass through while blocking short wave radiation (solar radiation). Figure 2.3 presents the energy transfer with a selective cover, the radiator radiates directly to the sky while convention occurs between the radiator and transparent cover and then between the cover and ambient.

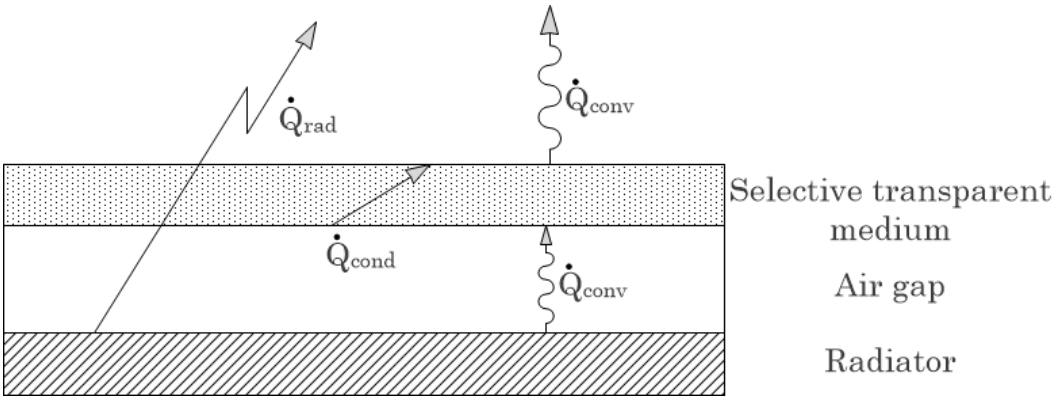

Figure 2.3 Energy flows with a selective cover

Wang *et al.* (2008) studied the effect of different cover materials on a night-sky radiation system. They found that the heat collecting efficiencies increased

from 52% without a cover to 58% and 61% for a polyethylene and polycarbonate cover respectively. Furthermore, the average cooling capacities recorded for a no cover, polyethylene and polycarbonate systems varied from 47 W/m^2 to 36 W/m^2 to 50 W/m^2 respectively, indicating that for heating purposes a cover would be perfect. In the case of cooling capacities the polyethylene reduces the capacity while the polycarbonate increases the cooling capacity slightly.

The placement of the radiator is the second aspect that should be considered in the design of a radiator. For an optimum radiating aperture area the ideal placement of the radiator should be in a horizontal position. Because of natural flow the radiator has to be tilted slightly. Meir *et al.* (2002) studied the effect of tilting the radiator. They found that the cooling capacity compared to that of horizontal placement is reduced by 1% and 7% for a tilt angle of 10° and 32° respectively. The reduction in the cooling capacity is ascribed to the decrease in aperture area as the tilt angle increases.

Meir *et al.* (2002) investigated the effect of the ratio between radiator aperture area and the volume of the storage tank. The aperture/volume ratio affects the minimum temperature reached during one night of cooling. Ratios that are too small will result in insufficient temperature drops, while too large a ratio delivers unnecessarily big temperature drops, and an increase in the system's sensitivity to the ambient air temperature. For example a ratio of 0.01 m^2/l and 0.5 m^2/l results in a temperature difference of 7 °C and 17.5 °C respectively. For cost and optimizing purposes this ratio is of utmost importance.

The third aspect which influences radiator design is mass flow rate. Al-Nimr *et al.* (1998) studied the effect of mass flow rates on a night-sky radiation system. Low flow rates have significant effects on the temperature difference of the tank for one cycle, but there is a limit on the cycles it can complete. Faster mass flow rates have little effect on the temperature difference of the tank, but more cycles could be achieved. Al-Nimr *et al.* (1998) concluded that while both flow rates resulted in different temperature reductions per cycle, at the end of a one night period the overall reduction in temperature in both low and high flow systems were the same. Therefore, low flow rates encountered in thermosyphon systems will have little or no negative influences on the system's performance.

In the case where a pump is used an extra heat load is added to the system. The pump is responsible for a heat load equal to 75% of its electric capacity (Meir *et al.*, 2002). To eliminate the unnecessary heat load the positions of the components need to be considered carefully to allow for natural circulation. Natural circulation requires the temperature drop between the inlet and outlet to be big enough to overcome internal friction and to allow thermosyphonic circulation (Erell and Etzion, 2000).

2.4 Previous Studies

Numerous studies has been done in the past on night-sky radiation as a alternative cooling method. As mentioned earlier, night-sky radiation could be implemented on systems which cool air or water. In this thesis the focus is on the cooling of water.

Identification and reduction or elimination of heat loads on buildings is the logical method to reduce building temperatures. Nahar *et al.* (1999) identifies the roof of a single storey building as being responsible for 50% of the heat load of the building. Therefore, Nahar *et al.* (1999) studied different passive cooling techniques for roof tops, which they ranked according to performance (from best to worse) evaporative, roof pond, white paint and insulation. A wet cloth is incorporated in the evaporative system and placed on the roof. The wetted cloth absorbs solar radiation and immediately dissipates the energy by evaporation. The evaporative method requires a large volume of water. In the case of the roof pond method a shallow pond covered with insulation material during the day to avoid evaporation and the effects of solar radiation on the solar pond is used. The insulation is removed at night to allow the water to radiate the captured energy to the sky, causing the water to cool. The roof pond is a system that can be used for cooling during summer and heating during winter. The other two methods studied are a roof painted white and a roof with insulation on the inside. For arid regions the roof pond solution is more feasible since evaporative systems require more water and the other methods studied are not effective enough for cooling.

In an effort to improve the performance of roof pond designs Runsheng *et al.* (2003) studied four different types of pond covers. Ranked from best to worst they are a floating cloth, movable insulation cover, open, and permanent insulation. The floating cloth caused stratification of the pond. Stratification happens when temperature layers form, the coldest layer is at the bottom and warmest at the top position. Stratification improves the performance since the coldest layer is in contact with the roof, which increases the heat transfer rate. The wet cloth blocks and absorbs a large amount of solar radiation which is immediately dissipated by evaporation. The movable insulation method requires a mechanical system, therefore it is least practical. The open pond has no insulated layer which allows solar heat loads to affect pond temperatures during the day, reducing its performance, while the permanently insulated pond just acts as an extra layer of insulation, therefore it is the worst option.

An alternative cooling method to a roof pond system is circulating water through a radiator. The water stored in a roof pond or tank is pumped, or flows naturally through a radiating panel. The radiator thermally radiates energy to the night-sky causing the water to cool. The radiator used in these systems is similar to conventional solar water heaters. Systems using a radiator

will now be considered.

Al-Nimr *et al.* (1998) compare the results of previous studies of night-sky radiation systems with radiators. The authors identify some shortcomings in previous studies and fill the gaps by creating a transient model which accounts for the effects of convection, conduction and radiation. The transient model is validated through a comparison between theoretical and experimental results. The system is a typical night-sky radiation set-up that consists of a 120 l storage tank and a 0.6 m^2 mild steel insulated radiator with polyethylene cover and a pump as indicated in Figure 2.4. The experiment resulted in a 15 °C difference in the temperature of the tank after one night.

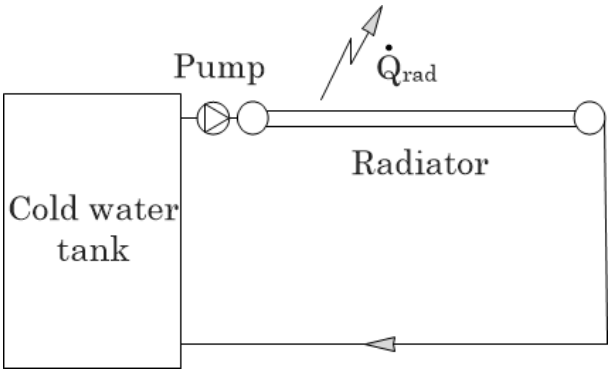

Figure 2.4 Typical layout of a night-sky radiation system

An in depth study was done by Erell and Etzion (2000), who focused on different types of radiation panels for a storage cooling pond with floating polystyrene as insulation. Water is pumped through three different radiators with apertures' of 2.78 m^2 and no covers. Radiator one consists of pipes, fins and insulation, radiator two consists of only pipes and fins. Radiator three consists of pipes with contoured aluminium fins. The insulation on radiator two and three were removed to study the effects of convection and radiation on the night-sky radiation system's performance. A theoretical model was developed to predict the performance of the system. For validation of the theoretical model the inlet and outlet temperatures of the radiator were compared to results obtained experimentally. The results indicated that fins should be removed to increase the cooling power. Therefore, Erell and Etzion (2000) suggest a radiator consisting only of pipes.

A radiation panel with no fins was tested by Meir *et al.* (2002). The radiator used was a polymer based radiator consisting of small channels. The radiator had a aperture of 5.4 m^2 and had no cover. Water was pumped from a 280 l tank to the inlet of the radiator panel, from here it trickled back to the tank. To remove energy added to the room, a radiant floor was proposed. Cooled water was pumped through pipes embedded in the concrete floor, extracting

stored heat from the concrete. A few case studies are solved theoretically and indicate that with modest air humidity and low ambient temperatures at night, sufficient cooling is obtained to keep the building within comfortable temperature limits. Thermal comfort as described by Holm and Engelbrecht (2005) is a room with a relative humidity of 50% and a temperature range from 16 °C to 32 °C with an optimum at 21 °C.

Dimoudi and Androutsopoulos (2006) investigated a design consisting of pipes embedded in a concrete roof. The pipes are unglazed and laid over an area of 2.71 m x 4.97 m. The pipes are exposed to the environment at the top and insulated at the bottom. Water is pumped through the pipes at night and then circulated through a concrete slab acting as thermal storage and a radiant cooling structure. The temperature reduction of the concrete slab during the night test period varied from 3 °C to 6 °C. Furthermore, the results provided indicate a room temperature of 28 °C. Dimoudi and Androutsopoulos (2006) suggest that such a system can contribute to the cooling of a building.

In an attempt to take advantage of a conventional solar water heater Wang *et al.* (2008) investigated the possibility of a dual system. A 1.4 m^2 radiator made of pipes and fins served as the radiating surface. The radiator is used to heat water during day time and cool water during night time. The positions of the components were carefully chosen, this made natural circulation possible. The layout of the natural flow dual system illustrated by Figure 2.5, allowed the system to work without a control system which would be responsible for controlling flow directions. When heated the water will flow to the hot storage tank and when cooled to the cold storage tank. Each storage tank has a volumetric capacity of 200 l. In the experiment a glazed and an unglazed radiator were tested. The results proved that the heat collecting efficiency (58% - 61%) is higher than that of conventional solar collectors. While the cooling capacity (36 W/m^2 - 50 W/m^2) is not as large as other values mentioned in literature.

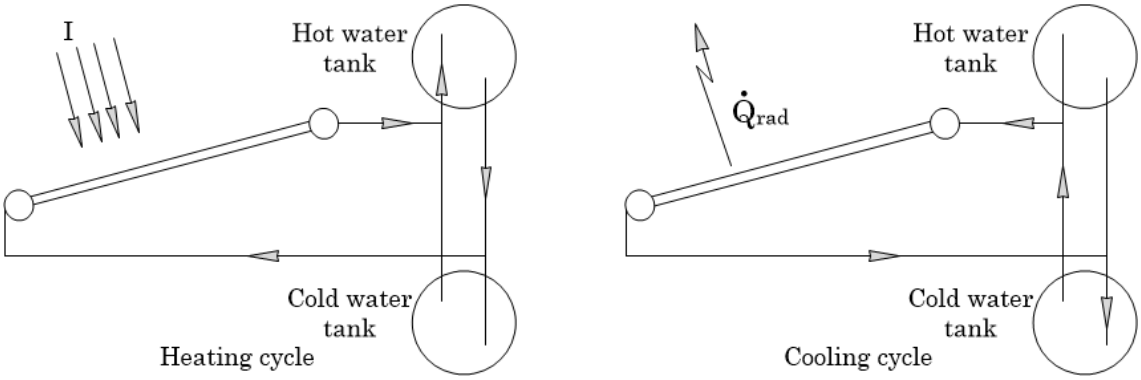

Figure 2.5 Layout of a natural flow dual system

The final system studied is that of Dobson (2005), he used a pool solar water heater as a radiator. The radiator has no cover and consists of various small channels. The fluid is pumped through the radiator at night and during the day the fluid is pumped through a convector situated in a room. The convector is responsible for removing the heat load the room is subjected to. A layout of the system is found in Figure 2.6.

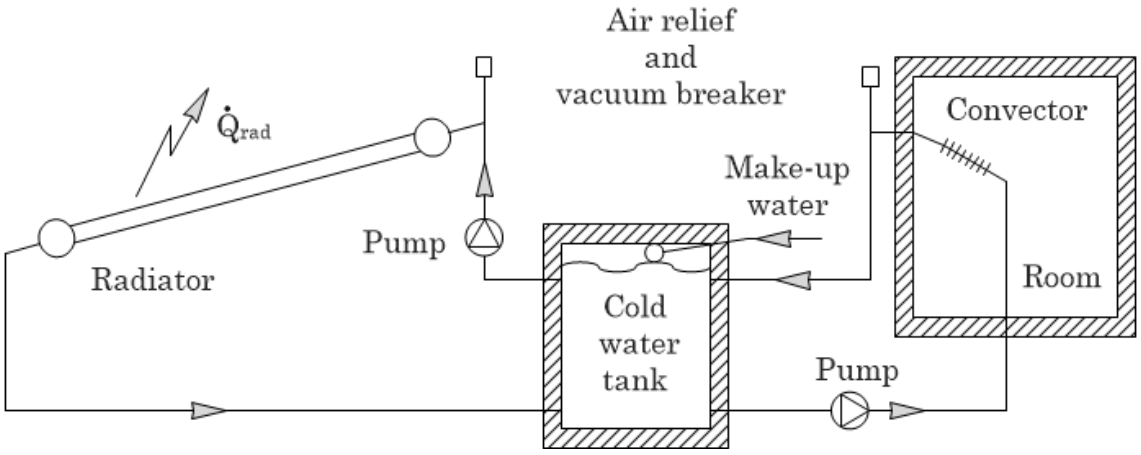

Figure 2.6 System which includes the cooling of a room

2.5 Stratified Tanks

Stratification of water in a tank occurs when the water forms levels with temperatures varying from cold at the bottom to hot at the top. Stratification only happens with no or low inlet mass flow rates as at high flow rates excessive mixing occurs and it is found in natural circulating solar water heater tanks with low flow rates. Compared to mixed tank, the use of a stratified tank increases a solar collector's performance by 38%.

As mentioned by Hollands and Lightstone (1989), a stratified tank performs better than a mixed tank since the mixing of fluids at different temperatures creates entropy. Entropy production is generally destructive in thermal devices. Apart from the creation of entropy, a decrease in performance could also be ascribed to the temperature of water exiting the tank. After water has been withdrawn from the tank, the water temperature of a mixed tank is higher than that of a stratified tank since the stratified tank withdraws the hottest water first. The colder layer is simply displaced upward by new cold water entering the tank. In the mixed tank water hotter than that of the stratified tank enters the solar panel. This will result in a reduction of the efficiency of the radiator since the surface temperature of the panel will be higher. The efficiency of a mixed system being lower than that of a stratified system causes the heating power to decrease. The same logic could be applied

to a system used for cooling. However according to Lunde (1980), after about three circulations through the tank the "efficiency" of both storage methods is more-or-less the same.

To ensure that the maximum cooling power is obtained, factors causing de-stratification need to be identified. These factors causing de-stratification then need to be eliminated or the effects caused by the factors need to be reduced. Hollands and Lightstone (1989) identified four de-stratification factors: jet mixing, plume entrainment, heat conduction and side losses. In this thesis the focus will be on one de-stratification factor, plume formation. The effects of plume formation are significant since changes of up to 35 °C have been recorded (Hollands and Lightstone, 1989).

Plume formation occurs when a hot fluid enters a cold tank from the bottom or when cold fluid enters a hot tank from the top. The entrance of the fluid is modelled as a fixed or variable inlet model. These two models are described by Hollands and Lightstone (1989). Cold water enters the hot water tank of the fixed inlet model at the top and moves downward, mixing each control volume until the mixed temperature is equal to the control volume's temperature a certain distance in. In the variable inlet model, it is assumed that cold water enters the hot water tank from the top. The water flows down without mixing until it finds the temperature which is closest to its own temperature and then settles or mixes with that water.

2.6 Heat Transfer Mechanisms

Heat is a form of energy transferred from one object to another due to a temperature difference between the objects. Heat between two objects will always flow from the higher temperature to the lower temperature, heat flow will stop when the two objects' temperatures are equal. Heat is transferred through three mechanisms namely conduction, convection and radiation.

2.6.1 Conduction

Conduction occurs when a particle with more energy transfers energy to an adjacent less energetic particle. Conduction heat transfer occurs when particles in liquids and gases collide and transfer energy while particles in a solid vibrate to transfer the energy. The rate of energy transfer by the medium is affected by the thermal conductivity (k) of the medium. The thermal conductivity is a measure of the ability of the material to conduct heat. Conduction heat transfer is calculated with

$$\dot{Q}_{cond} = \frac{T_{hot} - T_{cold}}{R_{cond}} \tag{2.6.1}$$

where $R = L/kA$ and A is the area perpendicular to the direction of heat transfer and L the thickness of the medium through which conduction occurs. Conduction is illustrated in Figure 2.7. The formula of conduction indicates that the heat transfer rate is influenced by the thermal conductivity, thickness and area of the medium.

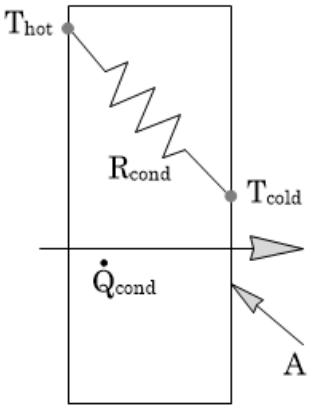

Figure 2.7 Illustration of conduction through an opaque material

2.6.2 Convection

Convection is the transfer of thermal energy between a solid surface and a gas or liquid in motion or stagnant. Convection is the combined effects of conduction and fluid motion. A stationary fluid in contact with a surface experiences only conduction while a moving fluid experiences conduction and convection. An increase in fluid motion increases the convection heat transfer coefficient (h).

The convection heat transfer is influenced by various factors such as surface geometry, nature of fluid, fluid properties and velocity of the fluid. The energy transferred due to convection between a surface and the ambient air is given by

$\dot{Q}_{conv} = \dfrac{T_s - T_{amb}}{R_{conv}}$, where T_s the surface temperature, T_{amb} the ambient temperature and R_{conv} the convection resistance

$R_{conv} = \dfrac{1}{hA_s}$, where h is the convection heat transfer coefficient and A_s the surface area, as presented in Figure 2.8.

Convection is either natural or forced. Forced convection is when an external source causes fluid flow, while natural convection is when flow occurs due to buoyancy forces induced by density variations caused by variation in temperatures.

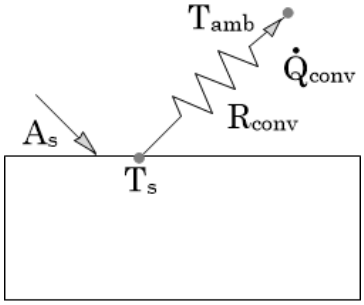

Figure 2.8 Illustration of convection

2.6.3 Radiation

Radiation is the energy emitted by a body above absolute zero in the electro magnetic wave length between 0.1 μm and 100 μm. No medium is required for this type of heat transfer. The thermal energy emitted by a body is given by

$$Q_{emit} = \sigma \epsilon A_s T_s^4$$

where σ is the Stephan Boltzmann constant, ϵ the emissivity, A_s the surface area and T_s the surface temperature in Kelvin. The maximum energy emitted by a body with high infra-red emittance and ambient temperature is in the range of 100 W/m^2.

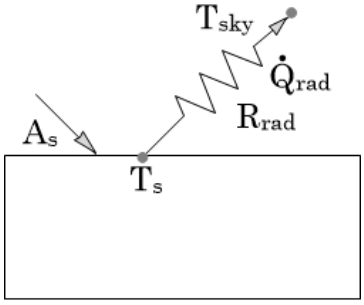

Figure 2.9 Illustration of radiation

The nett energy emitted from a body to the sky as illustrated by Figure 2.9 is given by

$$\dot{Q}_{rad} = \frac{T_s - T_{sky}}{R_{rad}}$$

where T_{sky} is the sky temperature in Kelvin and R_{rad} the radiation resistance.

$$R_{rad} = \frac{1}{\sigma \epsilon A_s (T_s^2 + T_{sky}^2)(T_s + T_{sky)}}$$

2.7 The Equations of Change

Building a one-dimensional transient model of a night-sky radiation system requires the application of the three fundamental laws: conservation of mass, conservation of energy and the conservation of momentum. The three laws are then applied to each control volume of the discretized system.

2.7.1 Conservation of Mass

The conservation of mass is mathematically known as the continuity equation. The equation is developed by applying a mass balance on a volume element fixed in space, through which a fluid is allowed to flow. The balance is expressed in words by

Rate of increase in mass = rate of mass in - rate of mass out

The physical statement can be translated to mathematical language and can produce Equation 2.7.1 Bird *et al.* (2007). This equation assumes one dimensional flow.

$$\frac{\partial \rho}{\partial t} = -\frac{\partial \rho v_x}{\partial x} \tag{2.7.1}$$

With the mass of control volume $m = \rho V$ where $V = \delta x \delta y \delta z$ and the mass flow rate $\dot{m} = \rho v \delta y \delta z$ where $\delta y \delta z$ is the area through which fluid flows. With equation (2.7.1) and the definition of mass and mass flow rate, Equation 2.7.2 could be derived.

$$\frac{\partial m}{\partial t} = -\partial \dot{m} \tag{2.7.2}$$

2.7.2 Conservation of Energy

The conservation of energy applied on a control volume provides the equation of change for energy. The equation is reduced by assuming one dimensional flow and neglecting the effect of kinetic energy on the fluid (Kays *et al.*, 2005).

$$\rho v \frac{\partial h}{\partial x} + \rho \frac{\partial h}{\partial t} - \partial \dot{Q} = 0 \tag{2.7.3}$$

Multiplying Equation 2.7.3 with the volume of the control volume, rearranging the terms and substituting $h = u + Pv$, Equation 2.7.4 can be derived

$$\frac{\partial mU}{\partial t} = -\partial \dot{m} h - \partial Q - \frac{\partial PV}{\partial t} \tag{2.7.4}$$

2.7.3 Conservation of Momentum

The conservation of momentum is mathematically presented as the equation of motion. This equation expressed in words, states

rate of increase in momentum = net rate of momentum + external forces.

where the net rate of momentum is the rate of momentum in minus the rate of momentum out. The external force acting on a control volume is gravity, therefore an mg term and shear force acting against the direction of flow. The motion equation is mathematically expressed by Bird *et al.* (2007) as

$$\frac{\partial \rho v}{\partial t} = -\frac{\partial \rho v v}{\partial x} - \frac{\partial P}{\partial dx} + \rho g - \frac{\partial \tau}{\partial y} \tag{2.7.5}$$

By multiplying Equation 2.7.5 with the volume of the control volume, the equation becomes

$$\frac{\partial m v}{\partial t} = -\partial \dot{m} v - \partial P A_x + mg - \partial \tau A_z \tag{2.7.6}$$

2.8 Fluid Properties

The properties of the water and air constantly change as the temperature of the medium changes. The constant pressure specific heat c_p can be assumed to be constant in the range of 0 °C to 80 °C.

Other properties such as the thermal conductivity, enthalpy dynamic viscosity and density, change with the temperature of the fluid. The changes in these properties are related to temperature assuming the pressure of the fluids to be constant. A curve can be fitted to data provided by Cengel and Ghajar (2011). An equation which is a function of temperature can then be used to calculate the desired fluid property at any desired temperature.

Using the Boussinesq approximation eliminates the constant change of density (Cengel and Ghajar, 2011). The approximation states that the change in density is insignificant except in terms where density is multiplied by gravity. For the terms with gravity the density will then be calculated with Equation 2.8.1.

$$\rho = \rho_{ref} - \beta_{ref}(T - T_{ref}) \tag{2.8.1}$$

The literature study provides the knowledge to design and theoretically model a night-sky radiation system for the cooling of a room in a building. The knowledge gained from the literature study will be used in the design criteria of the experimental set-up (Chapter 3).

3 Design Criteria of the Experimental Set-Up

The design of the experiment involves three different natural circulation cycles; a cooling, heating and convector cycle. The major components in these cycles are the cold and hot water storage tanks, a room with convector, a control and a swimming pool solar collector (radiator). These components are visible in the night, day and convector cycles depicted in Figure 3.1.

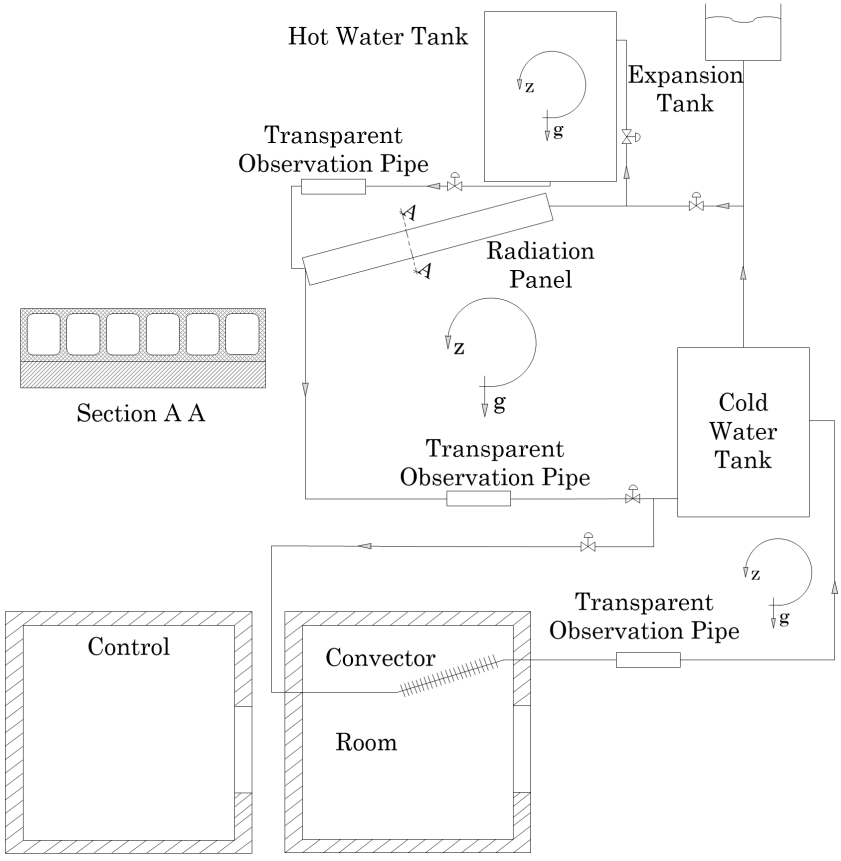

Figure 3.1 Layout of the experimental night-sky radiation system incorporating a radiation panel

3.1 Description of the Three Cycles

The night cycle or cooling cycle cools hot water flowing from the cold water storage tank to the radiator. The radiator radiates energy to the cold sky. The radiation causes a decrease in the temperature of the water, the decrease in temperature causes a increase in the density of the water. The cold fluid flows downward towards the tank and completes the cycle. The cooling cycle is illustrated in Figure 3.2 (a), natural circulation in the night and day cycle.

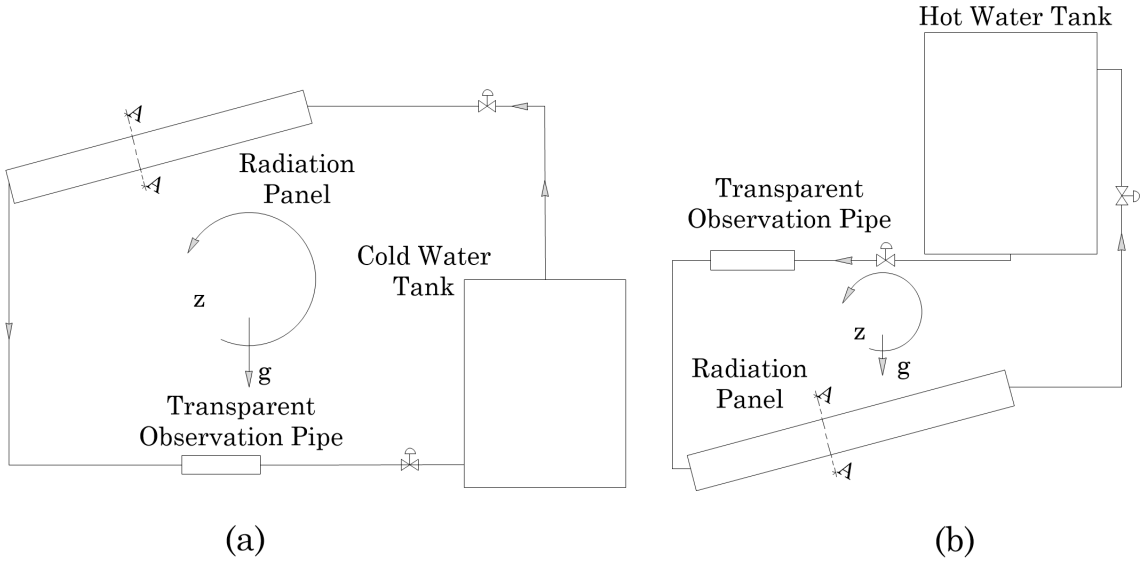

Figure 3.2 Natural circulation in the night (a) and day cycle (b)

Figure 3.2 (b) depicts the day cycle. Cold water flows from the hot water storage tank and enters the radiator. During the day the radiator acts as a solar collector, the radiator absorbs solar radiation and converts it to thermal energy. The thermal energy is transferred to the water causing an increase in water temperature. The density of the water decreases causing the heated water to be pushed upwards to the tank by the colder denser water.

The convector cycle shown in Figure 3.3 also operates during day time. This cycle is used to cool a room subjected to a heat load. Water flows from the cold water storage to the convector situated in the room. The convector absorbs energy from the room causing the air temperature to decrease and the water temperature to increase. Similar to the water in the day cycle the heated water rises to a higher position causing the water to flow back to the cold water storage to complete the cycle.

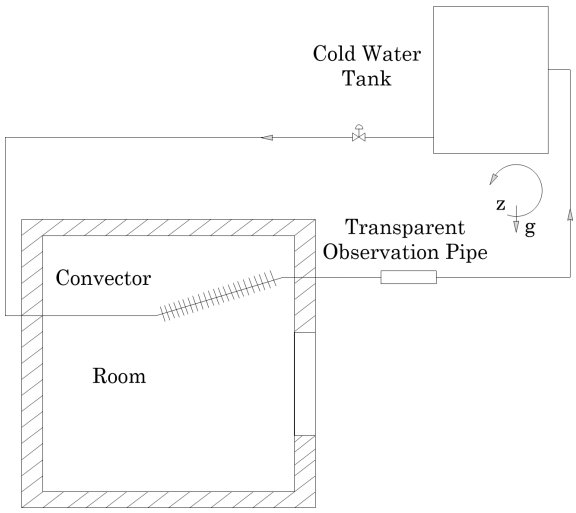

Figure 3.3 Natural circulation in the convector room cooling cycle

3.2 Radiator

A swimming pool solar collector is a commercially available product which matches the criteria for night-sky radiation, it has no fins and consists of numerous small channels. The 50 mm inner diameter (ID) manifold directs water into small channels of 4.7 mm x 7 mm made of black ultra violet resistant polypropylene with a life expectancy of 15 years. The black surface provides high emittance values of 0.97, and is unglazed. At the bottom a super wood board acts as support and insulation. Figure 3.4 presents a schematic diagram of the radiator manifold and cross section.

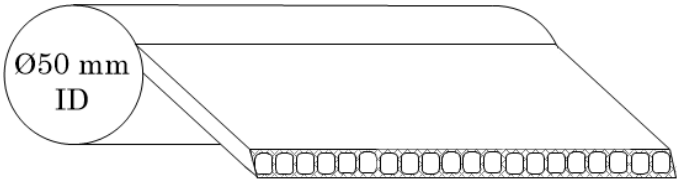

Figure 3.4 Schematic diagram of radiator's manifold and cross section

Using a radiator with similar characteristics as a solar collector engenders the option of a dual system. A dual system implies that the radiator could be used for night-sky radiation and also act as a solar water heater. Since the efficiency of the swimming pool solar water heater would be lower due to it not being glazed as in the conventional solar water heaters, it would only be used as a pre-heater for a geyser.

When considering a dual system, the positioning of the radiator becomes an issue. For cooling purposes the ideal position would be horizontal (0°). Heating, on the contrary, requires a tilt angle equal to the latitude of the specific location. The main purpose of this design is to cool water, therefore it was decided to tilt the radiator slightly by 5° to allow natural flow. The small tilt angle has negligible effects on the cooling power of the night sky radiation system.

3.3 Tanks

The system design requires two water storage tanks; one tank for the cold water storage and one for the hot water storage. These tanks have a capacity of 150 l and 68 l respectively.

To limit plume formation in the cold water tank during the night cycle, the inlet of the cold water tank is at the bottom and the outlet at the top. Cold water will now enter at the bottom of the tank and, without forming a plume, push the hot water out at the top. During the convector cycle the inlet and outlets of the tank are switched, cold water leaves the tank at the bottom while hot water enters from the top. For the hot water tank the outlet is placed at the bottom of the tank while the inlet is placed two -thirds from the bottom of the tank (Chinnery, 1971).

3.4 Rooms

Two identical square rooms with dimensions of 1.2 m x 1.2 m x 1.3 m high are required, one with a convector and the other without one. The room without a convector serves as a control. Structural stiffness is provided by a mild steel angle iron frame with a removable lid for access. The frame is covered with 1 mm thick galvanized sheet metal. The interior of the galvanized steel is lined with a 23 mm thick polystyrene board for insulation purposes. A perspex window is installed on the south facing side of the room to allow visual inspection of the room. Figure 3.5 illustrates the layout of the room with the convector.

3.5 Convector

The convector consists of 7 copper tubes with aluminium fins attached to the tubes. In an experiment similar to the one did in this study Naude (2013) selected this convector. A convector with closely packed fins has a greater surface area but the heat transfer coefficient reduces due to the added resistance to air flow due to the fins. Therefore, it is important to determine the

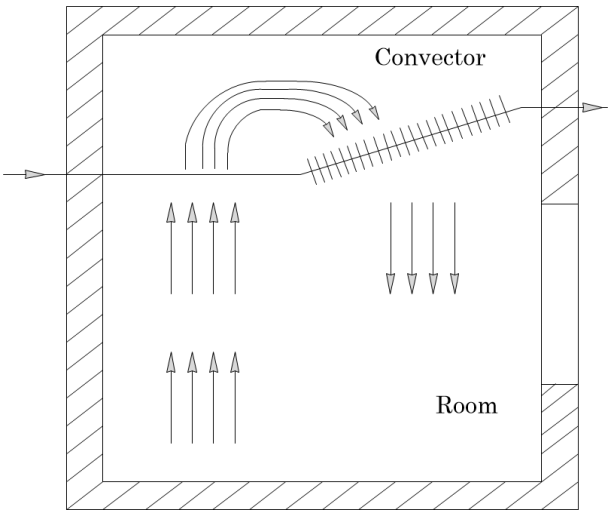

Figure 3.5 Layout of the room indicating flow over the convector

optimum fin spacing. After doing calculations described in Appendix B.2, it was decided to use the same convector with fin spacing of 7 mm, since the calculations provided a fin spacing of 7.45 mm. The temperature of the system changes continuously, therefore the optimum fin spacing will also change continuously

The convector is installed at the top section of the room at an angle of 5° to allow natural circulation of the water. The inlet side of the convector is the lowest point and located 40 mm below the top section of the roof. Figure 3.5 depicts the flow of air in the room.

4 Experimental Set-Up

In this chapter the experimental set-up aspects such as the instrumentations measurements, control and start-up procedure are discussed. Measurements include the measurement of temperatures at various positions and water and air velocities. The experiment is controlled with valves that need to be opened or closed manually, to ensure the activation of the cycles at the desired time. A certain procedure needs to be followed to ensure that no air bubbles are trapped in the system, thereby blocking the thermosyphonic flows.

4.1 Measurements and Control

Accurate measurements of temperature were taken with a computer and commercially available data acquisition (DAQ) hardware and software (National-instruments, 2014). The velocity measurements in the room were taken with a hot wire anemometer, while the water velocity measurements were taken visually.

4.1.1 Temperature Measurement and Calibration

For temperature measurement copper and constantan (type T) thermocouples were used. Twenty-nine temperature measurements at various locations were recorded. Five equally spaced thermocouples were placed in each tank, six in the room, five in the control and one at each inlet and outlet of the convector and radiator, the most important temperatures being those in the tanks, room and control. Other temperatures taken were the inlet and outlet of the radiator and convector and the top and bottom of the radiator, with the final thermocouple measuring the ambient temperature.

The thermocouples consist of two wires, a copper wire and a constantan wire. At the point of measurement the two wires are welded together to create a junction. A change in temperature induces a voltage which can be converted to a temperature. This phenomenon is known as the Seebeck Effect. The voltage at the junction is sent to the DAQ and the DAQ sends multiple voltage measurements to the computer. The software converts the voltages into

temperatures measured in °C and records them. A sample rate of 10 Hz was selected for the experiment.

Credible results require the calibration of measurement equipment. The calibrated temperature ranges from -5 °C to 80 °C. Temperature steps were taken from -5 °C to 0 °C and then at intervals of 10 °C. The calibration set-up as depicted in Figure 4.1, consists of a 9142 field metrology well, a platinum resistance temperature detector (RTD) (the available model was a PT-100) and the thermocouples (Fluke corporation, 2014). The calibration certificate of the RTD can be found in Appendix A.1. The RTD was last calibrated on the 4th of February 2013.

The thermocouples were connected to the DAQ which was connected to the computer from where the temperature of the thermocouples could be read. The field metrology well was set to the required calibration temperature, where it cooled the billet in which the thermocouples and RTD were inserted. The RTD was connected to a Hewlett Packard 34401A multimeter (Agilent-tecnologies, 2012). The resistance value reading of the multimeter could be converted to a temperature. When the temperatures of the thermocouples and the resistance of the RTD reached equilibrium, the temperatures and resistance were recorded.

Thermocouple temperature readings were compared to those of the PT-100. The final step of the calibration was to adjust the thermocouples' readings to those of the PT-100. This is done by applying the linear regression correction function onto the data.

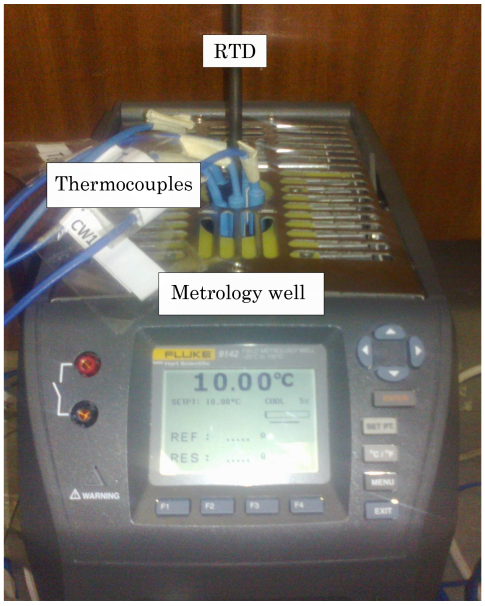

Figure 4.1 Figure illustrating calibration set-up including a Fluke 9142 field metrology well unit

Results obtained from calibration and the regression applied to it are shown in Table 4.1. Coefficients A and B were used in the correction Equation 4.1.1 to calculate corrected temperature values. The coefficient of determination R^2 value indicated how close the data is to the fitted regression line, a value of one indicates a good fit. Additional calibration information can be found in Appendix A.

$$T_{correct} = A + B * T_{thermocouple} \tag{4.1.1}$$

Table 4.1 Correction coefficients and the coefficient of determination

	A	B	R^2
T_{room1}	0.417	1.000	1.000
T_{room2}	0.347	1.002	1.000
T_{room3}	0.345	0.997	1.000
T_{room4}	0.465	0.998	1.000
T_{room5}	0.416	1.000	1.000
T_{room6}	0.498	1.000	1.000
T_{room1c}	0.348	0.995	1.000
T_{room2c}	0.354	0.991	1.000
T_{room3c}	0.470	1.000	1.000
T_{room4c}	0.365	1.004	1.000
T_{room5c}	0.461	0.999	1.000
T_{conin}	0.259	1.007	1.000
T_{conout}	0.270	1.004	1.000
T_{rinCW}	0.426	1.002	1.000
T_{routCW}	0.303	1.002	1.000
T_{rinHW}	0.338	0.998	1.000
T_{routHW}	0.482	0.994	1.000
T_{rt}	0.239	1.004	1.000
T_{rb}	0.295	0.992	1.000
T_{CW1}	0.187	1.004	1.000
T_{CW2}	0.280	1.003	1.000
T_{CW3}	0.167	1.005	1.000
T_{CW4}	0.301	1.002	1.000
T_{CW5}	0.279	1.005	1.000
T_{HW1}	0.423	1.000	1.000
T_{HW2}	0.513	0.996	1.000
T_{HW3}	0.387	0.990	1.000
T_{HW4}	0.410	0.998	1.000
T_{HW5}	0.518	0.998	1.000
T_{amb}	0.274	1.005	1.000

The temperature difference error was further reduced by forming similar thermocouple pairs. The pairs formed were those of the tanks, room, control and inlet and outlet temperatures. Thermocouples with nearly similar temperatures were chosen to form pairs. Tables A.1 to A.5 in Appendix A show the temperature of the thermocouple pairs at the different calibration temperatures.

4.1.2 Filtering of Temperature Data

Once the calibration was completed the recorded temperatures appeared to be noisy, as depicted in Figure 4.2. Further investigation of this behaviour suggested that the noise must have been generated by the module since there was no amplification. Noise can be removed from data by inserting a filter before recording or on recorded data.

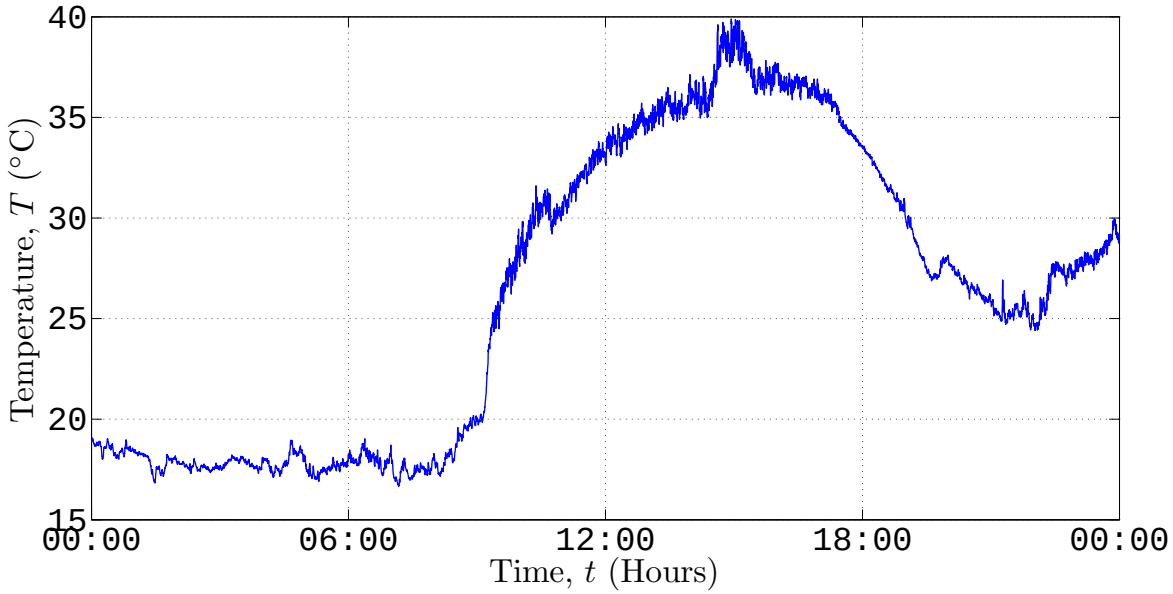

Figure 4.2 Noise recorded of the temperature as a function of time

During this experiment noise was removed after data was recorded by using Matlab's built in smoothing function. This function has various methods of smoothing, including a moving average method which was chosen to reduce the noise in the data. The moving average method calculates a new average value for each data point. The average is determined by a specified number of data points before and after each data point. The effect of the noise removal is illustrated in Figure 4.3.

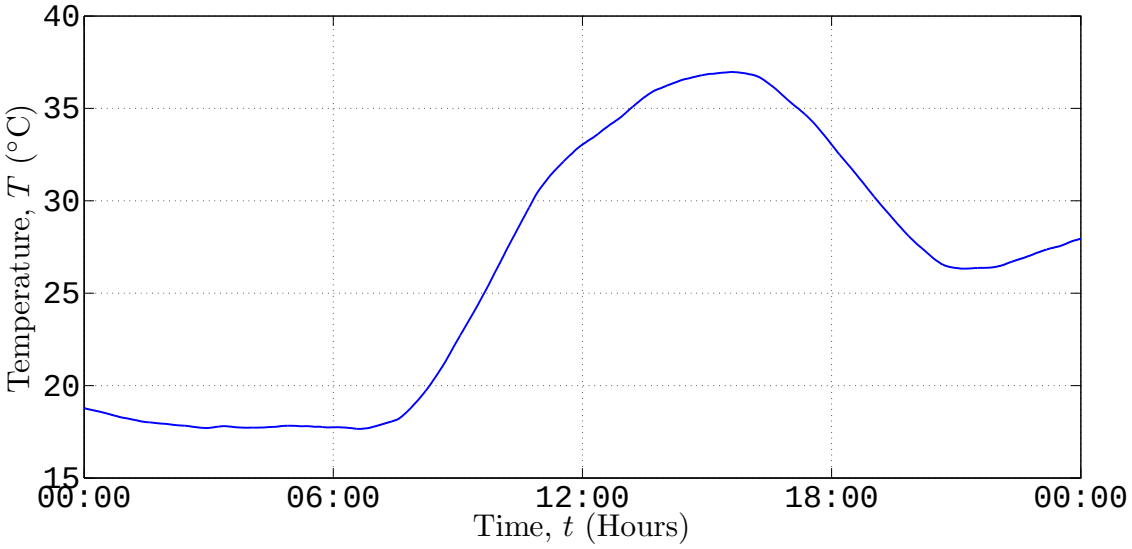

Figure 4.3 Smoothed temperature as a function of time

4.1.3 Air and Water Velocities

Air flow rates were measured using a AIRFLOW thermal anemometer (model TA5). The anemometer has a probe that can be extended up to 1 m, this feature made measurements possible without opening the room (Airflow, 2014).

The anemometer heats a very thin wire situated at the tip of the probe, to above the temperature of the surroundings. Air flowing past the wire causes the wire to cool. The wire's resistance changes due to a change in temperature. The resistance is used to calculate air velocities with a correlation between the air velocity and wire resistance.

The TA5 anemometer used has a velocity range from 0.25 m/s to 30 m/s. Since natural circulation is implemented air velocities are very low. To reduce errors in measurements a shroud placed under the convector directs flow to a single square outlet of (136 mm x 165 mm). At the outlet, eight airflow measurements at different positions were taken, the average of the eight measurement served as the airflow rate over the convector.

Transparent observation sections inserted in each loop made the visual inspection of water flow rates possible. A colourant injected into the fluid with a syringe and needle can be tracked through a 0.6 m section. The distance travelled together with the time travelled is then used to calculate the maximum velocity of the fluid. Knowing that the fluid flow is laminar, since it could be observed visually, the average velocity of the fluid could be calculated. Cengel and Cimbala state that the average fluid velocity of laminar flow is equal to half of the maximum velocity of the fluid.

4.2 Start-up and Running of Experiment

Natural circulation is a key aspect of the design. Since no pumps were used air trapped inside the system would cause the water thermosyphonic system to malfunction due to the blocking of the water flow by the surface tension between the bubble and the pipe. To prevent air being trapped in the system, the system was designed to allow an air bubble to find its way to the expansion tank, as seen in Figure 3.1. Water needs to enter the system at the lowest point and then gradually fill the system from bottom to top pushing all the air out.

Once the system is filled it becomes operational. For the experimentation period it was decided to manually close and open the valves. This was done at 08:00 and 17:00 each day.

5 Theoretical Modelling

In this chapter a method whereby the transient performance of a night-sky radiation system as depicted in Figure 5.1 is determined, is presented. The system is divided into three cycles. the night, hot water and convector cycles. The physical model representing the system is then discretized. The conservation of mass, energy and momentum are then applied to the unique control volumes.

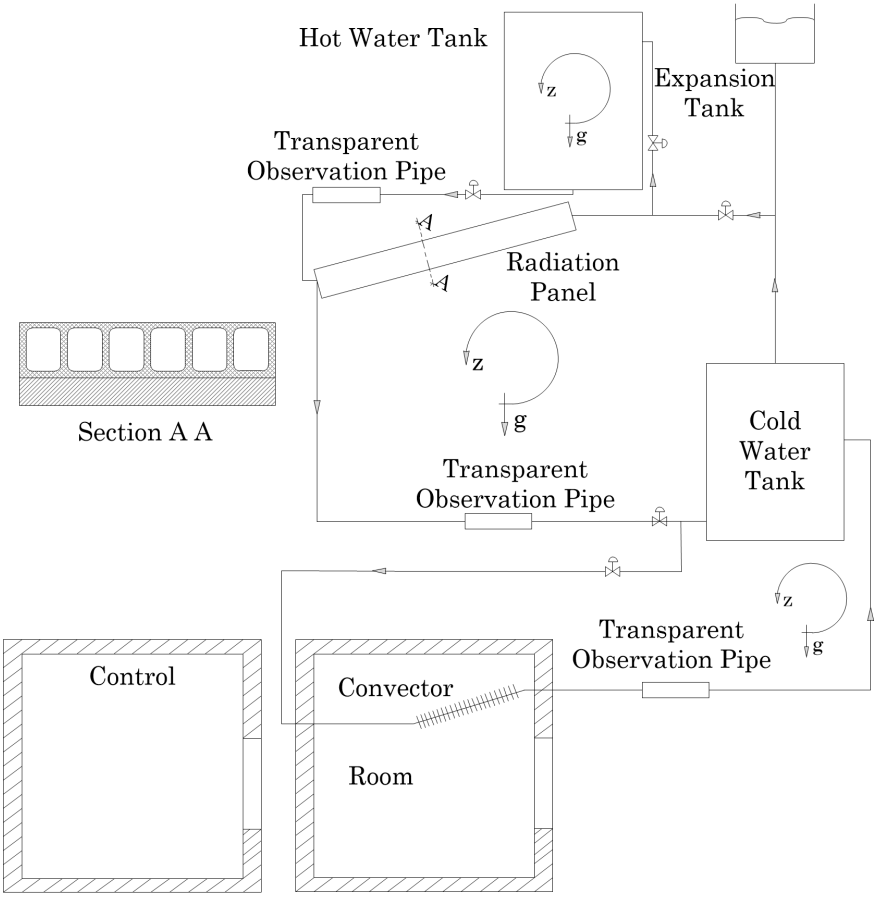

Figure 5.1 Layout of the experimental night sky radiation system incorporating a radiation panel. (Figure 3.1 repeated for convenience.)

5.1 Night Cycle

During the night, water circulates naturally through the radiator. The radiator thermally radiates energy to the sky and extracts heat from the water. The water cools and due to gravity and change in density, flows to a lower position and enters the tank. Hotter water from the tank in return is pushed into the radiation panel to complete the cycle. Consider the discretized loop in Figure 5.2, the loop consists of a radiator, cold water tank, manifold and pipes. The theoretical model requires the application of the conservation of mass, energy and momentum to each of the indicated control volumes.

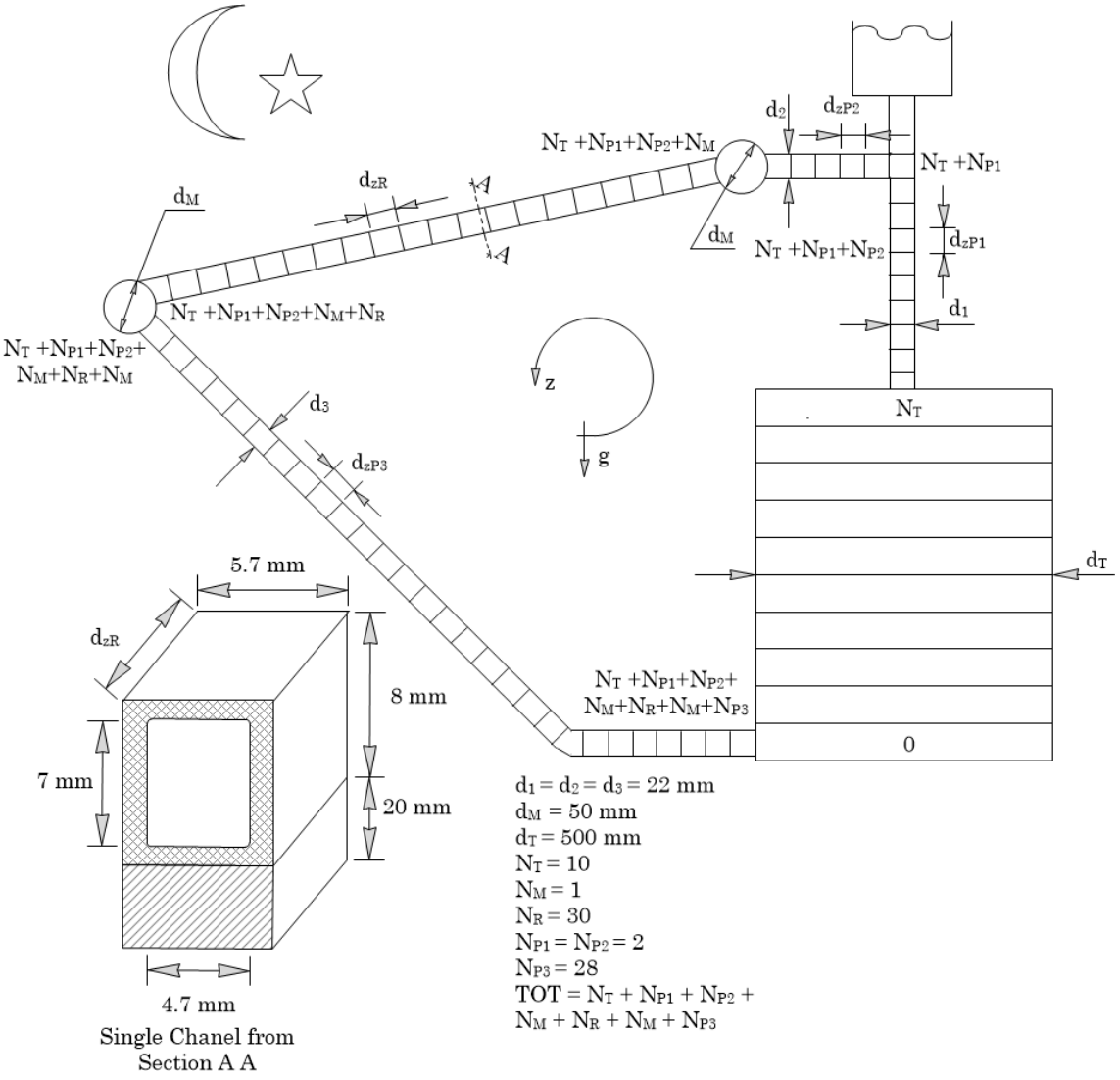

Figure 5.2 Discretized loop for night cycle operation

5.1.1 Conservation of Mass

The mass of the control volume for the next time step can be calculated by applying the conservation of mass. The conservation of mass involves the mass in and outflow of the control volume. With the mass at the next time step the conservation of energy can be applied to determine the temperature of the control volume for the next time step.

Applying the general statement of conservation of mass

$$\frac{\Delta m}{\Delta t} = \sum \dot{m}_{in} - \sum \dot{m}_{out} \qquad [\text{kg/s}] \tag{5.1.1}$$

to each unique component shown if Figure 5.3, with manipulation equation (5.1.1) becomes

$$m^{t+\Delta t} = m^t + \Delta t(\sum \dot{m}_{in} - \sum \dot{m}_o ut) \qquad [\text{kg/s}] \tag{5.1.2}$$

where $m = \rho A_x \Delta z$, $A_x = \pi d^2/4$ and $\dot{m} = \rho v A_x = \rho G$ since $v = G/A_x$.

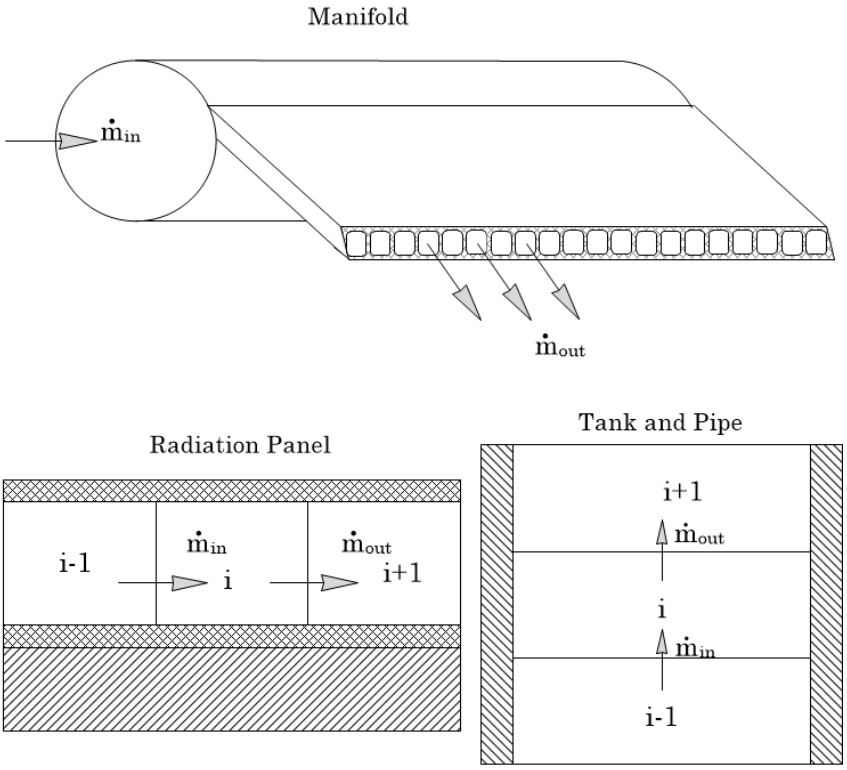

Figure 5.3 Diagram indicating the mass flow through the typical i$^{\text{th}}$ control volume of each component

5.1.2 Conservation of Energy

In order to predict the temperature of a control volume for the next time step, the conservation of energy needs to be applied to that control volume. The conservation of energy considers the flow of energy due to mass flow, conduction, convection and radiation as indicated in Figure 5.4.

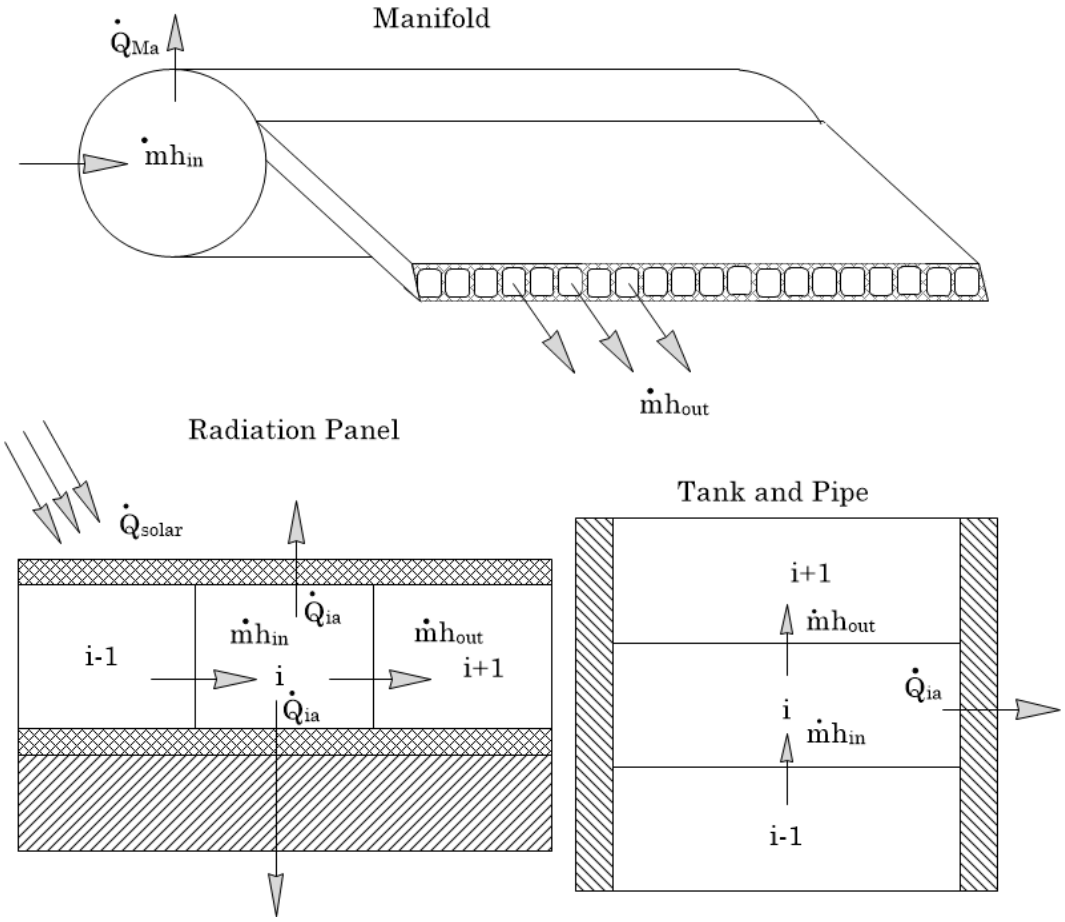

Figure 5.4 Diagram indicating energy flow of the typical i^{th} control volume of each component

With the flow of energy known, a thermal resistance diagram of the unique control volumes is constructed. The thermal resistance diagram presented in Figure 5.5, includes convection, conduction and radiation as heat transfer mechanisms.

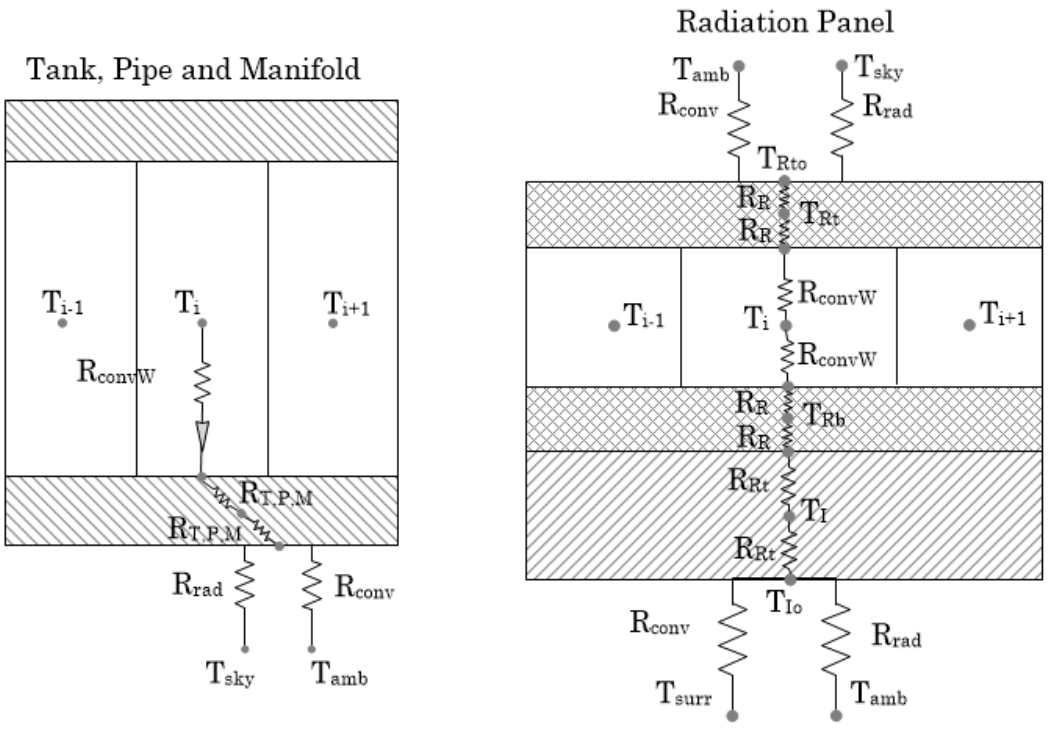

Figure 5.5 Thermal resistance diagram for the typical ith control volume

Applying the general statement of conservation of energy to each unique control volume in Figure 5.2 and ignoring kinetic and potential energy

$$\frac{\Delta mU}{\Delta t} = \sum \dot{m}h_{in} - \sum \dot{m}h_{out} + \dot{Q}_{in} - \dot{Q}_{out} - \frac{P\Delta V}{\Delta t} \qquad [\text{W}] \qquad (5.1.3)$$

where enthalpy, $h = u + PV$, the equation becomes

$$\frac{\Delta mH}{\Delta t} = \sum \dot{m}h_{in} - \sum \dot{m}h_{out} + \dot{Q}_{in} - \dot{Q}_{out} \qquad [\text{W}] \qquad (5.1.4)$$

and specific enthalpy could be expressed as $h = c_pT$, now the equation becomes

$$\frac{\Delta mc_pT}{\Delta t} = \sum \dot{m}h_{in} - \sum \dot{m}h_{out} + \dot{Q}_{in} - \dot{Q}_{out} \qquad [\text{W}] \qquad (5.1.5)$$

and with manipulation

$$T^{t+\Delta t} = \frac{(mc_pT)^t}{mc_p^{(t+\Delta t)}} + \left(\frac{(mc_p)^t\Delta t}{mc_p^{(t+\Delta t)}}\right)\left(\sum \dot{m}h_{in} - \sum \dot{m}h_{out} + \dot{Q}_{in} - \dot{Q}_{out}\right) \qquad [\text{W}] \qquad (5.1.6)$$

The heat transfer rate calculated with

$\dot{Q} = (T_{hot} - T_{cold})/R$

where typically $R = 1/hA$; $R = L/kA$ and $R = 1/\varepsilon\sigma A(T_{hot}^2+T_{cold}^2)(T_{hot}+T_{cold})$ for convection, conduction and radiation respectively.

The convection heat transfer rate is influenced by the convection heat transfer coefficient. Loveday and Taki (1996) studied the effect of wind on the heat transfer of building walls. The radiator can be modelled as a building wall, therefore equation (5.1.7) for a flat surface is used as suggested by Loveday and Taki (1996). In this equation v is the wind speed.

$$h = 18.6v^{0.605} \tag{5.1.7}$$

The tank and pipe's external convection heat transfer coefficients are calculated by using the Nusselt number where $h = Nuk/D_h$. The Nusselt number is affected by the wind speeds, wind speeds greater than zero result in external forced convection. Cengel and Ghajar (2011) suggest equation (5.1.8) for this scenario and for wind speeds equal to zero natural convection is assumed, and equation (5.1.9) is used.

$$Nu = \{0.3 + \frac{0.62Re^{1/2}Pr^{1/3}}{(1+(0.4/Pr)^{2/3})^{1/4)}}\}\{(1+(Re/282500)^{5/8})\}^{4/5} \tag{5.1.8}$$

$$Nu = \{0.6 + \frac{0.387Ra^{1/6}}{(1+(0.559/Pr)^{9/16})^{8/27}}\}^2 \tag{5.1.9}$$

The internal convection heat transfer coefficient depends on the cross section of the component. For the analysis internal forced convection is assumed. The Nussult number is taken as the average of the constant surface temperature and constant heat transfer rate conditions. Using values suggested by Cengel and Ghajar (2011), the Nussult number for circular sections is 4.01 and for rectangular sections is 3.53.

The energy balance at the top of the radiator is influenced by radiation, conduction and convection, with radiation responsible for a significant portion of heat loss. As indicated earlier radiation is affected by the sky temperature which is affected by the relative humidity of the air. Low relative humidities result in low sky temperatures and high radiation heat transfer rates.

The radiator radiates energy to the cold sky, which acts as a heat sink. The sky temperature can be calculated using the ambient air temperature and relative humidity. The sky temperature is calculated with (Mills, 2009):

$$T_{sky} = \left(\epsilon_{sky}(T_{amb} + 273.15)^4\right)^{1/4} - 273.15 \tag{5.1.10}$$

where $\epsilon_{sky} = 0.741 + 0.00162T_{dp}$ at night and $\epsilon_{sky} = 0.727 + 0.00160T_{dp}$. The dew point temperature is calculated with equation (5.1.11) where $A = 7.625$ and $B = 243.04$ °C (Lawrence, 2005).

$$T_{dp} = \frac{B\Big(\ln(RH) + \frac{A_1 T_{amb}}{B+T_{amb}}\Big)}{A - \ln(RH) - \frac{AT_{amb}}{B+T_{amb}}} \tag{5.1.11}$$

The required fluid properties are calculated using equations imitating data provided by Cengel and Ghajar (2011). The equations describe a curve which is fitted to the data, these curve fits and equations describing them are presented in Appendix C. The equations assume constant pressure therefore they are only functions of temperature.

5.1.3 Conservation of Momentum

By applying the conservation of momentum to the cycle, the volumetric flow rate of the next time step is calculated. The new volumetric flow rate is used to calculate the mass flow rate of the control volumes for the next time step. Gravity is only present in the conservation of momentum, therefore the Boussinesq approximation will be used.

Applying the general statement of the conservation of momentum to each unique control volume shown in Figure 5.2.

$$\frac{\Delta mv}{\Delta t} = \sum \dot{m} v_{in} - \sum \dot{m} v_{out} + (P_{in} - P_{out})A_x - mg - \tau A_z \qquad [\mathrm{N}] \tag{5.1.12}$$

Dividing by A_x and summing around the loop, the pressure terms cancel out and the equation becomes

$$\frac{\Delta}{\Delta t}\sum \frac{mG}{A_x^2} = \sum (\frac{G}{A_x})^2(\rho_{in} - \rho_{out}) + \sum \rho g \Delta z \sin(\theta) - \sum \frac{\tau A_z}{A_x} \qquad [\mathrm{N/m^2}] \tag{5.1.13}$$

where $\tau = C_f \rho G^2 / 2A_x^2$, $A_z = \pi d \Delta z$ and $\theta = -\pi/2; \pi/2$ if the gravity acting against the flow θ is negative and with the flow θ is positive. Dividing by Δz and in the limit, as Δz and A_x tend to zero and integrating around the loop Equation 5.1.13 becomes

$$\frac{\partial}{\partial t}\oint \rho v_z = -\oint \frac{\partial \rho v_z^2}{\partial z} - \oint \frac{\partial P}{\partial z} - \oint \rho g_z - \oint \frac{\partial \tau}{\partial z} \qquad [\mathrm{N/m^3}] \tag{5.1.14}$$

where $\oint \frac{\partial P}{\partial z} - = 0 \qquad [\mathrm{N/m^3}]$

or explicitly as

$$G^{t+\Delta t} = \sum \frac{G^t \rho_i^t \Delta z}{\rho_i^{t+\Delta t} \Delta z} + \Delta t \frac{M + B - F}{\sum_1^{N_{TOT}} \rho_i^{t+\Delta t} \Delta z / A x_i} \tag{5.1.15}$$

where

$M = \sum((\rho_{in} - \rho_{out}) G^2 / A x_i^2)$

$B = \sum(\rho_b g \Delta z Sin(\theta))$

$F = \sum(\tau \pi D_i (\Delta z_i + \Delta z_{minor}) / A x_i)$

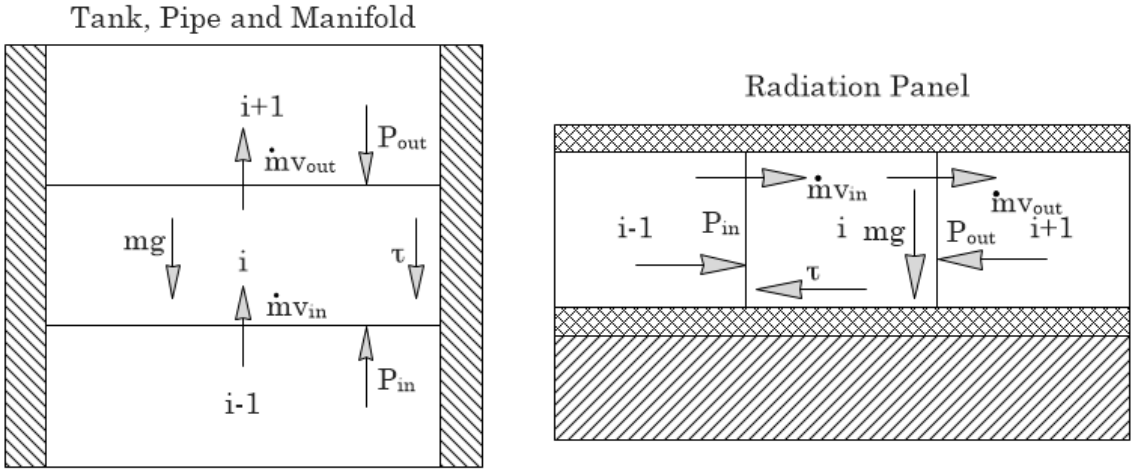

Figure 5.6 Diagram indicating the forces acting in on the unique i th control volume

5.2 Hot Water and the Convector Cycle

Two more cycles need to be modelled, a convector cycle and a heating cycle. The two models are modelled separately, the important cycle being the convector cycle, requiring the model to predict the room and convector's behaviour, while the hot water cycle predicts the temperature of the hot water tank. The hot cycle as presented in Figure 5.7 could be solved by the same procedure described in Section 5.1.

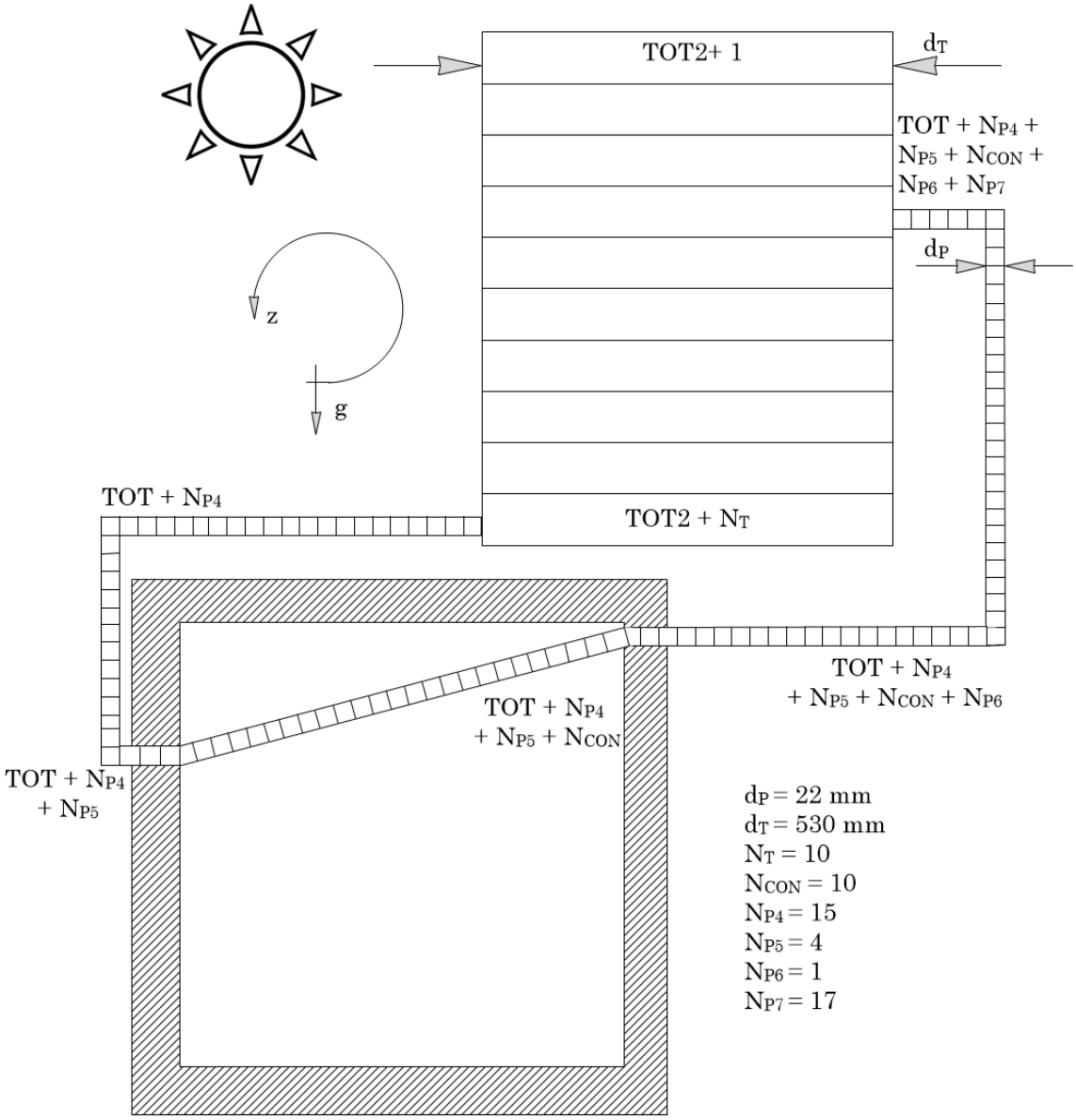

Figure 5.7 Discretized loop for day cycle operation

5.2.1 Room

The experimental room is subjected to a solar load causing the temperature inside the room to increase. The effects of the solar load are removed by means of the cooling water flowing through a convector situated inside the room. The convector absorbs energy from the room causing a decrease in temperature. A small portion of the heat is lost to the environment and not removed by the convector.

The solar load is affected by the thermal capacity of the room, solar irradiation,

the position of the sun and and the outside weather conditions. As the position of the sun changes, the solar load varies due to the change in aperture area of the room. For instance at sunrise the western side has no solar load, but as the day progresses this load changes causing the eastern side to have no load while the western side is subjected to a solar load.

To calculate the aperture area the sun's position at any point in time needs to be known. The position of the sun is affected by the day, time of day and location of experiment. The position of the sun is described by two angles namely the solar azimuth describing the sun's position measured clockwise from south and the zenith describing the angle of incidence on a horizontal surface, as indicated in Figure 5.8 (Stine and Geyer, 2001).

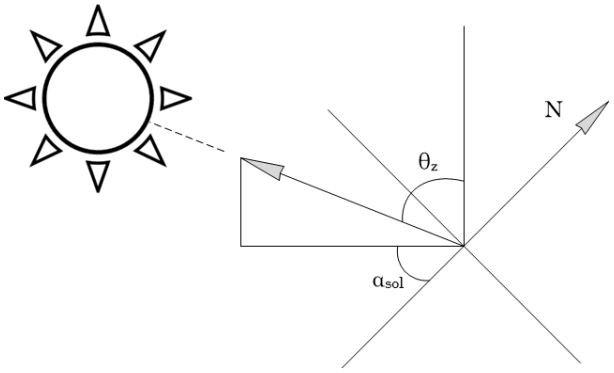

Figure 5.8 Diagram indicating solar zenith and azimuth angle

The solar azimuth is defined as

$$\alpha_{sol} = sign(\omega)|cos^{-1}(\frac{\cos\theta_z sin(\phi) - sin(\delta)}{sin(\theta_z)cos(\phi)})| \tag{5.2.1}$$

where ϕ is the latitude, ω the hour angle, θ_z the zenith angle and δ the declination. The hour angle is defined as $\omega = 15 - t_{sol} - 12$ where the solar time is

$t_{sol} = t + 4(Longitude - TimezoneLongitude) + EOT$

and the equation of time is

$EOT = 229.2(0.000075{+}0.001868cos(B){-}0.032077sin(B){-}0.014615cos(2B){-}0.04089sin(2B))$

and $B = \frac{(\text{day of year}-1)360}{365}$.

Finally the declination is given by

$\delta = 0.006918{-}0.399912cosB{+}0.070257sinB{-}0.006758cos2B{+}0.000907sin2B{-}0.002679cos3B + 0.00148sin3B$

The zenith angle can now be calculated using Equation 5.2.2

$$\theta_z = cos^{-1}(cos\phi cosBcos\omega + sin\phi sin\delta) \tag{5.2.2}$$

With the zenith and azimuth known, aperture area followed by solar the load on the room, can be estimated. The load can be calculated using $\dot{Q}_{sol} = \alpha I A$ where I is the direct solar radiation, A the aperture area and α the absorbency of the sheet metal.

$A = WH \cos\alpha_{sol} \cos\theta_z$

With the known solar load on the room the temperature of the room can be calculated with Equations 5.1.3 to 5.1.6. The steel is very thin and has a high conductivity. Therefore the outside and inside temperatures of the galvanized steel sheet are assumed to be equal. The room is also subjected to convection heat losses on the outside. The convection heat transfer coefficient is a function of wind speed, Loveday and Taki (1996) discuss numerous correlations of wind speed and heat transfer coefficients on building facades. For this specific case, a flat surface subjected to varying wind speeds the best correlation is

$h = 1.7v + 5.1$

where v is the wind speed. Difficulties with the calculation of room flow were encountered, it was then assumed that an equal amount of energy was removed from each level of the control volume. The energy removed was calculated with

$\dot{Q} = (T_{avg_{room}} - T)/R$ where $T_{avg_{room}}$ is the average room temperature, T the water temperature and R the total resistance of the convector

$R = R_{conv_W} + R_{cond} + R_{par}$ where $R_{par} = (1/R_{conv_A} + 1/R_{fin})^{-1}$

5.2.2 Convector

The convector removes the energy added to the room. The convector is situated in the top section of the room. Air flows through the convector, is cooled and finds its way to the bottom, allowing new hotter air to enter the convector, and in this way natural convective circulation is initiated. The physical dimensions describing the number of fins, fin thickness, fin pitch, number of pipes and pipe wall thickness of the convector can be found in Table 5.1.

Table 5.1 Convector dimensions and information

Description	Value	Unit
Fin Size (L x H)	0.135 x 0.065	m
Fin Thickness	1	mm
Number of fins per metre	160	-
Fin pitch	7	mm
Pipe Diameter OD	15	mm
Pipe Wall Thickness	0.7	mm
Number of pipes	7	-
Length of finned pipe	1	m

Figure 5.9 depicts the installed convector with a diagrammatic cross section. The dimensions of the diagrammatic cross section can be found in Table 5.1

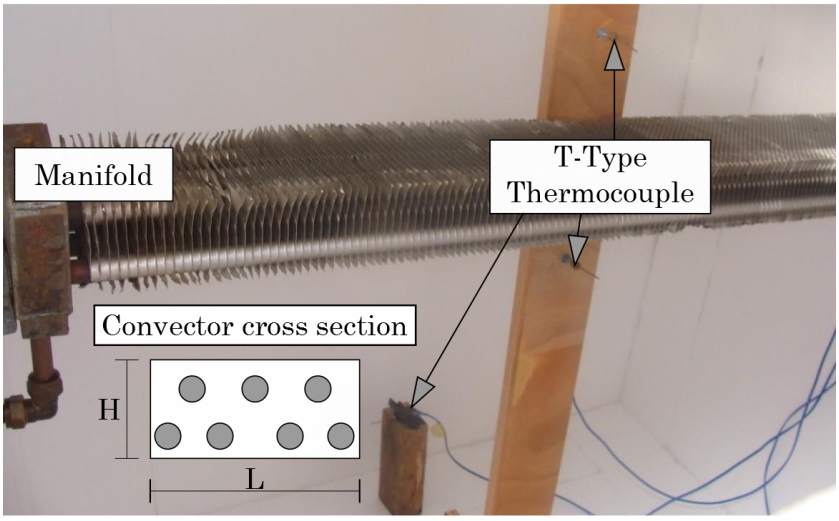

Figure 5.9 Picture of the installed convector with diagrammatic cross section

Figure 5.10 illustrates a diagrammatic side view of the convector. The diagram indicates the airflow and water flows with the convection and conduction resistances. The normal conduction resistance for a cylinder is used for the tubes, $R_{cond} = \ln(r_o/r_i)/2\pi Lk$. The convection resistances for the water and air side are calculated as follow $R_{conv} = 1/hA$, while the fin resistance adds a fin efficiency to the equation, $R_{fin} = 1/hA\eta$. It is necessary to calculate convection heat transfer coefficients for the water, base of tube and fins of the convector.

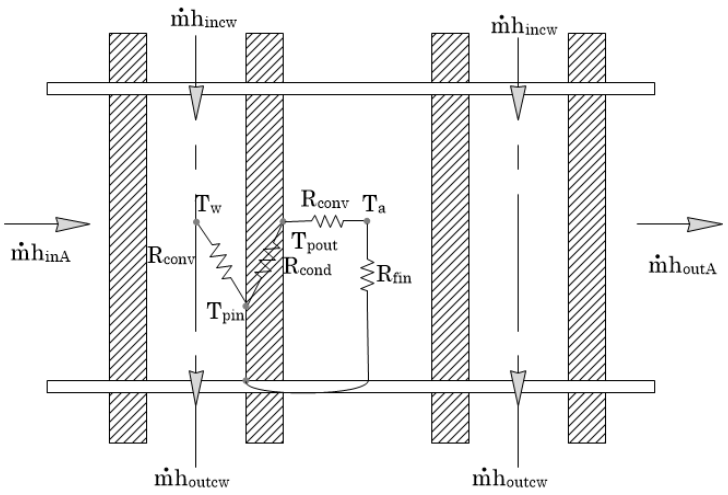

Figure 5.10 Side view of convector indicating air and water flows and conduction and convection resistances

The water heat transfer coefficient is calculated as done earlier in Section 5.1.2, while the fin heat transfer coefficient is calculated as described by Mills (2009).

$$h_{fin} = (1.07\Delta T/L_{fin})^{1/4} \text{ for } 10^4 < Gr < 10^9 \tag{5.2.3}$$

$$h_{fin} = 1.3\Delta T)^{1/3} \text{ for } 10^9 < Gr < 10^{12} \tag{5.2.4}$$

where $Gr = \dfrac{\beta \Delta T g \rho^2 L_{fin}^3}{\mu}$, and β the coefficient of volumetric expansion, ΔT the temperature difference between the fin surface and air, and L_{fin} the length of the fin along which natural convection takes place. It is assumed that the air acts as an ideal gas, therefore $\beta = 1/T$ with T in Kelvin.

The efficiency of the fin is calculated using a method described by Cengel and Ghajar (2011)

$$\eta = \frac{\tan mL_c}{mL_c} \tag{5.2.5}$$

where $L_c = L_{fin} + 0.5t_{fin}$ and $m = \sqrt{\dfrac{2h_{fin}}{k_{fin}t_{fin}}}$

The tube bank Nusselt number can be calculated using Mills (2009)

$$Nu = 0.36 + \frac{0.518Ra_D^{1/4}}{(1 + (0.559/Pr)^{9/16})^{4/9}} \quad \text{for} \quad 10^{-6} < Ra_D < 10^9 \tag{5.2.6}$$

$$Nu = \left(0.6 + 0.387\left(\frac{Ra_D}{(1+(0.559/Pr)^{9/16})^{16/9}}\right)^{1/6}\right)^2 \quad \text{for} \quad Ra_D > 10^9 \quad (5.2.7)$$

where $Ra_D = \dfrac{\beta \Delta T g \rho^2 D^3 Pr}{\mu}$, where D is the diameter of the tubes and Pr the Prandtl number of air. Flow occurs through a staggered arranged tube bank causing the direction and speed of flow to change. The change in fluid speed and direction cause the Nusselt number to change. To compensate for the change in the Nusselt number Mills (2009) suggests a correction factor

$\Phi = 1 + 2/3P_L$

where $P_L = S_L/D$ S_L is the distance between the rows of tubes and D is the diameter of the tubes. The corrected Nusselt number can now be calculated using the correction factor, Nusselt number and N number of tube rows. With the corrected Nusselt number known, the convection coefficient is calculated by $h = Nu_D k/D$, where Nu_D is calculated with Equation 5.2.8.

$$Nu_D = Nu\frac{1+(N-1)\Phi}{N} \quad (5.2.8)$$

5.2.3 Hot Water Cycle

To solve the hot water cycle the same procedure is followed as in Section 5.1. The hot water cycle consists of the radiator, hot-water tank and pipes. First the cycle is discretized as indicated in Figure 5.11. Then the conservation of mass, energy and momentum is applied to the control volumes.

Solar radiation is absorbed by the radiator and converted to thermal energy. The conversion of energy causes an increase in the radiator temperature, the thermal energy of the radiator is then transferred to the water by conduction and convection.

The amount of radiation converted to thermal energy is calculated by

$\dot{Q}_{in} = \alpha I A_a$

where α is the absorptivity of the radiator, I the direct solar radiation and A_a the aperture area. The aperture area is influenced by the sun's position and the tilt angle (θ_{tilt}) of the radiator. The aperture area is calculated by

$A_a = A\sin((90 - \alpha_{sol}) - \theta_{tilt})$

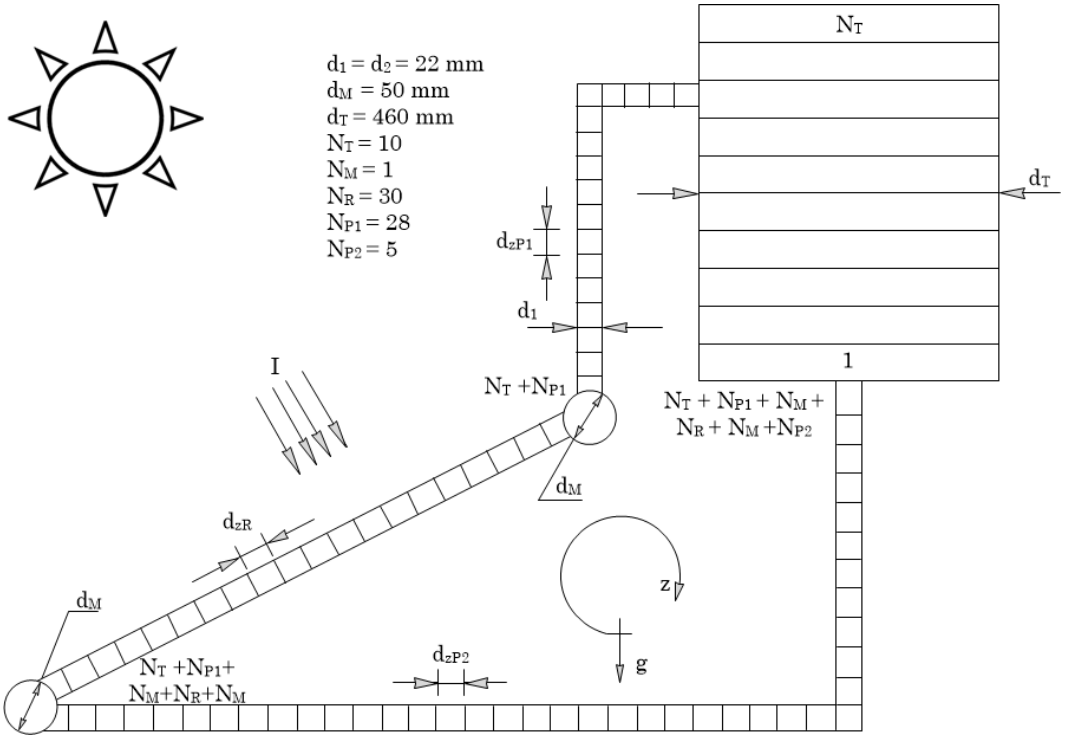

Figure 5.11 Discretized day cycle

5.3 Solution Algorithm

In this section the theoretical model algorithm used is described. The algorithm discretizes the system, and applies the conservation of mass, energy and momentum to these unique control volumes. These conservation equations are solved for each time step providing the user the predicted temperature and velocity. A logic flow structure illustrates the flow of the developed theoretical model programmed in Fortran. The logic flow diagram is followed by a more in depth layout of the program, describing the equations and programming procedure.

5.3.1 Logic Flow Diagram

The program uses Fortran as a coding language because Fortran was specifically designed for scientific and numerical computing and is very fast. The program starts by assigning geometric parameters, initial temperatures and fluid properties. Environmental information supplied by the university of Stellenbosch's weather station is read into the program.

The program enters a time loop, and depending on the time, either the convector or night cycle is solved. The cycles are solved by applying the conservation of mass, energy and momentum to the control volumes for each time step.

Every 30 seconds the desired information is printed to files and is used for further evaluation of the system.

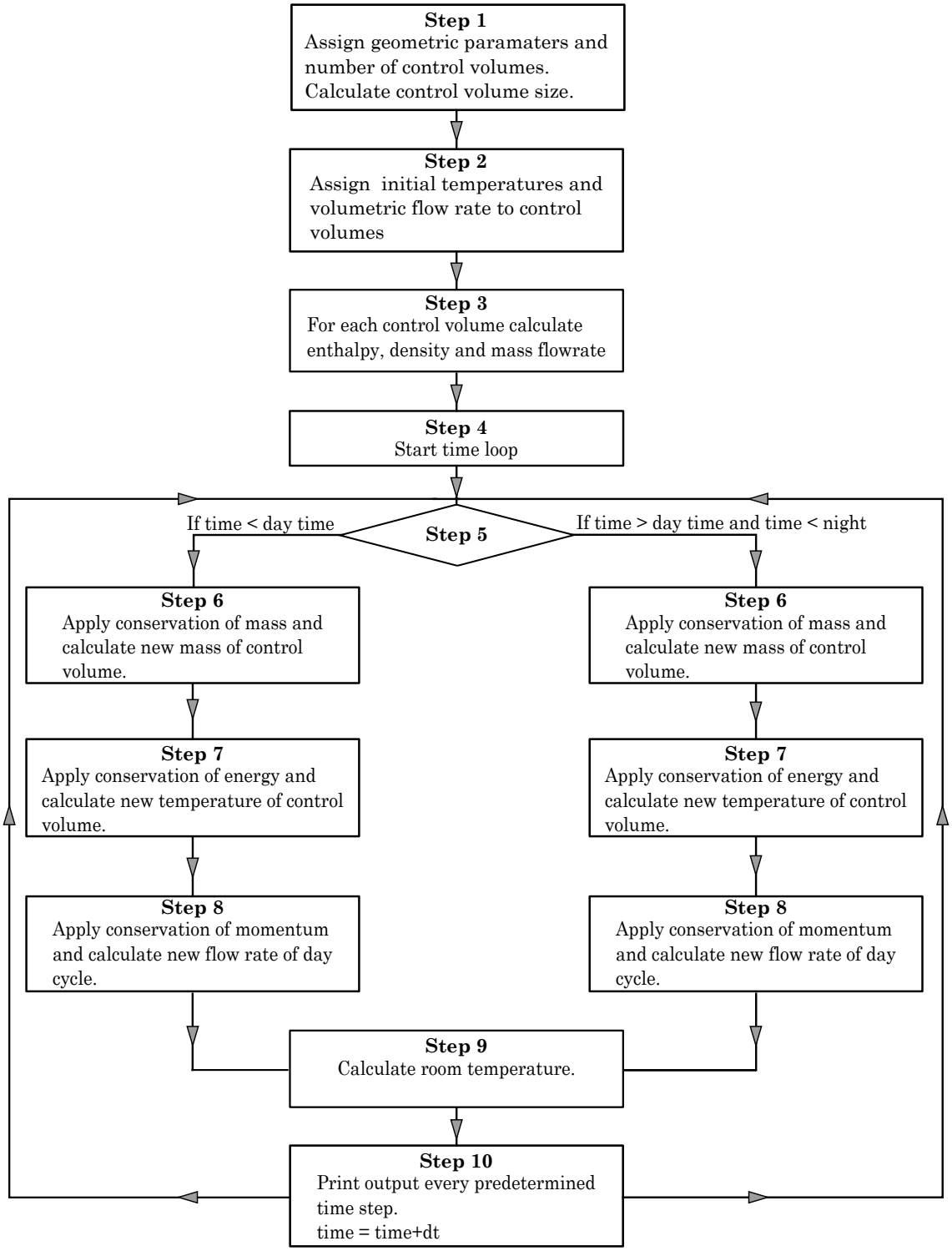

Figure 5.12 Logic flow chart

5.3.2 Main Program

An explicit numerical solution method is used to solve Equations 5.1.2 and 5.1.6, applied to the discretized control volumes of the night, day and convector cycles.

Input of geometrical and initial values. $T_{initial} = 15\ ℃,\ G = 10^{-6}\ m^3/s,$ $\Delta t = 0.01\ s,\ \sigma = 5.68e^{-8},\ g = 9.81\ m/s^2$

Table 5.2 Geometrical input values

	Length (m)	Diameter (m)	Thickness (m)	Number of Control Volumes	Theta (°)
Pipe 1	$L_{P1} = 0.21$	$D_P = 0.0163$	$t_P = 0.0022$	$N_{P1} = 02$	-90
Pipe 2	$L_{P2} = 0.20$	$D_P = 0.0163$	$t_P = 0.0022$	$N_{P2} = 02$	00
Pipe 3	$L_{P3} = 2.80$	$D_P = 0.0163$	$t_P = 0.0022$	$N_{P3} = 28$	04
Pipe 4	$L_{P4} = 1.50$	$D_P = 0.0163$	$t_P = 0.0022$	$N_{P4} = 15$	00
Pipe 5	$L_{P5} = 0.40$	$D_P = 0.0163$	$t_P = 0.0022$	$N_{P5} = 04$	90
Pipe 6	$L_{P6} = 0.10$	$D_P = 0.0163$	$t_P = 0.0022$	$N_{P6} = 01$	00
Pipe 7	$L_{P7} = 1.30$	$D_P = 0.0163$	$t_P = 0.0022$	$N_{P7} = 13$	-90
Pipe 8	$L_{P8} = 0.26$	$D_P = 0.0163$	$t_P = 0.0022$	$N_{P8} = 02$	00
Pipe 9	$L_{P9} = 0.21$	$D_P = 0.0163$	$t_P = 0.0022$	$N_{P9} = 02$	90
Tank	$L_T = 0.68$	$D_T = 0.560$	$t_T = 0.0040$	$N_T = 10$	90 or -90
Manifold	$L_M = 1.20$	$D_M = 0.0460$	$t_M = 0.0020$	$N_M = 01$	00
Radiator	$L_R = 3.00$	$D_R = 0.0055$	$t_R = 0.0005$	$N_R = 30$	05
Convector	$L_{CON} = 1.00$	$D_{CON} = 0.018$	$t_{CON} = 0.001$	$N_{CON} = 10$	05

$N_{TOT} = N_T + N_{P1} + N_M + N_R + N_M + N_{P2}$
$N_{TOT2} = N_{TOT} + N_{P3} + N_{P4} + N_{P5} + N_{CON}$
Calculate length of each control volume. dz=l/N
Input of material properties

Table 5.3 Material properties input values

	Specific Heat (J/kgK)	Thermal Conductivity (J/kgK)	Density (kg/m^3)	Emissivity	Absorbtivity
Tank	$c_{pT} = 1670$	$k_T = 0.20$	$\rho_T = 942$	$\epsilon_T = 0.80$	$\alpha_T = 0.20$
Pipe	$c_{pP} = 2300$	$k_P = 0.45$	$\rho_P = 942$	$\epsilon_P = 0.80$	$\alpha_P = 0.20$
Radiator	$c_{pR} = 1925$	$k_R = 0.12$	$\rho_R = 910$	$\epsilon_R = 0.99$	$\alpha_R = 0.75$
Manifold	$c_{pM} = 1925$	$k_M = 0.12$	$\rho_M = 910$	$\epsilon_M = 0.80$	$\alpha_M = 0.75$
Insulation	$c_{pIns} = 1200$	$k_{Ins} = 0.04$	$\rho_{Ins} = 16$	$\epsilon_{Ins} = 0.50$	$\alpha_R = 0.20$

Calculate mass of various materials in control volumes with geometrical and material properties.

do i=1,N_{TOT}
Assign initial temperature, volume, diameter,cross-sectional area,perimeter area, length, thickness and emissivity to each control volume
Calculate ρ *and* $\dot{m}$ *for each control volume using initial conditions.*
Where $\rho_i = -0.004T_i^2 - 0.05877T_i + 1000.482$,
$\dot{m}_i = G\rho_i$
end do

5.3.2.1 Night and Convector

Start with night cycle procedure
Start time cycle
$t_{endNIGHT} = (15)(3600)/\Delta t$

do j = 1, $t_{endNIGHT}$
$t = t + \Delta t$
Reset momentum terms.
$C_1 = 0, C_2 = 0, M_{in} = 0, M_{out} = 0, D_{Mass} = 0, F = 0$

Start with night cycle.
do i = 1, N_{TOT}
Calculate density, $\rho_i = -0.004T_i^2 - 0.05877T_i + 1000.482$.
Calculate mass, $m_i = \rho_i V_i$.
Calculate mass flow rate, $\dot{m}_i = G\rho_i$.
Calculate enthalpy, $h_i = 4.182e^3T_i - 1.52e^2$.
Assign values to $\dot{m}_{in/out}$, $h_{in/out}$ *and* $\rho_{in/out}$ *using upwind differencing*
$\dot{m}_{out} = \dot{m}_i$, $h_{out} = h_i$ *and* $\rho_{out} = \rho_i$

if (G >= 0) then
then $\dot{m}_{in} = \dot{m}_{i-1}$, $h_{in} = h_{i-1}$ and $\rho_{in} = \rho_{i-1}$
else $\dot{m}_{in} = \dot{m}_{i+1}$, $h_{in} = h_{i+1}$ and $\rho_{in} = \rho_{i+1}$

Applying the conservation of mass, calculate new control volume mass.
$m_i^{t+\Delta t} = m_i^t + \Delta t(\dot{m}_{in} - \dot{m}_{out})$

Calculate thermal conductivity of water k_w,
where $k_w = -9.485e^{-6}T^2 + 0.002T + 0.560$
Calculate radiation, convection and conduction resistance value of each control volume, where $R_{rad} = 1/A\epsilon\sigma(T_s^2 + T_\infty^2)(T_s + T_\infty)$, $R_{conv} = 1/hA$ *and* $R_{cond} = l/kA$.
Applying the conservation of energy, calculate new temperatures
$T_i^{t+\Delta t} = \frac{(m_i c_{p_i} T_i)^t}{(m_i c_{p_i})^{t+\Delta t}} + \frac{\Delta t}{(m_i c_{p_i})^{t+\Delta t}}(\dot{m}_{in}h_{in} - \dot{m}_{out}h_{out} + \dot{Q}_{in} - \dot{Q}_{out})$

Calculate the dynamic viscosity of water.
$\mu = -3.014e^{-9}T^3 + 3.261e^{-7}T^2 - 4.818e^{-5}T + 1.756e^{-3}$
Calculate the Reynolds number and shear stress. $Re = \rho V D_h/\mu = 4\rho|G|/D\mu$

if Re < 1 then $C_f = 16$
if $1 <=$ Re & Re $<= 1181$ then $C_f = 16/Re$
if Re > 1181 then $C_f = 0.079Re^{-0.25}$
$\tau = C_f G^2 \rho/2Ax_i$

Calculate ρ *of buoyancy term.* $\rho_b = \rho_{ref} - \beta_{ref}(T_i - T_{ref})$

Calculate the sum of the buoyancy terms.
$B = \sum_1^{N_{TOT}}(\rho_b g \Delta z Sin(\theta))$
Where $\theta < 0$ *for gravity acting against flow and* $\theta > 0$ *for gravity acting in flow direction.*

Calculate the sum of the momentum flux difference terms.
$M = \sum_1^{N_{TOT}}((\rho_{in} - \rho_{out})G^2/Ax_i^2)$

Calculate the sum of the friction terms.
$F = \sum_1^{N_{TOT}}(\tau\pi D_i(\Delta z_i + \Delta z_{minor})/Ax_i)$

Calculate the new volumetric flow rate of the night cycle.
$G^{t+\Delta t} = \sum_1^{N_{TOT}} \frac{G^t \rho_i^t \Delta z}{\rho_i^{t+\Delta t}\Delta z} + \Delta t \frac{M+B-F}{\sum_1^{N_{TOT}} \rho_i^{t+\Delta t}\Delta z/Ax_i}$

Set old control volume temperatures and night cycle volumetric flow rates equal to new values.
$T^t = T^{t+\Delta t}$ and $G^t = G^{t+\Delta t}$

Stop if $t = t_{endDAY}$

Start with the convector cycle procedure
$t_{endDAY} = (9)(3600)/\Delta t$

Follow the same procedure as the day cycle, except
do i $= (N_{TOT} + 1), (N_{TOT2} + N_T)$
where $T_{(N_{TOT2}+1)} = T_1, T_{(N_{TOT2}+2)} = T_2, T_{(N_{TOT2}+3)} = T_3,$ *etc.*

5.3.2.2 Room

Define geometrical values
H = 1.3 m, $W_N = W_S = W_E = W_W$ =1.2 m, N_{Room} = 10, t_{steel} = 0.001 m, t_{Ins} = 0.023 m

Material properties input

Table 5.4 Material properties input values

	Specific Heat (J/kg K)	Thermal Conductivity (W/m K)	Density (kg/m^3)	Thickness (m)
Air	$c_{p_A} = 1006$	$k_A = 0.5$	$\rho_A = 1.2$	$t_A = 0.0040$
Steel	$c_{p_{Steel}} = 502$	$k_{Steel} = 45.3$	$\rho_{Steel} = 7833$	$t_{Steel} = 0.001$
Insulation	$c_{p_{Ins}} = 1200$	$k_{Ins} = 0.04$	$\rho_{Ins} = 16$	$t_{Ins} = 0.023$

Location coordinate input
Latitude = -28.4°, Longitude = 18.85°, TimezoneLONG = 30°
Insert day, decimal time and solar irradiation at time of calculation.

Calculate mass, $m = \rho * V$ *where* $V = H * W * t$

Call angles and areas, two subroutines which calculate the angle of the sun and the area influenced by the sun.

Assign initial steel and insulation temperatures and calculate enthalpy of air
$h_i = f(T_i) = 1.726e^{-1}T^4 - 19.024T^3 + 746.826T^2 - 6.845e^{-3}T + 24391.87$

Start calculations
do i =1, N_{Room}

Calculate radiation, convection and conduction resistances respectively as done in previous section.

if (i = N_{Room}) then

Calculate new steel temperatures:
$T_{Steel}^{t+\Delta t} = T_{Steel}^{t} + \frac{\Delta t}{(mc_p)^{t+\Delta t}}(\dot{Q}_{in} - \dot{Q}_{out})$
where $\dot{Q}_{out} = (T_{Steel} - T_{Ins})/R_{cond}$ and $\dot{Q}_{in} = IA\alpha + (T_{Steel} - T_{Sky})/R_{par}$
and $R_{par} = (1/R_{con]} + 1/R_{rad})^{-1}$

Followed by the new insulation temperatures
$T_{Ins}^{t+\Delta t} = T_{Ins}^{t} + \frac{\Delta t}{(mc_p)^{t+\Delta t}}(\dot{Q}_{in} - \dot{Q}_{out})$

where $\dot{Q}_{in} = (T_{Steel} - T_{Ins})/R_{cond}$ and $\dot{Q}_{out} = (T_{Ins} - T_i)/R_{cond}$

Calculate new air temperature of control volume.

$T_i^{t+\Delta t} = \frac{(m_i c_{p_i} T_i)^t}{(m_i c_{p_i})^{t+\Delta t}} + \frac{\Delta t}{(m_i c_{p_i})^{t+\Delta t}}(\dot{m}_{in} h_{in} - \dot{m}_{out} h_{out} + \dot{Q}_{in} - \dot{Q}_{out})$

5.3.2.3 Solar Angles and Solar Load

Receive month, day, time, latitude longitude and timezone longitude.

Start calculating sun angles.

Calculate day of the year (DOY) followed by β *where* $\beta = (DOY - 1)365/360$

Calculate the equation of time (EOT), solar time (t_s) *and the hour angle* (ω).
$EOT = 229.2\frac{7.5e^{-5}+1.868e^{-3}cos(\beta)-3.208e^{-2}sin(\beta)-1.462e^{-2}cos(2\beta)-4.089e^{-2}sin(2\beta)}{60}$
$t_s = t + 4(Longitude - TimezoneLONG)/60 + EOT$
$\omega = 15(t_s - 12)$

Calculate the sun angles, declination (δ), *zenith* (θ_z) *and solar azimuth* (α_s).
$\delta = 6.918e^{-3} - 3.999e^{-1}cos(\beta) + 7.026e^{-2}sin(\beta) - 6.758e^{-3}cos(2\beta) + 9.070e^{-4}sin(2\beta) - 2.679e^{-3}cos(3\beta) + 1.480e^{-3}sin(3\beta)$
$\theta_z = acos(cos(Latitude)cos(\delta)cos(\omega) + sin(Latitude)sin(\delta))$
$\alpha_s = sign(\omega)|acos(cos(Zenith)sin(Latitude) - sin(\delta)/sin(\theta_z)cos(latitude))|$

Return solar azimuth and zenith.

End of angle calculation.

Receive room dimensions, solar azimuth, zenith and irradiance.

Start calculating solar loads.

Calculate irradiance areas.
New height, $H = H\cos\theta_)$
Calculate irradiance areas.
if $\alpha_s < 90$ then
$A_N = 0$, $A_E = 0$
$\theta = \alpha_s$, $W_S = W_S\cos\theta$ and $A_S = HW_S$
$\theta = 90 - \alpha_s$, $W_W = W_W\cos\theta$ and $A_W = HW_W$
$A_T = W_S W_W\cos\theta_z$

if $\alpha_s == 90$ then
$A_N = 0$, $A_E = 0$, $A_S = 0$
$\theta = 90 - \alpha_s$, $W_W = W_W \cos\theta$ and $A_W = HW_W$
$A_T = W_S W_W \cos\theta_z$

if $\alpha_s > 90$ & $\alpha_s < 180$ then
$A_E = 0$, $A_S = 0$
$\theta = 180 - \alpha_s$, $W_N = W_N \cos\theta$ and $A_N = HW_N$
$\theta = 90 - \alpha_s$, $W_W = W_W \cos\theta$ and $A_W = HW_W$
$A_T = W_N W_W \cos\theta_z$

if $\alpha_s == 180$ then
$A_E = 0$, $A_S = 0$, $A_W = 0$
$\theta = 180 - \alpha_s$, $W_N = W_N \cos\theta$ and $A_N = HW_N$
$A_T = W_N W_W \cos\theta_z$

if $\alpha_s > 180$ & $\alpha_s < 270$ then
$A_S = 0$, $A_W = 0$
$\theta = 180 - \alpha_s$, $W_N = W_N \cos\theta$ and $A_N = HW_N$
$\theta = \alpha_s - 270$, $W_E = W_E \cos\theta$ and $A_N = HW_E$
$A_T = W_N W_E \cos\theta_z$

if $\alpha_s == 270$ then
$A_N = 0$, $A_S = 0$, $A_W = 0$
$\theta = \alpha_s - 270$, $W_E = W_E \cos\theta$ and $A_N = HW_E$
$A_T = W_N W_E \cos\theta_z$

if $\alpha_s > 270$ & $\alpha_s < 360$ then
$A_N = 0$, $A_W = 0$
$\theta = \alpha_s - 270$, $W_E = W_E \cos\theta$ and $A_N = HW_E$
$\theta = \alpha_s$, $W_S = W_S \cos\theta$ and $A_S = HW_S$
$A_T = W_S W_E \cos\theta_z$

if $\alpha_s == 0$ or $\alpha_s == 360$ then
$A_N = 0$, $A_E = 0$, $A_W = 0$
$\theta = \alpha_s$, $W_S = W_S \cos\theta$ and $A_S = HW_S$
$A_T = W_S W_E \cos\theta_z$

Now calculate solar load
$\dot{Q}_{Nin} = IA_N$, $\dot{Q}_{Sin} = IA_S$, $\dot{Q}_{Ein} = IA_E$, $\dot{Q}_{Ein} = IA_W$, $\dot{Q}_{Tin} = IA_T$

Return solar loads.

End of solar load calculation.

5.3.3 Tank Variable Inlet Model

In order to create an accurate model of the tank, a variable inlet model is used. This model only affects the energy equation, thus affecting the temperature. The hot water tank and convector cycle both have an outlet at the bottom and an inlet at the top. Hot water enters the tank from the top; if the water entering the tank is warmer than the top layer it rests at the top layer displacing all the other layers downward. If the water entering the tank is colder than the top layer, it travels down the tank without disturbing the layers it travels trough. The water entering the tank finds a level with temperature equal to or greater than itself and displaces the layers beneath it downward.

The concept explained above is implemented in the program as described below. The night cycle uses the same principal except water enters from the bottom and displaces the layers to the top.

Convector Cycle Tank

do $i = 1, N_t$

$h_{out} = 4182T_i - 152$
if $(G > 0)$ then
$h_{in} = 4182T_{i-1} - 152$
else
if $(i == N_T)$ then
$h_{in} = 4182T_1 - 152$
else
$h_{in} = 4182T_{i+1} - 152$
end if
end if

$\dot{m} = G\rho$

if $(T_{in} >= T_1)$then
$\dot{m}h_{in_i} = \dot{m}\big(4182T_{in} - 152\big)$
$\dot{m}h_{out_i} = \dot{m}h_{out}$
else

if $(T_{in} <= T_i)$then
q=i
end if

do $n = 1, N_T$
if $(n < q)$ then
$\dot{m}h_{in_i} = 0$
$\dot{m}h_{in_i} = 0$
end if

if $(n = q)$ then
$\dot{m}h_{in_i} = \dot{m}\big(4182T_{in} - 152\big)$
$\dot{m}h_{out_i} = \dot{m}h_{out}$
end if

if $(n >= q)$ then
$\dot{m}h_{in_i} = \dot{m}h_{in}$
$\dot{m}h_{in_i} = \dot{m}h_{out}$
end if

end do
end if

Applying the conservation of energy calculate new temperatures of the tank control volumes.
$T_i^{t+\Delta t} = \frac{(m_i c_{p_i} T_i)^t}{(m_i c_{p_i})^{t+\Delta t}} + \frac{\Delta t}{(m_i c_{p_i})^{t+\Delta t}}(\dot{m}h_{in_i} - \dot{m}h_{out_i} + \dot{Q}_{in} - \dot{Q}_{out})$

6 Results

In this chapter results obtained experimentally and theoretically will be presented and discussed. Data provided by the weather station of the University of Stellenbosch was used to theoretically simulate the system (Stellenbosch-weather, 2014). The theoretical and experimental results are compared to prove the validity and accuracy of the theoretical model. Figure 6.1 depicts the experimental set-up, the solar panel, room and control, all facing north.

The experiment was carried out over an extended period in April 2014. The weather conditions during this period varied from clear to cloudy skies, with most days enjoying sunny sumer weather. For winter conditions the experiment was carried out only on the night cycle, this experiment took place during clear sky conditions in June and is presented in Section 6.4.

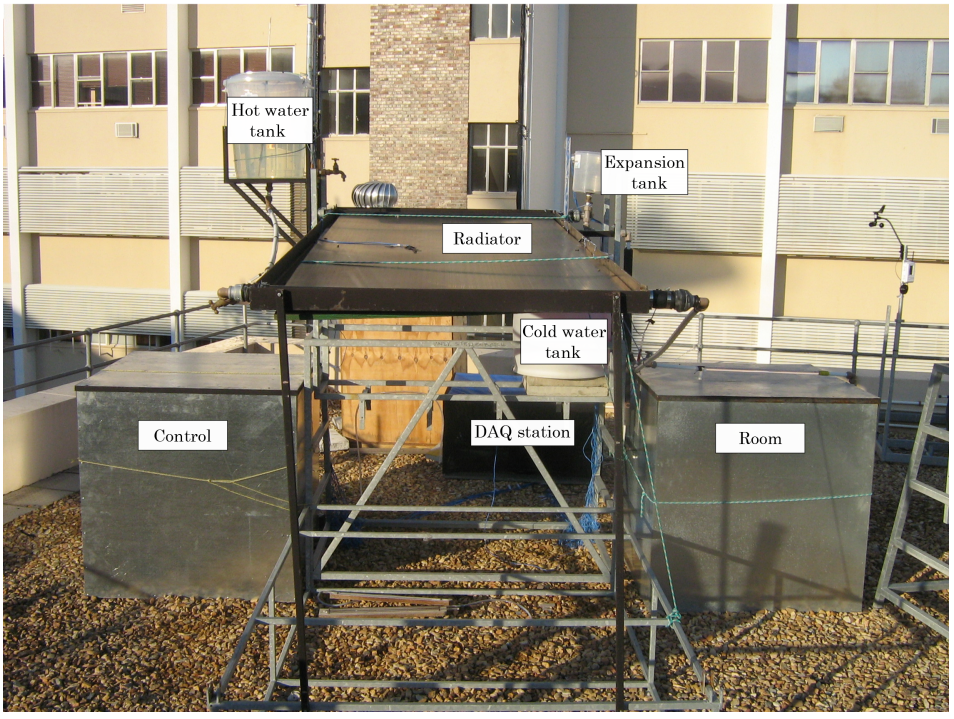

Figure 6.1 Experimental night-sky radiation system facing north

6.1 Cold Water Tank

Five equally spaced thermocouples measured the temperatures in the 150 l cold water tank. The temperatures of the thermocouples are presented in Figure 6.2. This representation of the temperatures illustrates the stratification of the cold water tank, the hottest layer being at the top and the coldest layer at the bottom. The presence of stratification indicates that the inlet and outlet were correctly chosen to minimize de-stratification by eliminating or reducing plume formation. Since the thermocouples are equally spaced the mathematical average of the tank is a good representation of the average tank temperature.

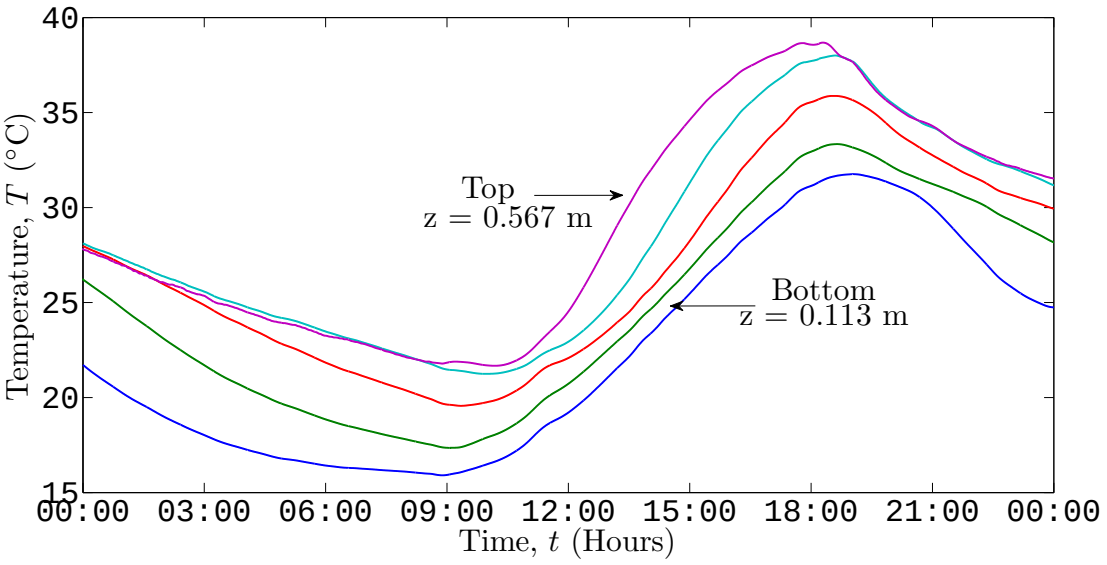

Figure 6.2 Temperature profile of the water in the cold water tank as a function of time illustrating temperature stratification

The theoretical model consists of 10 equally sized control volumes, as in the experiment, a mathematical average would also be a good representation of the tank temperatures. These averages can be compared to indicate the validity of the theoretical model. Figure 6.3 represents the comparison of the theoretical model with the results obtained experimentally.

The temperature of the tank as illustrated in Figure 6.3, varies from a minimum of 20 °C to a maximum of 35 °C. The theoretical model is a good representation of the experimental results, since it imitates the behaviour of the experiment. The minimum and maximum of the theoretical model vary with a maximum of 2 °C. The low predicted tank temperature of the morning of the 10^{th} of April is ascribed to the presence of clouds during the night. The model does

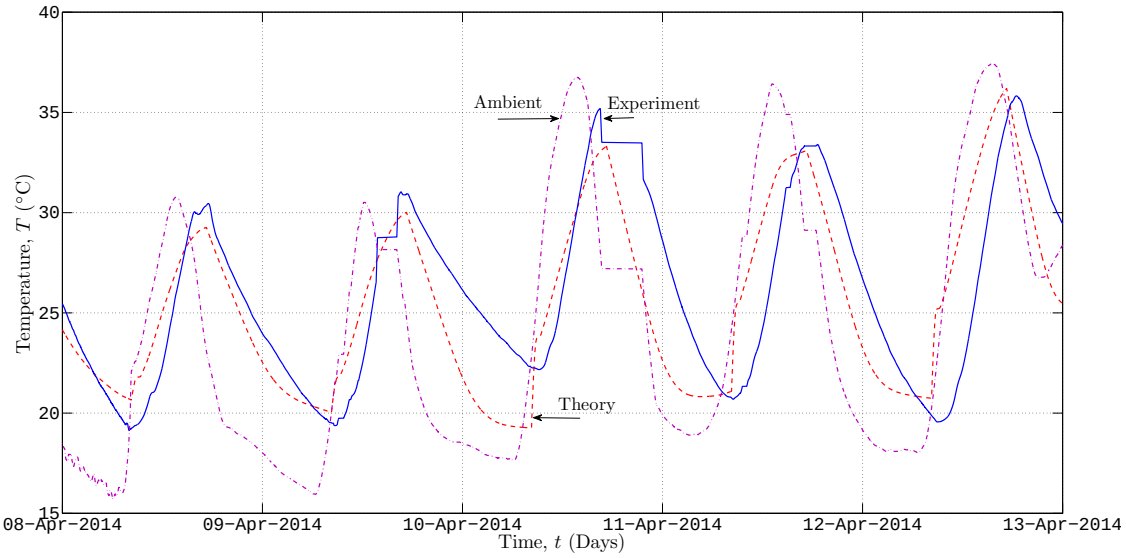

Figure 6.3 Comparison between the theoretical and experimental water temperatures in the cold water tank

not take the effect of clouds into account, therefore the theoretical model over predicts the system's cooling performance.

The rate of energy dissipated and absorbed by the water in the cold water tank during the day and night can be calculated with

$$\dot{Q} = mc_p(T_{start} - T_{end})/(\Delta t)$$

where $m = \rho_{avg}V$ and ρ_{avg} are equal to the density at the average of start and end temperatures. With the measured data and the method described the rate of energy absorbed from the room and the rate of energy dissipated by the radiator can be calculated. The same method is used for the theoretical model, the values calculated are presented in Table 6.1.

The heat removal rates are affected by the weather conditions and vary from 39 W/m^2 to 75 W/m^2. The heat removed by the system corresponds to heat removable rates of 60 W/m^2 recorded by Dobson (2005) and Okoronkwo *et al.* (2014). The theoretical model closely predicts the heat removal rates of the experiment. The difference in heat removal rates can be ascribed to the inability of the theoretical model to predict accurately the water temperature.

Table 6.1 Daily rate of energy absorbed and dissipated in cold water tank

April	Experiment			Theory		
	$\dot{Q}_{dissipated}$ (W)	W/m^2	$\dot{Q}_{absorb}$ (W)	$\dot{Q}_{dissipated}$ (W)	W/m^2	$\dot{Q}_{absorb}$ (W)
7	196.46	54.57		150.72	41.87	
			192.33			95.98
8	208.44	57.90		166.79	46.33	
			211.51			200.75
9	142.41	39.56		194.21	53.95	
			219.87			234.09
10	208.52	57.92		233.18	64.77	
			244.58			349.67
11	273.01	75.92		236.63	65.73	
			237.42			306.40
12	163.80	45.50		205.62	57.12	
			282.64			405.29

The energy removed from the air in the room by the convector is absorbed by the water in the tank. This rate at which energy is removed by the convector can be converted to watts removed per cubic meter (W/m^3) of air. The values for the experiment varied from a minimum of 102 W/m^3 to a maximum of 150 W/m^3. A building of 6 m x 8 m x 2.5 m with the long wall facing east was considered. Calculations shown in Appendix B suggest that the building requires an average cooling rate of 22.71 W/m^3. When comparing these results it appears that the system is capable of delivering sufficient cooling when the sizing of the system is done correctly.

6.2 Room

The room consists of a mild steel frame covered with galvanized sheet metal and insulated with polystyrene. The room has six thermocouples, four placed in the middle at different heights, one above and below the radiator, the other lower, with the lowest at the same height as two thermocouples at the eastern and western side of the room.

An average of the bottom three thermocouples and top two represents the temperature of the top and bottom sections. The mathematical average of the calculated averages and the measured temperature represents the room's average temperature.

The control has five installed thermocouples; three in the middle at different heights with the lowest being the same height as the thermocouples at the eastern and western side. An average temperature of the room is calculated using an average of the bottom three measurements and the top two. Figure 6.4 represents the comparison of the the room with the control.

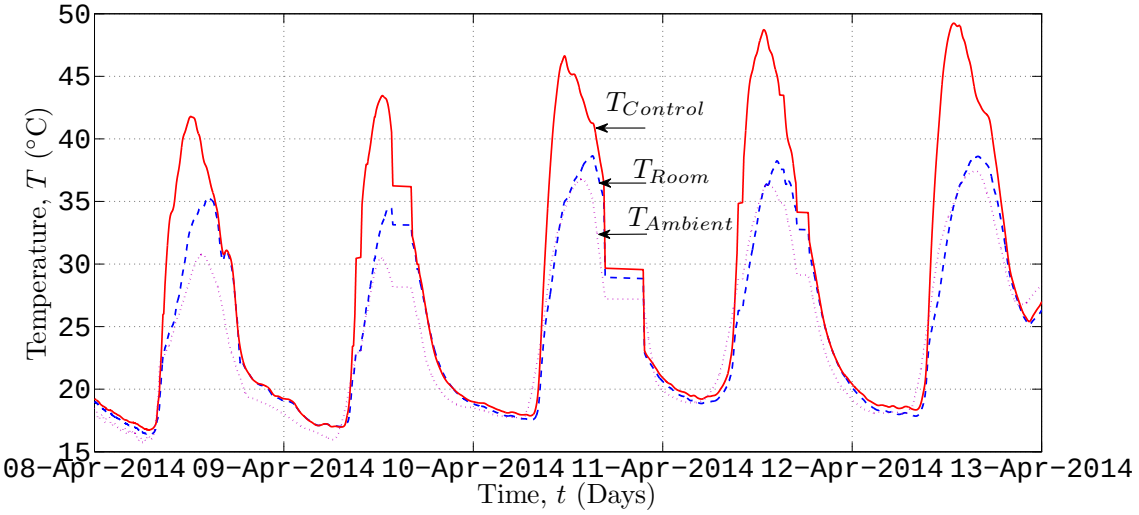

Figure 6.4 Comparison of the measured room and control temperatures

Figure 6.4 indicates the difference between the temperature of the room and the control during the day. The room temperatures vary from a minimum of 16 °C to a maximum of 38 °C. The control also has a minimum of 16 °C and a maximum of 49 °C. To validate the theoretical model the measured room temperature is compared to the theoretically calculated temperatures.

Consider Figure 6.5; this figure shows the comparison between the theoretically calculated room temperature and experimentally measured room temperature. The comparison proves that the theoretical model is a good approximation of the experiment. The temperature profile of the theory follows the temperature profile of the experiment with a maximum deviation of 4 °C at the peaks. The deviation is ascribed to the placement of the room. During experimentation adjacent structures throw shadows on the room, the theoretical model does not take the effect of these shadows into account.

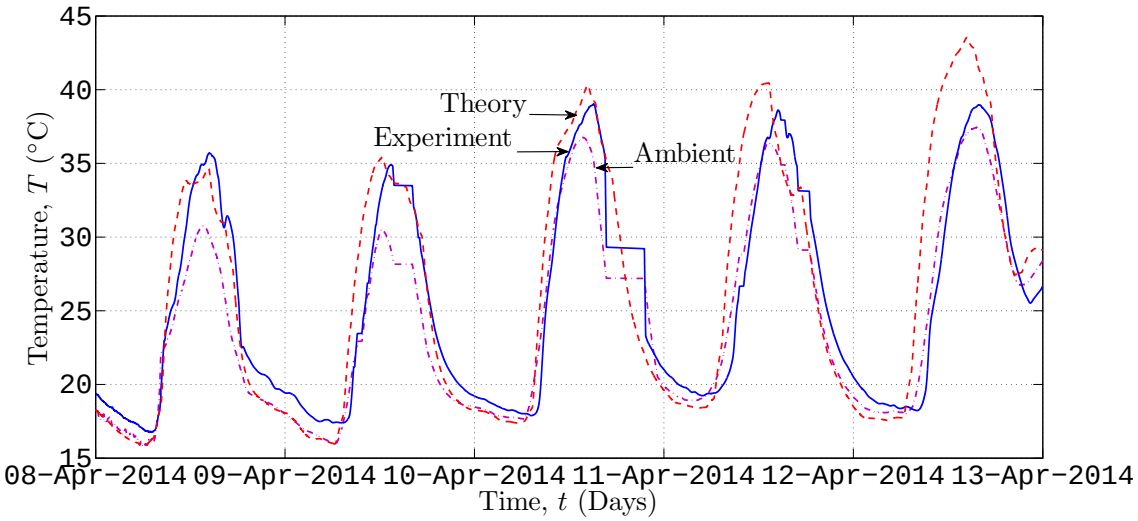

Figure 6.5 Comparison of the measured room and theoretically calculated temperatures

The energy in the room during day above 20 °C is calculated with

$$Q = mc_p(T - T_{ref})$$

where T_{ref} is the reference temperature $T_{ref} = 20$ °C. When comparing the energy in the room and the control, a cooling efficiency can be calculated, $\eta_{cooling} = 1 - Q_{room}/Q_{control}$. The efficiencies for the experiment and theory are presented in Table 6.2. The heat removal efficiency varies from 0.162 to 0.422, the theory has a lower efficiency than the experimentation. The difference can be ascribed to the higher predicted room temperature of the theoretical model.

Table 6.2 Experimental and theoretical cooling efficiency as defined

April	Experiment	Theory
	$\eta_{cooling}$	$\eta_{cooling}$
7	0.162	0.170
8	0.322	0.235
9	0.422	0.239
10	0.301	0.223
11	0.364	0.193
12	0.381	0.218

6.3 Hot Water Tank

Five equally spaced thermocouples measured the water temperature of the 68 l hot water tank. Low flow rates and, as described in Section 3.3, the strategically placed inlet and outlet, caused water in the tank to be stratified. Consider Figure 6.6, stratification is visible with the temperature difference measured at different heights in the tank. The lowest temperature is at the bottom of the tank, and the highest at the top. The temperatures vary from 2 °C to 10 °C. The system during its best performance, heated the water from 24 °C to 62 °C per 8 hour period.

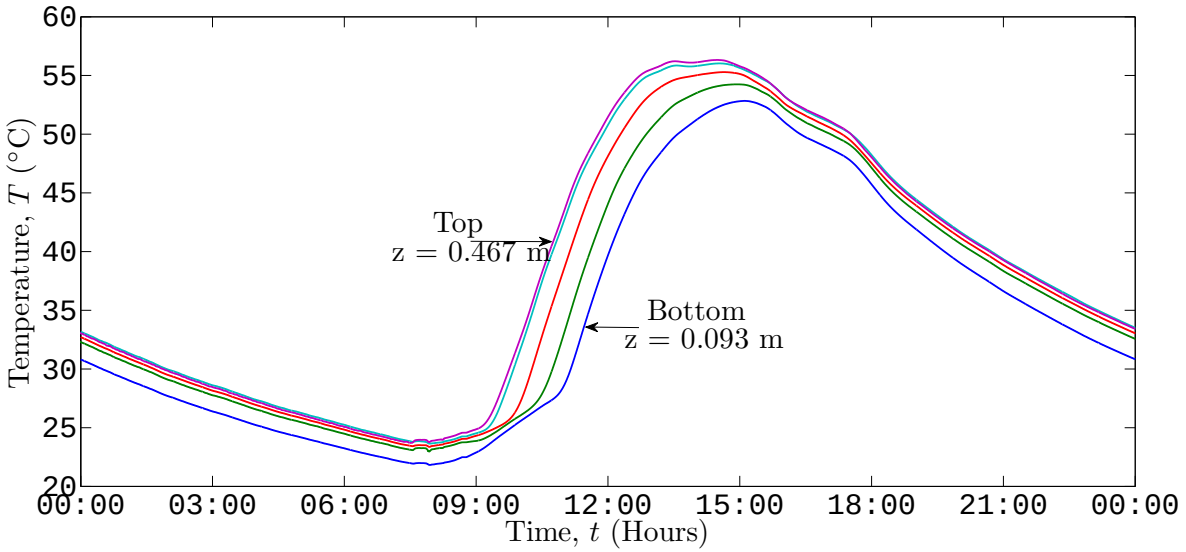

Figure 6.6 Temperature profile in the hot water tank as a function of time illustrating temperature stratification

The procedure followed to calculate the average temperature of the water in the cold water tank is the same as the calculation of the hot water tank's temperature. The comparison of the calculated averages, measured and predicted, are presented in Figure 6.7. The theoretically calculated values correlate closely with the experimentally determined values. The theoretical model predicts only the heating cycle and not the cooling of the tank, which occurs after sunset. It was assumed that the tank temperature would be equal to the ambient temperature of the next morning. Temperature differences between the theory and the experiment at the peaks vary from as little as 0 °C to 5 °C, suggesting that the assumption of the water temperature being equal to the ambient temperature the next morning, is reasonable.

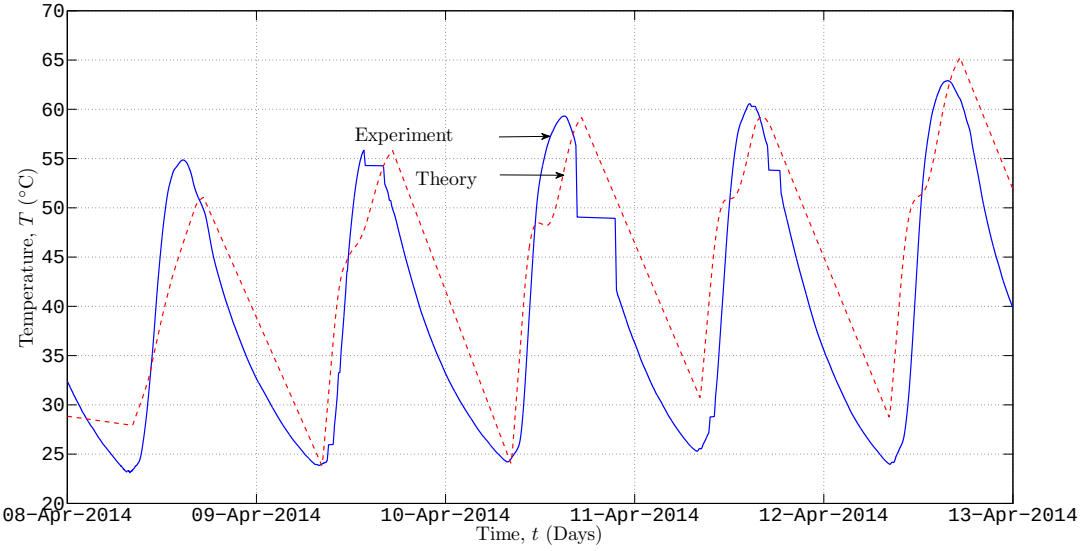

Figure 6.7 Comparison of the measured and theoretically calculated hot water temperatures as a function of time

The energy storing rate of the heating cycle can be calculated by

$$\dot{Q} = mc_p(T_{end} - T_{start})/\Delta t$$

where m is the mass of the water in the tank, $m = \rho_{avg}V$ and ρ_{avg} is the density at the average temperature between the end (maximum temperature reached) and the start of the day (minimum temperature). Δt is the time elapsed between the start temperature and end temperature measurements. With the method described the energy collecting rate as presented in Table 6.3 can be calculated using the relevant measurements.

Table 6.3 Hot water tank temperatures and energy collecting rate

April	T_{start} (°C)	T_{end} (°C)	Δ t (s)	$\dot{Q}_{collected}$ (W)
7	27.41	48.50	25890	230.356
8	23.31	54.75	25860	343.672
9	23.88	55.61	20000	448.352
10	24.38	59.31	24600	400.964
11	25.35	60.25	22500	437.851
12	24.15	62.74	26100	417.263
13	28.99	54.76	21700	335.345
14	25.82	42.79	17000	282.629

The energy collected during the day cycle varies from a minimum of 230 W to a maximum of 448 W. Consider a 100 l water tank at 10 °C over a period of

9 hours. The system is capable of increasing the water temperature by 35 °C to 45 °C. The radiator serves as a satisfactory solar collector considering the design of the collector. This is not a good design for a solar water heater because the tilt angle is too small and there is an absence of glazing for all year round use. The system can definitely serve as a pre-heater for the geyser. A 100 l geyser without a pre-heater requires 645 W of energy to heat water from 10 °C to 60 °C, the pre-heater will reduce the energy required to 196 W. Therefore the energy required is reduced to 30% of the initial requirement.

6.4 Winter Weather Experimental Conditions

The system was tested during typical Stellenbosch summer weather. For the sake of thorough investigation of the system's performance it was also tested during typical Stellenbosch winter weather conditions. Figure 6.8 illustrates the temperature of the cold water tank for two days. The cold water tank temperature does not reach the low temperatures experienced at night with a temperature difference of 5 °C between the water and ambient temperature at its lowest. Investigating the energy dissipated per square metre of radiating surface, resulted in 56.57 W/m^2 and 55.83 W/m^2 for the two nights. These values are close to those recorded during summer operation, with no significant increase or decrease in cooling capacity.

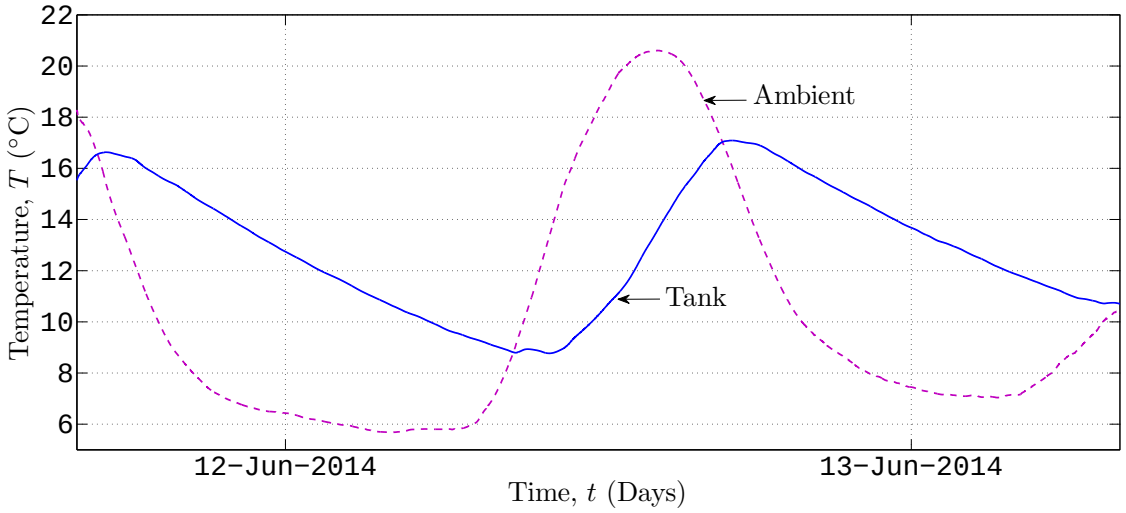

Figure 6.8 Comparison of the measured ambient and cold water tank temperatures as a function of time

The system was also tested to ensure that it can operate without a control system. This test required the valves of the convector and night cycle to be open at all times to allow the fluid to flow in the direction determined by buoyant forces. Figure 6.9 presents the control and room temperatures measured during the test. The large temperature difference of 9 °C between the control and room on the 18th of April proves that the system is capable of operating without a control system.

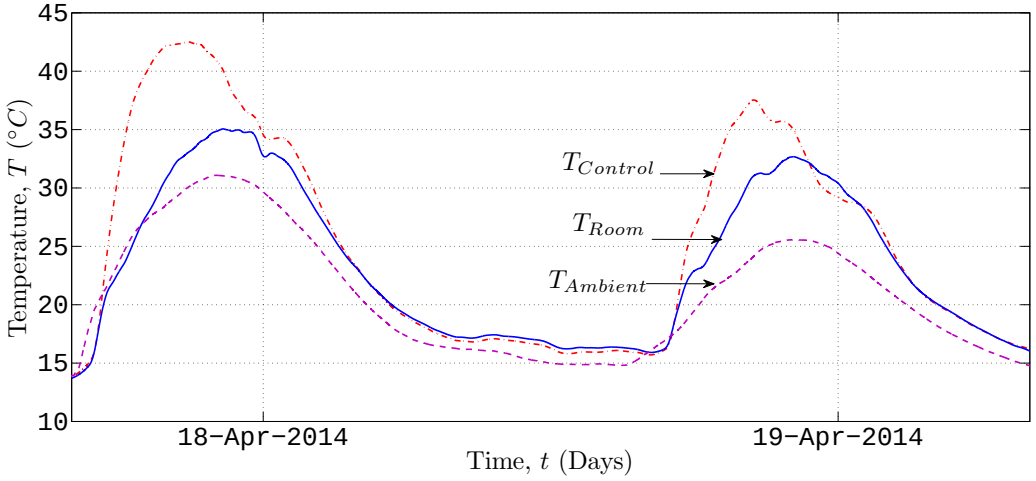

Figure 6.9 Comparison of measured and theoretically calculated water temperature as a function of time in a night-sky radiation system with no control system

6.5 Flow

The water flow rate measurements were taken as described in 4. Figure 6.10 presents the setup used to inject the dye.

Table 6.4 shows measurements for the convector, hot and cold water cycles. The water flow rates recorded show that the hot water flow rates are much higher than the flow rates of the cold water cycle. The effect of the flow rates is visible in a comparison between Figure 6.2 and Figure 6.6. The comparison between the hot water tank and cold water tank indicates a smaller difference in the temperature of the top layer and bottom layer of the hot water tank. The temperature difference between the two layers is an indication of the level of stratification. It is known that high flow rates cause de-stratification, causing the level of stratification to be low. The hot water tank has high flow rates compared to those of the cold water tank, hence the low level of stratification of the hot water tank compared to that of the cold water tank.

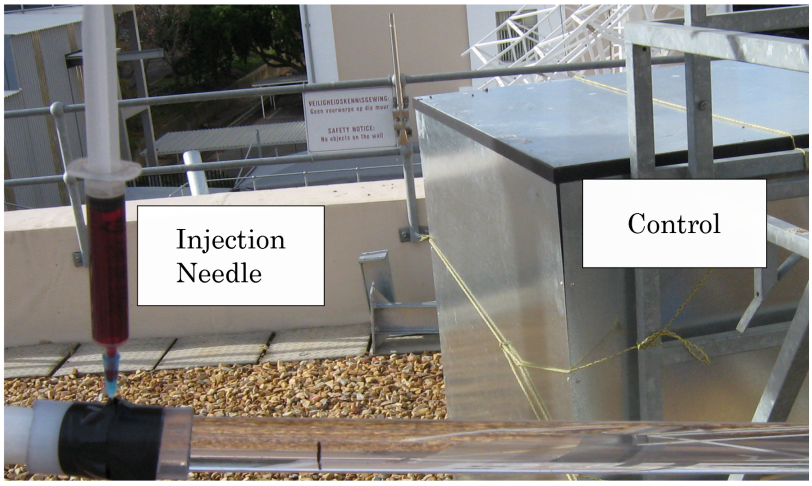

Figure 6.10 Dye injection into the water flowbb

Table 6.4 Measurements of hot and convector water velocities and room air speeds for 10 and 11 April 2014

Time	Hot water cycle (m/s)	Convector (m/s)	Cold water cycle (m/s)	Room air speed (m/s)
09:31	0.025	0.015		0.250
10:26	0.054	0.023		0.270
11:41	0.051	0.030		0.340
12:37	0.042	0.029		0.340
13:30	0.036	0.029		0.270
14:29	0.030	0.026		0.250
15:29	0.014	0.023		0.160
16:32	0.000	0.007		0.050
21:03			0.026	
21:44			0.025	
22:12			0.025	
23:12			0.020	
00:12			0.020	
01:15			0.018	
02:15			0.017	
03:15			0.016	
04:15			0.014	

The measured low flow rates in the hot water, convector and cold water cycles show a laminar flow regime. The theoretical assumption is verified by Figure 6.11 (a) indicating a laminar profile. A diagrammatic sketch of Figure 6.11 (a) can be found in Figure 6.11 (b) . The colourant injected into the stream indicates highly-ordered motion with smooth stream lines.

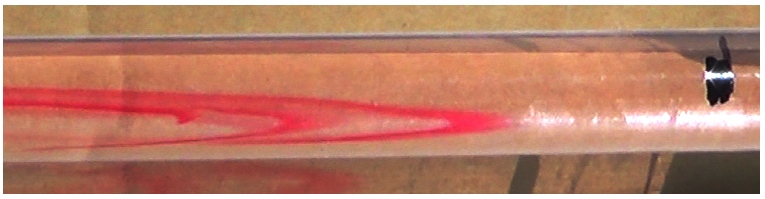

(a)

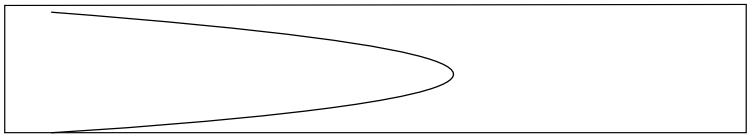

(b)

Figure 6.11 Laminar profile made visible by dye (a) diagrammatic representation of the visible laminar profile (b)

The airflow measurement in the room varied from 0.25 m/s to 0.05 m/s as shown in Table 6.4. The air velocity was measured using a shroud that directed the flow through the convector to a central position. Eight readings were taken at the outlet of the shroud at a specific location and an average of those readings was taken.

6.6 Sensitivity Analysis

Grid dependence and time step dependence will be considered in this section. The increase in the number of control volumes requires a decrease in the time step. The time step dependence indicates the effect of the time step when the control volumes are constant and the time step is increased or decreased.

6.6.1 Grid Dependence

In this section data of the base case of the theoretical model and altered theoretical model are presented. The base case, is the theoretical model used to provide the results presented in this thesis. The altered theoretical model investigates the effect of the number of control volumes used. The number of control volumes used in the model are increased and decreased. An increase in

the number of control volumes reduces the size of the control volumes, thereby improving the accuracy of the model. It is necessary to adjust the time step of the program with the change in the number of control volumes. For the sake of comparison the time step was kept constant to indicate the effect the number of control volumes has on the runtime of the program. When the number of control volumes is reduced the size of the control volumes increase. The three scenarios investigated are presented in Table 6.5 and the comparison of the predicted temperature as a function of time is presented in Figure 6.12..

Table 6.5 Program runtime with variation in control volumes

System	Number of Control Volumes	Δt (s)	Run Time (min:sec)
Fewer Control Volumes	62	0.1	01:03
Base case	119	0.1	01:45
More Control Volumes	182	0.1	02:30

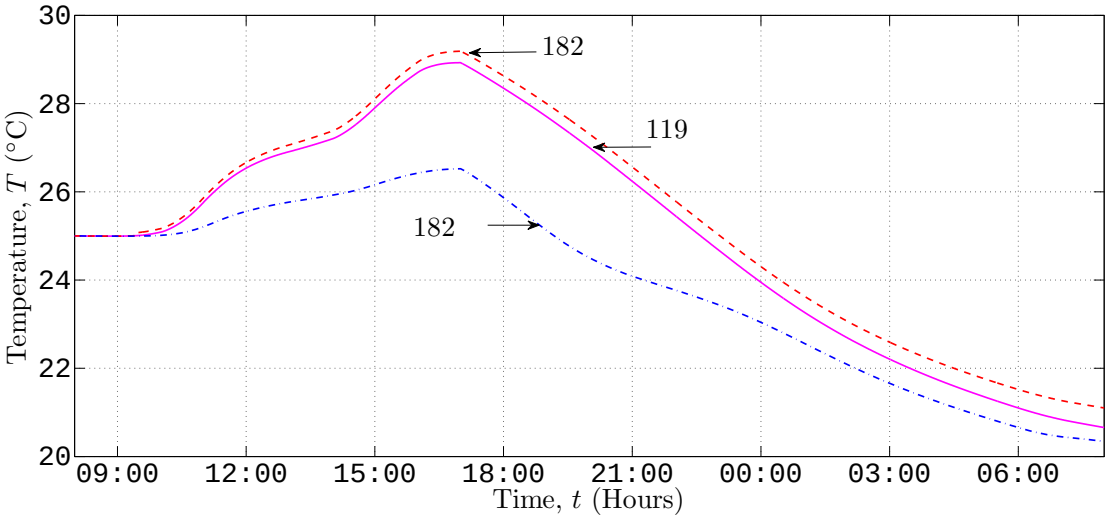

Figure 6.12 Comparison of the tank water temperature as a function of time of the base case, more and fewer control volume

The comparison indicates that extra control volumes increase the runtime of the program. The runtime indicated by Table 6.5 is the runtime of the program for one days' prediction. Extra control volumes increase the accuracy of the model but the runtime of the program needs to be considered. The increase in accuracy illustrated by Figure 6.12 must be weighed against the extra runtime.

Figure 6.12 illustrates how the temperature values of the theoretical model change with the number of control volumes. The increase of control volumes increases the accuracy of the theoretical model. A small change (< 1 °C)is visible in the tank water temperature of the theoretical model, the gain in accuracy is not worth the additional time, since the program needs to produce results for a few consecutive days. This would cause the difference in runtime to be even larger.

6.6.2 Time Step Dependence

In this section the change in the theoretical predicted values due to a change in the time step is discussed. When the time step selected is too large the predicted temperature increases above the maximum expected temperature of 80 °C and the program is forced to abort. A small time step on the other hand increases the runtime of the program. Table 6.6 presents the runtime for one day's predicted tank temperature.

Table 6.6 Program runtime of one day's predicted tank temperature for different time steps

Δt (s)	Number of Control Volumes	Run Time (mm:ss)
0.01	119	17:45
0.10	119	01:45
0.20	119	00:52

Table 6.6 indicates the increase in the program runtime with the decrease in the time step. The effect of the time step on the predicted temperature now needs to be addressed. This is done by comparing the predicted tank temperature at the three different time steps. Figure 6.13 illustrates the predicted tank temperature as a function of time for one day's operation. The figure indicates that for the specific time step choices, the predicted tank temperature does not differ with the change in time step size. The only effect the three considered time steps has is that on the runtime of the program. It is thus in the interest of the user to use the largest time step possible to reduce the runtime of the program.

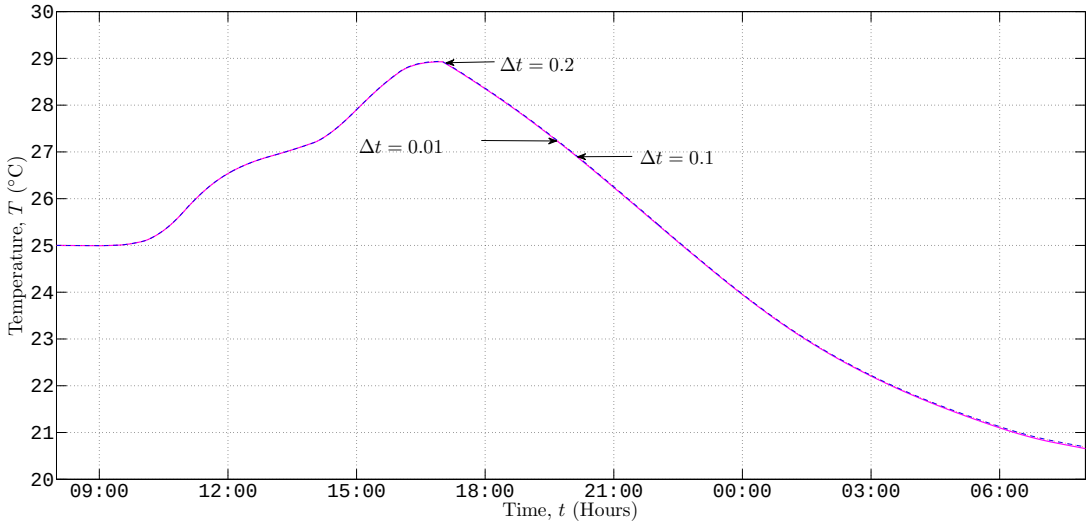

Figure 6.13 Comparison of the tank temperature as a function of time of the three time step sizes

6.7 Optimization

The optimization of the night and convector cycles is an important but complex process. The convector cycle is responsible for the cooling of the room while the night cycle is responsible for the cooling of the water. The three important components of the night-sky radiation system are the radiator, convector and storage tank. The storage tank connects the two cycles and acts as an energy storage unit. Heat absorbed from the room by the convector is stored in the water during the day, at night the water circulates through the radiator, which emits the stored energy. The size of such a system will depend on the room heat load or building heat load and the desired comfort level.

In an attempt to reduce the system's variables, a radiator area to tank volume ratio is calculated. The effect of this ratio at night is presented in Figure 6.14. A high ratio is sensitive to the ambient temperature, and produces a large temperature drop in the cold water tank for one night of cooling. This large ratio is presented by $A_R/V_{CWT} = 0.052$ m^2/l, while a lower value is less sensitive to the environment but produces a smaller temperature drop in tank temperature, as shown by $A_R/V_{CWT} = 0.007$ m^2/l.

A pattern similar to the night cycle is seen in Figure 6.15, a representation of the tank temperatures during the day. A smaller ratio causes a small temperature increase while a large ratio leads to a large temperature increase in the cold water tank temperature.

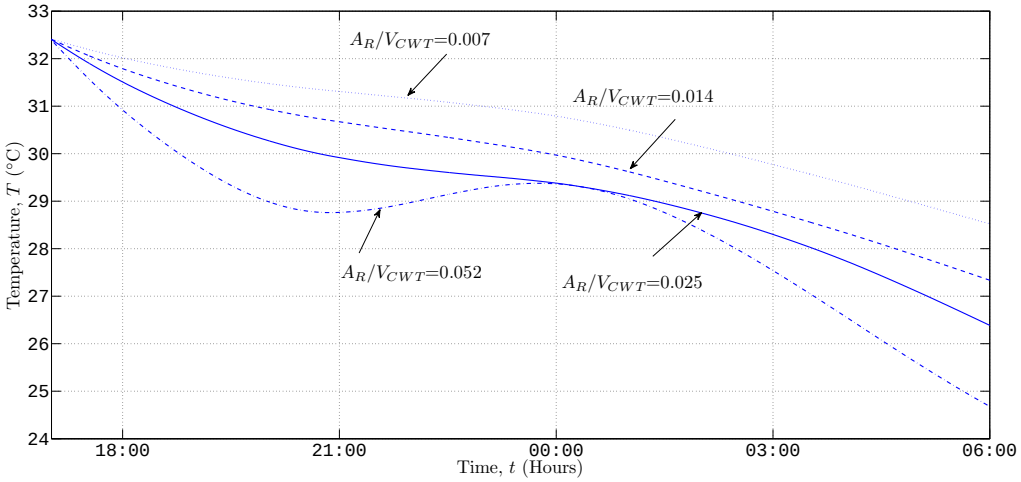

Figure 6.14 Effect of the ratio of radiator area to tank volume A_R/V_{CWT} on the tank water temperature as a function of time (at night)

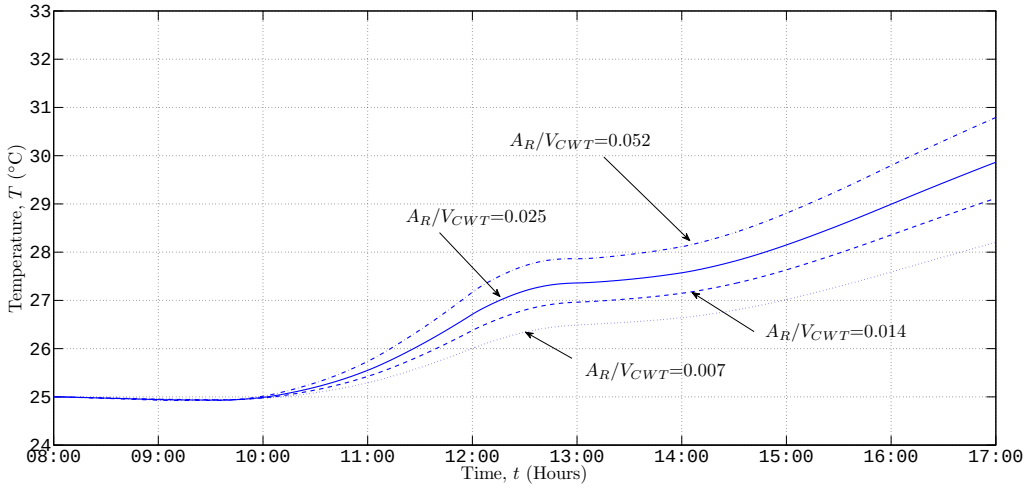

Figure 6.15 Effect of the ratio of radiator area to tank volume A_R/V_{CWT} on the tank water temperature as a function of time (during the day)

The optimization process comprises four steps. During step one, the size of the convector is determined by the available space determined by the size of the room. Then an ratio of radiator area to tank volume is chosen. Then the area is chosen according to budget or available space. Lastly tank volume is calculated according to the chosen ratio of radiator area to tank volume.

The size of the convector determines the heat removal rate from the room. To ensure that the maximum heat is removed from the room, the maximum size of the convector is selected. The maximum size of the convector is affected by the available space in the room. A small convector results in insufficient heat removal causing the room to reach temperatures above 25 °C, selected as the comfort level for this project.

The next step is to choose an ratio of radiator area to volume. Choosing an ratio of radiator area to volume too small could possibly lead to the system not being able to handle two or more consecutive hot days. To compensate for the effect of one or two consecutive hot days a ratio that is less sensitive to the ambient air temperature $A/V = 0.007$ m^2/l is chosen. The decision is made possible by interpreting Figures 6.14 and 6.15, these figures represents the storage tank water temperature characteristics of the night-sky radiation system.

The radiator area or number of radiators now need to be selected. Consider Figure 6.16. The temperature profiles of the room are presented for the base case, optimized with one radiator and optimized with two radiators. The option using two radiators produces the most favourable results with room temperatures not exceeding 29 °C on the first day of operation, the temperature of days two and three exceeds 30 °C but only after 17:00 when the cooling is turned off. During operating hours the room remains a comfortable temperature and does not exceed 27 °C for the double radiator set-up and 29 °C for the single radiator set-up.

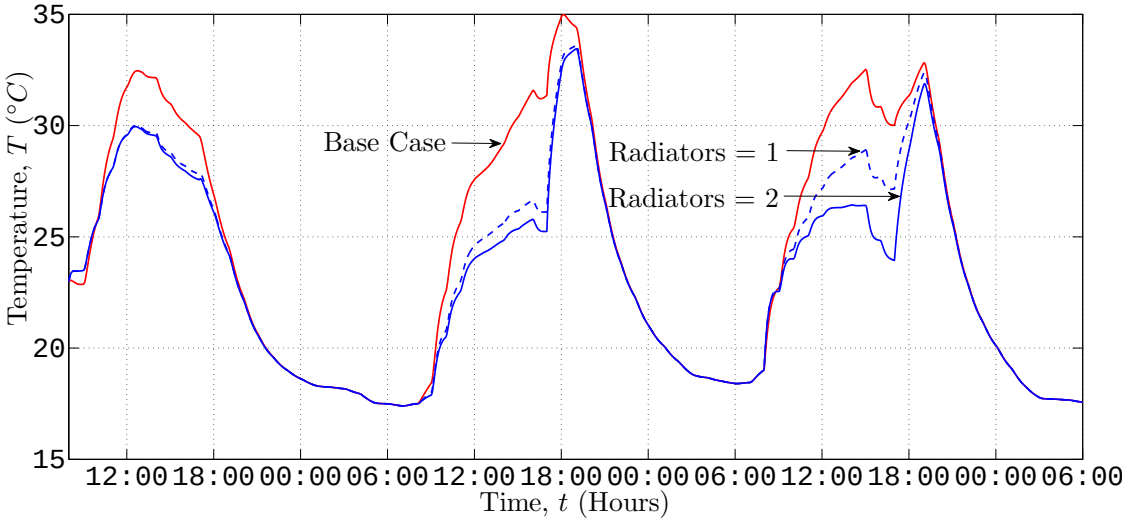

Figure 6.16 Room temperature as a function of time for the base case and optimized systems with one and two radiators each of 3.6 m^2

With the room temperatures known, the cold water tank temperature needs to be considered. Figure 6.17 presents the temperature profile of the three operating days. The temperature in the original system varies much more than that in the optimized system with one radiator and a slightly bigger tank, while in the system with two radiators there is an overall temperature drop during the three-day period. The optimized system with two radiators yields favourable results if only the room temperatures are considered, the tank temperatures indicate that the system with two radiators and the chosen ratio of radiator area to volume ratio of 0.007 m^2/l is over-sized for the actual experimental set-up.

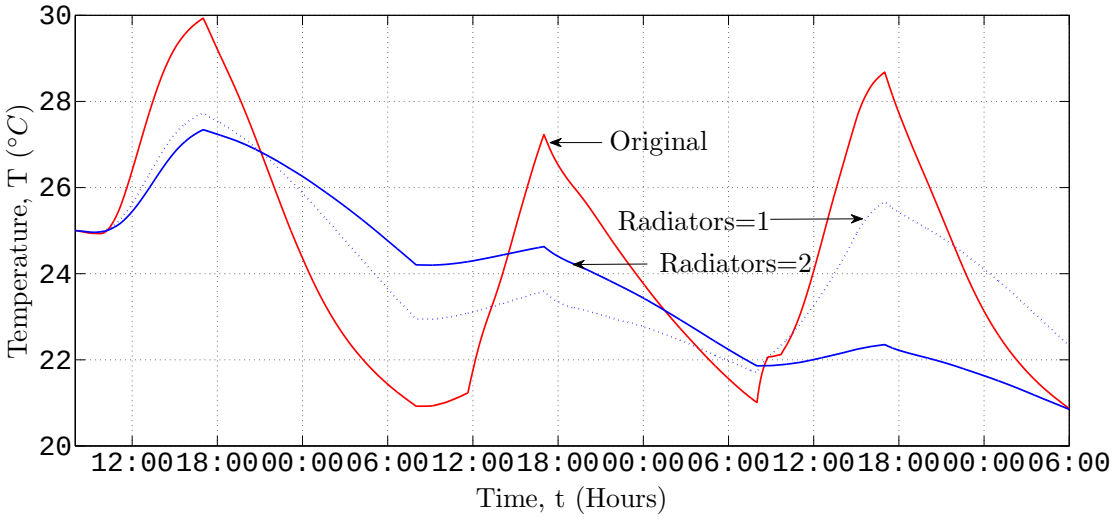

Figure 6.17 Tank temperatures in original and optimized system with one and two radiators

The cooling factor parameter will now be considered. The cooling factor is the ratio of the energy dissipated to the energy absorbed in one day of operation. A ratio lower than one indicates a lack of cooling, while a ratio of one indicates a balanced system. This ratio is used to indicate whether the system is over or undersized. Considering the cooling factor for the three days, it can be seen that the system with one radiator has a cooling factor of 1.5 while the system with two radiators has a cooling factor of 3.1. This is another indication of an oversized system. The radiator dissipates three times more energy than absorbed during the three days. To reduce this ratio the size of the convector could be increased, but this is unnecessary since the room temperature is already within an comfortable range of 16 °C to 32 °C.

A temperature performance parameter created indicates the thermal comfort level in the room. The performance parameter is calculated when the room temperature exceeds 25 °C. The time step is multiplied by the difference in

room temperature and the pre determined comfort level temperature of 25 °C. The three scenarios investigated produced the results presented in Table 6.7.

Table 6.7 Comparison of original with optimized system

	Day	Base	Optimized	
		Case (°C s)	One Radiator (°C s)	Two Radiators (°C s)
$\sum \Delta t(T_r - 25)$	1	244 913	95 119	92 459
$\sum \Delta t(T_r - 25)$	2	258 704	14 375	4 130
$\sum \Delta t(T_r - 25)$	3	778 228	170 258	17 765
Cost (R)		5 050	13 084	18 216

The values presented in Table 6.7 are an indication of the time when the temperature of the room is above 25 °C. A high value suggests that the room was above 25 °C for an extended period or that the room temperature is extremely high for a short period. The results of Table 6.7 clearly indicate that the optimized system with two radiators has the best comfort level due to the low values of the temperature performance parameter. The additional cost of R 5 000 for the optimized system with two radiators needs to weighed against the thermal comfort gained. The cost of the system was calculated with the base cost of 1000 R/m for the convector, 1000 R/m^2 for the radiator and 3 R/l for the water tank. A cost calculation of the base case and two optimized systems is presented in Appendix B.3.

7 Discussion and Conclusions

In this chapter the results obtained through experimentation and theoretical models are discussed. The validity of the theoretical model and the application of a night-sky radiation system are considered.

7.1 Validity of Theoretical Model

Results obtained from five consecutive days of experimentation were used to validate the developed theoretical model. The temperatures of the cold water tank, hot water tank and room were used to compare the results obtained experimentally and theoretically. The theoretical model used data supplied by the weather station of the University of Stellenbosch, situated close to the experiment location.

The theoretical model yielded results that predict the performance of the system favourably. Figure 6.3 and Figure 6.5 confirm the validity of the theoretical model. The tank temperature deviation from the experimental results is ascribed to cloud cover at night. Clouds cause an overestimation of radiation, resulting in a predicted tank temperature much lower than that of the experiment. Keeping the effect of cloud cover in mind, the theoretical model can be used to predict the system's performance throughout the year for clear skies.

Optimization of the system is a method used to theoretically determine the size of the system needed to deliver the optimum performance. The method used produced credible results with a room temperature that was reduced to acceptable temperatures within a comfortable range of 16 °C to 29 °C.

Furthermore the temperature profile of the tank water obeys the quality of the area to volume ratio chosen. Small area/volume ratios yield systems with a low sensitivity to the environment and small change in temperatures. The opposite is true for large area/volume ratios.

The analysis of the theoretical model includes grid and time step dependence analysis. These analyses prove the effect of control volume size and time step sizes. The model is very sensitive to the grid size and less sensitive to the time step size. When larger control volumes are used the accuracy of the

model drops, the computational time also decreases. Therefore the control volume size where decreased, and the theoretical model's accuracy as well as the computational time increased. The increase in accuracy needs to be weighed against the extra runtime required, especially when the program needs to predict more than one day of operation.

The theoretical model developed for the hot water cycle also accurately predicted the behaviour of the experimental system. The model deviated from the experimental results at the minimum and maximum. The deviation and imitation of the experiment are illustrated in Figure 6.7. The experiment was capable of adding a maximum of 448.35 W of energy to the hot water tank.

7.2 Application of a Night-Sky Radiation System

The experiment shows that cooling a building by taking advantage of naturally occurring phenomena, in this case night-sky radiation and density induced circulation, is possible. The system operates without any non renewable energy inputs, this is done by placing components at positions that allow natural flow. Since natural circulation is the driving force, a test was done to prove that the system can operate without a control system. The absence of a control system and other mechanical or electrical components reduces the operational cost of the system since maintenance cost is eliminated.

Consider a room of 6 m x 8 m x 2.5 m with the long wall facing east. When the room is subjected to typical summer conditions the room requires 30 W/m^3 of heat removal throughout the day to ensure that the room remains at a comfortable 25 °C. The current experiment without any optimization resulted in 150 W/m^3 heat removed at its maximum performance. This evidence indicates that with optimization night-sky radiation is capable of providing reasonable heat removal.

The investigation of the heating cycle produced results that prove that the system could be used to pre-heat water for a geyser. The heating cycle was capable of collecting energy at a maximum rate of 448 W. It was proved that the heating cycle could reduce the load on a 100 l geyser by 30%.

To conclude, the theoretical model is a favourable representation of the experiment and can be used in practice. The theoretical model allows the researcher to optimize the system for specific needs. The night-sky radiation system is definitely a renewable cooling method that can be used in future for cooling. The system was also proven to be capable of pre-heating water for the geyser, providing a means of saving more energy, thus causing a further reduction in greenhouse gas emissions.

8 Recommendations and Future Work

In this chapter recommendations for future experimentation are considered. The section could be used by an other student to gain ideas for improving or studying the effects of alterations in the experimental set-up. The recommendations for future studies include:

1. Incorporating a radiative heat exchange unit
2. Studying the effect of forced convection in the room
3. Incorporating a solar pond and a radiator in the system
4. Creating an user friendly interface for architects
5. Using heated water for space heating

These four recommendations will now be briefly discussed.

The first recommendation to be considered is replacing the original convector with a radiating surface. A concrete slab embedded with pipes through which the cooled night water flows can act as such a surface. The water will extract the heat the concrete slab absorbs from the room. The concrete slab could then be used as an heat sink during the day and additionally to that be used as an heat source during the night. When the water is cooled at night, it will flow through the concrete, extracting the absorbed thermal energy of the day.

When the heat capacity of 1 kg concrete and 1 kg water are compared, it is found that water has a higher heat storing capacity (4185 J/K) than that of concrete 840 J/K this implies that the mass of concrete would be five times more than that required by water to store the same amount of energy. The water needed is only one third of the volume of the concrete. When considering a building with concrete floors or ceilings, this is a feasible concept.

The second recommendation is that the effect of forced convection on the heat removal rate of the room be tested. This was not done in the current study

since it would require an electrical component. The use of forced convection might help to increase the heat removal rate of the convector and thereby create a more efficient cooling system.

The third recommendation is the combination of a solar pond system and a radiator. In addition to the radiator this type of system also uses the solar pond as a radiating surface, thereby increasing the total area subjected to night-sky radiation. More radiation would mean that more energy could be dissipated during the night. It also means that the required radiator area decreases which reduces the cost of the system, the extra cost of building a solar pond also needs to be considered before implementing this alteration.

The fourth recommendation is the creation of a user friendly interface that could be used by architects. This would assist them in designing green buildings in the future.

The final recommendation or operating condition that needs some consideration is the use of the hot water not for the preheating of geyser water but for the heating of the room. Typical South African weather requires heating of the room during the winter especially in the inland region. Studies need to be done to determine if enough heat could be collected and stored to heat a room.

References

Agilent-tecnologies (2012 May). Eighth edition edn.
Available at: http://cp.literature.agilent.com/litweb/pdf/34401-90004.pdf

Airflow (2014 August).
Available at: http://www.tsi.com/uploadedFiles/SiteRoot/Products/Literature/Manuals/ta5th

Al-Nimr, M., Kodah, Z. and Nassar, B. (1998). A theoretical and experimental investigation of a radiative cooling system. *Solar energy*, vol. 63, no. 6, pp. 367–373.

Bird, R.B., Stewart, W.E. and Lightfoot, E.N. (2007). *Transport phenomena*. John Wiley & Sons.

Botha, F., Dobson, R. and Harms, T. (2013). Simulation of a syngas from a coal production plant coupled to a high temperature nuclear reactor. *Journal of Energy in Southern Africa*, vol. 24, no. 2, pp. 37–45.

Cengel, Y. and Ghajar, A. (2011). *Heat and Mass Transfer: Fundamentals and Applications*. McGraw-Hill Education. ISBN 9780077366643.

Cengel, Y.A. and Cimbala, J.M. (). Fluid mechanics, fundamentals and applications, 2006. *Copyright*, vol. 7, p. 956.

Chinnery, D. (1971). *Solar water heating in South Africa*. South African Council for Scientific and Industrial Research.

Dimoudi, A. and Androutsopoulos, A. (2006). The cooling performance of a radiator based roof component. *Solar energy*, vol. 80, no. 8, pp. 1039–1047.

Dobson, R. (2005). Thermal modelling of a night sky radiation cooling system. *Journal of Energy in Southern Africa*, vol. 16, no. 2, p. 21.

Erell, E. and Etzion, Y. (2000). Radiative cooling of buildings with flat-plate solar collectors. *Building and Environment*, vol. 35, no. 4, pp. 297–305.

Fluke corporation, h.s.d. (2014 August).
Available at: http://assets.fluke.com/manuals/914243ugeng0000.pdf

Givoni, B. (1977). Solar heating and night radiation cooling by a roof radiation trap. *Energy and buildings*, vol. 1, no. 2, pp. 141–145.

Hollands, K. and Lightstone, M. (1989). A review of low-flow, stratified-tank solar water heating systems. *Solar Energy*, vol. 43, no. 2, pp. 97–105.

Holm, D. and Engelbrecht, F. (2005). Practical choice of thermal comfort scale and range in naturally ventilated buildings in South Africa: technical paper. *Journal of the South African Institution of Civil Engineering= Joernaal van die Suid-Afrikaanse Instituut van Siviele Ingenieurswese*, vol. 47, no. 2, pp. p–9.

Kays, W.M., Crawford, M.E. and Weigand, B. (2005). *Convective Heat and Mass Transfer*. McGraw-Hill.

Lawrence, M.G. (2005). The relationship between relative humidity and the dewpoint temperature in moist air: a simple conversion and applications. *Bulletin of the American Meteorological Society*, vol. 86, no. 2.

Loveday, D. and Taki, A. (1996). Convective heat transfer coefficients at a plane surface on a full-scale building facade. *International Journal of Heat and Mass Transfer*, vol. 39, no. 8, pp. 1729–1742.

Lunde, P.J. (1980). Solar thermal engineering: space heating and hot water systems. *New York, John Wiley and Sons, Inc., 1980. 635 p.*, vol. 1.

Meir, M., Rekstad, J. and LØvvik, O. (2002). A study of a polymer-based radiative cooling system. *Solar Energy*, vol. 73, no. 6, pp. 403–417.

Milford, R. (2009). Greenhouse gas emission baselines and reduction potentials from buildings in South Africa.

Mills, A. (2009). *Heat Transfer*. Pearson Education. ISBN 9788131727133.

Nahar, N., Sharma, P. and Purohit, M. (1999). Studies on solar passive cooling techniques for arid areas. *Energy Conversion and Management*, vol. 40, no. 1, pp. 89–95.

National-instruments (2014 August).
Available at: `http://sine.ni.com/nips/cds/print/p/lang/en/nid/207535`

Naude, J. (2013). Night sky radiation cooling system. Tech. Rep., University of Stellenbosch.

Okoronkwo, C., Nwigwe, K., Ogueke, N., Anyanwu, E., Onyejekwe, D. and Ugwuoke, P. (2014). An experimental investigation of the passive cooling of a building using nighttime radiant cooling. *International Journal of Green Energy*, vol. 11, no. 10, pp. 1072–1083.

Robinson, B.S., Dorwart, J. and Sharp, M.K. (2013). US space cooling potentials for ambient sources with thermal energy storage. *International Journal of Ambient Energy*, , no. ahead-of-print, pp. 1–14.

Runsheng, T., Etzion, Y. and Erell, E. (2003). Experimental studies on a novel roof pond configuration for the cooling of buildings. *Renewable Energy*, vol. 28, no. 10, pp. 1513–1522.

Stellenbosch-weather (2014 August).
Available at: `http://weather.sun.ac.za/`

Stine, B. and Geyer, M. (2001). *Power from the sun*.

Stoecker, W. and Jones, J. (). Refrigeration and air conditioning, 1982. *Mc GrawHill Book Co, New York*.

Wang, Y., Cui, Y., Zhu, L. and Han, L. (2008). Experiments on novel solar heating and cooling system. *Energy Conversion and Management*, vol. 49, no. 8, pp. 2083–2089.

Winkler, H. (2005). Renewable energy policy in South Africa: policy options for renewable electricity. *Energy Policy*, vol. 33, no. 1, pp. 27–38.

Winkler, H. (2007). Energy policies for sustainable development in South Africa. *Energy for sustainable Development*, vol. 11, no. 1, pp. 26–34.

Appendices

A Calibration and Thermocouple Pairs

Calibration done with the fluke 9142 field metro-logy well, RTD and Hewlett Packard multimeter gave the following results depicted in Figures A.1 to Figures A.4. These figures illustrate the difference between the temperature measured by the T type thermocouple and the PT-100 RTD ($\circ$) at the set point temperature. The set point temperature is the pre determined calibration temperature. The temperature difference after the application of the correction factors provided by the applied regression, is also indicated ($+$).

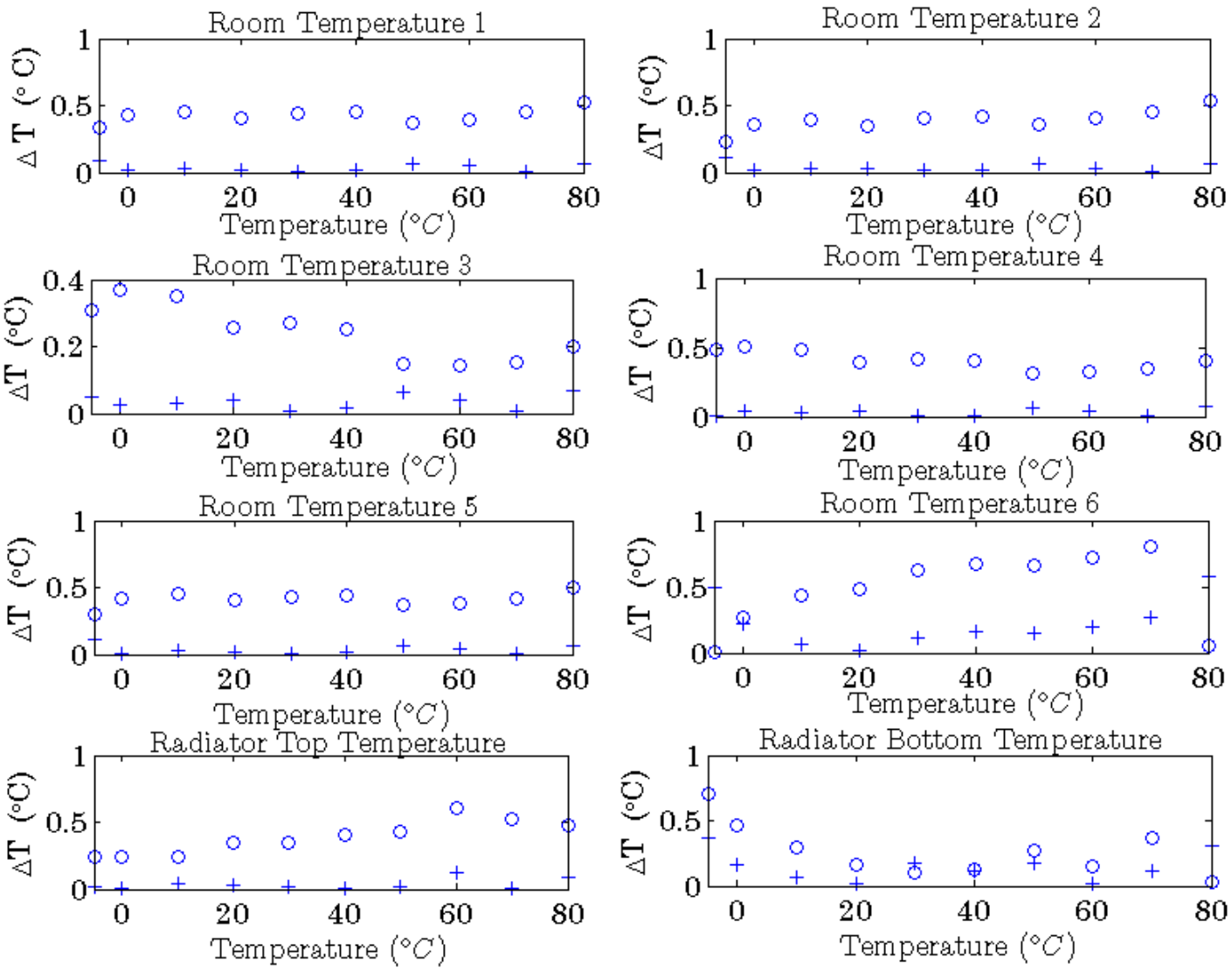

Figure A.1 Graphs illustrating thermocouple temperature difference

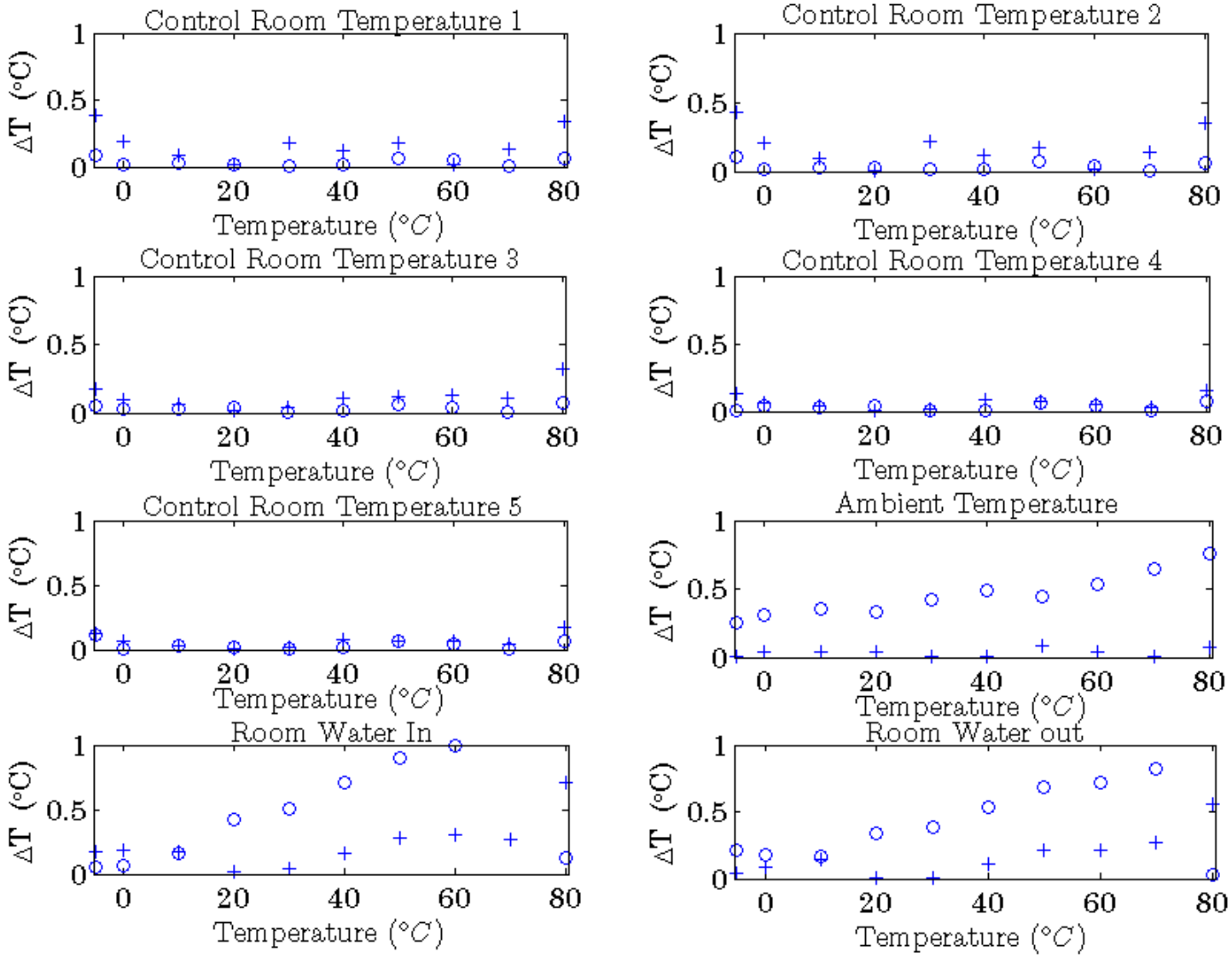

Figure A.2 Graphs illustrating thermocouple temperature difference continued

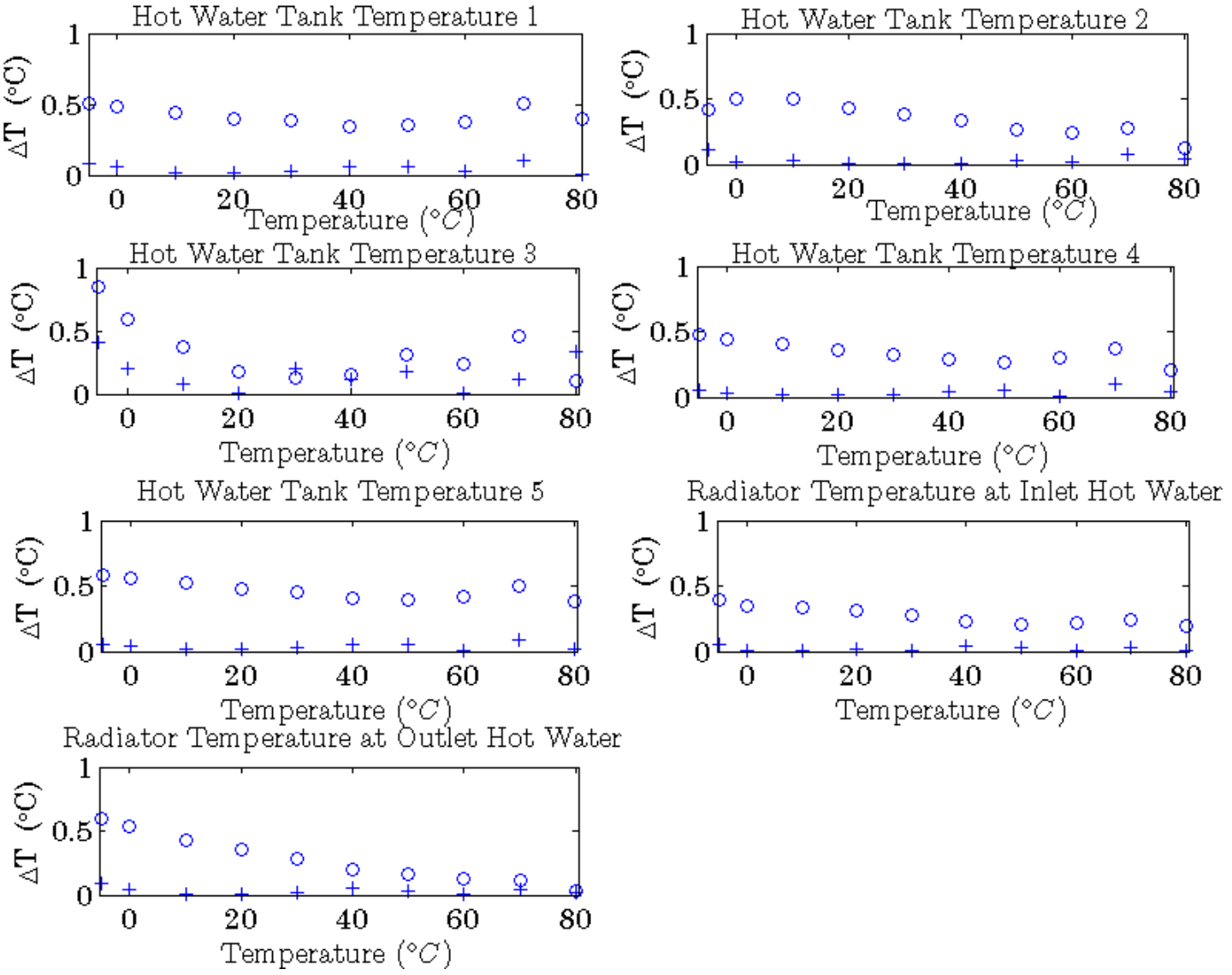

Figure A.3 Graphs illustrating thermocouple temperature difference continued

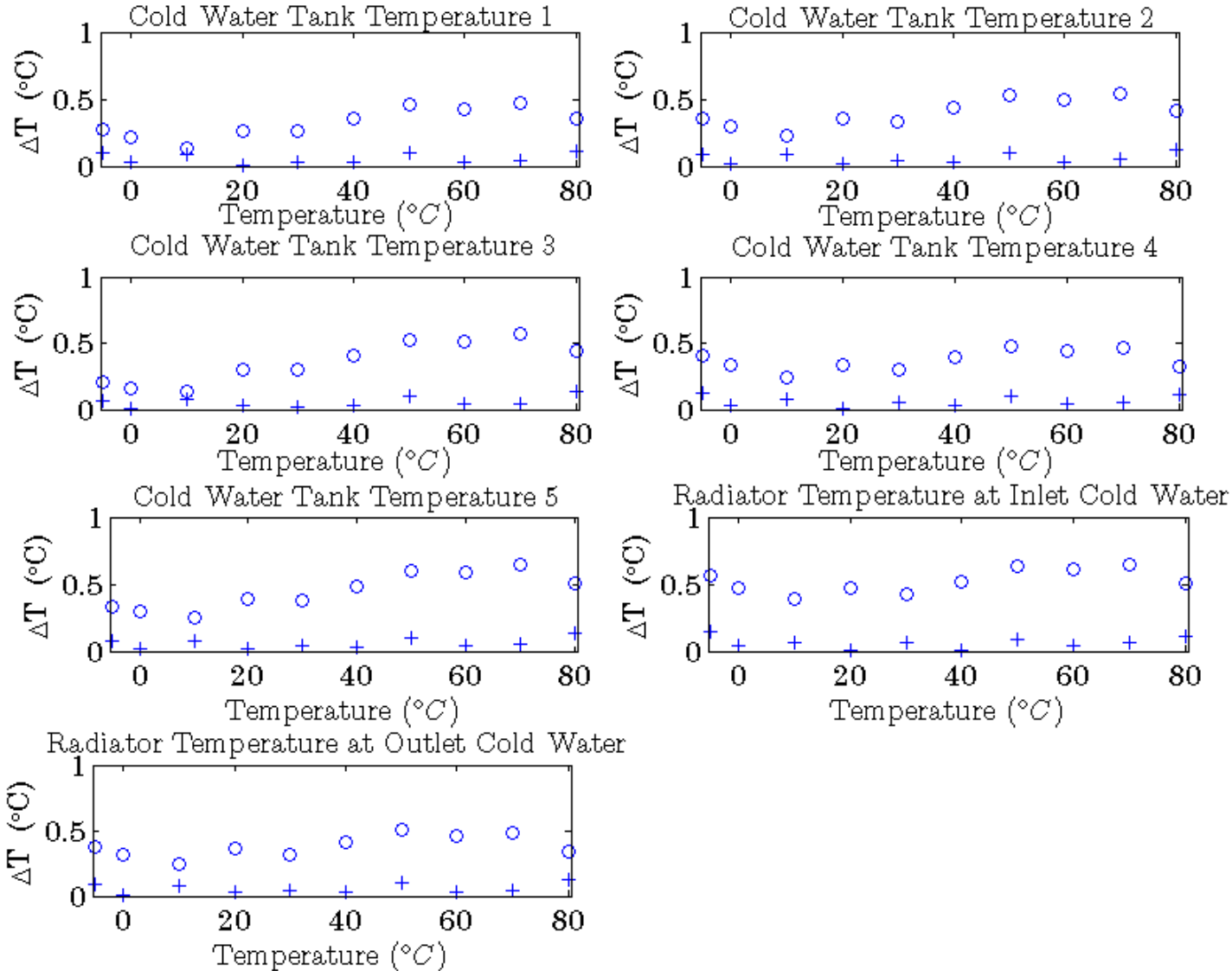

Figure A.4 Graphs illustrating thermocouple temperature difference continued

In an effort to reduce the temperature difference error thermocouple pairs with more or less the same temperature were used. The pairs formed where the inlet and outlet temperature of the radiator and convector, the temperature in the room, control, cold water tank and hot water tank. Tables A.1 to A.5 present the temperature of the selected thermocouple pairs at the pre determined calibrated temperatures.

Table A.1 The temperatures of hot water tank thermocouple pairs at calibration temperatures

Set Point (°C)	T_{HW1} (°C)	T_{HW2} (°C)	T_{HW3} (°C)	T_{HW4} (°C)	T_{HW5} (°C)
-5	-4.855	-4.655	-4.848	-4.829	-4.823
0	0.093	0.164	-0.009	0.120	0.109
10	10.039	10.031	9.907	10.039	10.043
20	20.025	20.007	19.803	20.019	20.017
30	30.032	30.013	29.748	30.028	30.031
40	40.028	39.969	39.674	40.008	40.015
50	50.015	49.985	49.589	50.008	50.009
60	59.981	59.972	59.515	59.948	59.963
70	69.838	69.868	69.431	69.837	69.847
80	79.844	79.884	79.327	79.886	79.861

Table A.2 The temperatures of cold water tank thermocouple pairs at calibration temperatures

Set Point (°C)	T_{CW1} (°C)	T_{CW2} (°C)	T_{CW3} (°C	T_{CW4} (°C)	T_{HW5} (°C)
-5	-4.620	-4.605	-4.588	-4.637	-4.593
0	0.176	0.180	0.207	0.171	0.189
10	9.941	9.940	9.937	9.927	9.933
20	19.916	19.912	19.898	19.924	19.908
30	29.861	29.863	29.848	29.881	29.863
40	39.967	39.964	39.960	39.968	39.969
50	49.992	49.996	49.991	49.995	49.994
60	59.927	59.927	59.922	59.921	59.919
70	69.922	69.919	69.923	69.918	9.915
80	79.677	79.679	79.693	79.675	79.689

Table A.3 The temperatures of room thermocouple pairs at calibration temperatures

Set Point (°C)	T_{room1} (°C)	T_{room2} (°C)	T_{room3} (°C)	T_{room4} (°C)	T_{room5} (°C)	T_{room6} (°C)
-5	-4.455	-4.431	-4.492	-4.546	-4.424	-4.044
0	0.187	0.186	0.176	0.166	0.196	0.428
10	9.962	9.962	9.959	9.959	9.958	10.052
20	19.846	19.857	19.862	19.862	19.840	19.846
30	29.881	29.873	29.885	29.895	29.883	29.780
40	39.845	39.848	39.848	39.858	39.844	39.705
50	49.790	49.793	49.791	49.791	49.786	49.579
60	59.775	59.759	59.764	59.764	59.769	59.523
70	69.729	69.734	69.737	69.727	69.741	69.458
80	79.704	79.710	79.699	79.699	79.703	80.352

Table A.4 The temperatures of control thermocouple pairs at calibration temperatures

Set Point (°C)	T_{room1c} (°C)	T_{room2c} (°C)	T_{room3c} (°C)	T_{room4c} (°C)	T_{room5c} (°C)
-5	-4.833	-4.866	-4.941	-4.906	-4.891
0	0.000	-0.013	0.049	0.084	0.082
10	9.906	9.903	10.001	10.023	10.027
20	19.812	19.808	19.992	20.012	20.003
30	29.727	29.762	30.043	30.022	30.028
40	39.673	39.667	40.074	40.051	40.044
50	49.589	49.592	50.075	50.030	50.029
60	59.504	59.498	60.086	60.009	60.025
70	69.449	69.452	70.047	69.968	69.981
80	79.326	79.318	79.528	79.697	79.677

Table A.5 The temperatures of inlet and outlet thermocouple pairs of the radiator and convector at calibration temperatures

Set Point (°C)	Radiator Hot water		Convector		Radiator Cold Water	
	T_{rinHW} °C	T_{routHW} °C	T_{conin} °C	T_{conout} °C	T_{rinCW} °C	T_{routCW} °C
-5	-4.822	-4.857	-4.344	-4.479	-4.666	-4.607
0	0.139	0.104	0.389	0.290	0.155	0.192
10	10.050	10.055	10.029	9.998	9.918	9.932
20	19.991	20.016	19.910	19.938	19.931	19.902
30	30.012	30.026	29.791	29.828	29.894	29.873
40	40.003	40.017	39.833	39.888	39.988	39.963
50	49.994	49.988	49.804	49.877	50.001	49.984
60	59.965	59.959	59.655	59.746	59.914	59.924
70	69.906	69.900	69.697	69.696	69.907	69.924
80	79.837	79.831	80.277	80.117	79.669	79.684

A.1 Calibration Certificate

RAPID INSTRUMENTATION CC

38, 1st Avenue, Boston,
Bellville, 7530
R.S.A.

Tel: (021) 948-0413
Fax: (021) 948-0435
Cell: 083 458 2497

P O Box 1050
Oakdale
7535
Reg. No. 2000/021703/23

CERTIFICATE OF CALIBRATION

South African National Accreditation System
Accredited Laboratory Number 366

sanas
Calibration Laboratory

Calibration of a	:	PLATINUM RESISTANCE THERMOMETER
Manufacturer	:	ISOTECH
Model Number	:	935-14-72
Serial Number	:	191069
Factory Number	:	N/A
Calibrated for	:	UNIVERSITY OF STELLENBOSCH
Address	:	Department of Mechanical Engineering Stellenbosch
Temperature	:	0 °C; + 50 °C; + 100 °C; + 180 °C; + 300 °C
Technical Signatory	:	M P ACKHURST
Calibrated by	:	M P ACKHURST
Checked by	:	S R ACKHURST
Date of Calibration	:	4 February 2013
Certificate Number	:	**RAP15738**
Issue Number	:	2

The South African National Accreditation System (SANAS) is a member of the International Laboratory Accreditation Co-Operation (ILAC) Mutual Recognition Arrangement (MRA). The MRA allows for the mutual recognition of technical test and calibration data by member accreditation bodies worldwide. For more information on the MRA please refer to www.ilac.org.

$0{,}0011611x^2$
$+2{,}32652102x$
$-243{,}7648049$

RAPID INSTRUMENATION CC
SANAS CALIBRATION LABORATORY 366

SUMMARY OF RESULTS				
Actual Temperature °C	UUT Reading Ω	UUT Reading °C	Correction °C	Uncertainty U °C
+ 0.097	100.0297	+ 0.076	+ 0.022	± 0.70
+ 50.020	119.4191	+ 50.057	- 0.037	± 0.70
+ 99.985	138.5377	+ 100.085	- 0.100	± 0.70
+ 179.823	168.4702	+ 179.978	- 0.154	± 0.70
+ 300.004	212.1331	+ 300.229	- 0.225	± 0.70
IMMERSION DEPTH: 150mm				

LABORATORY STANDARDS AND EQUIPMENT USED FOR MEASUREMENTS		
Standards of Equipment	Serial Number	Certificate Number
ASL F250 Digital Thermometer	1344029856	TH\DG-6460
Pt100 Probe	PT100 1-20	TH\DG-6460
Calibrator	RAP01G	

PROCEDURE/S UTILISED	
1016	Determination of Uncertainties
2001	Ice Point
2003	Calibration of RTD / PT100

METHOD
The UUT was calibrated according to laboratory standards, the results of which were traceable to National Measuring Standards for Temperature.

The reported expanded uncertainty is based on a standard uncertainty multiplied by a coverage factor k = 2 providing a level of confidence of approximately 95%, the uncertainty of measurement has been estimated in accordance with the principles defined in the GUM, Guide to Uncertainty of Measurement, ISO, Geneva, 1993.

The accuracy of the equipment used during calibration is traceable to the National Measuring Standards as maintained in the Republic of South Africa or International Measuring Standards.

The measurement results recorded in this certificate were correct at the time of calibration. The subsequent accuracy will depend on factors such as care, handling and frequency of use. It is recommended that recalibration be undertaken at an interval that will ensure that the instrument remains within the desired limits.

Signed: Certificate No: RAP15738

M P ACKHURST
Technical Signatory

B Calculations

B.1 Cooling Load

In order to determine if the cooling delivered by the system is adequate the required cooling load on a room situated in Cape Town, South Africa is calculated. The method used is described by Stoecker and Jones, the load is calculated for a east facing dark office building. The building's east and west walls are 8 m long, while the south and north facing walls are 6 m long with a height of 2.5 m. The east facing wall has a window of 3 m x 1.2 m with venetian blinds.

The required cooling load is influenced by lighting, solar load on walls and window and number of occupants and their activity. The solar load varies throughout the day, therefore the cooling load for the building is calculated for the time of operation which is from 8:00 to 17:00. The wall consists of ordinary brick of 0.09 m brick with plaster of 0.008 m on both sides. The conduction heat transfer coefficient (k) of the brick and plaster is equal to 1.39 W/Km. The resistance of the wall is calculated by adding the resistances as shown in Figure B.1.

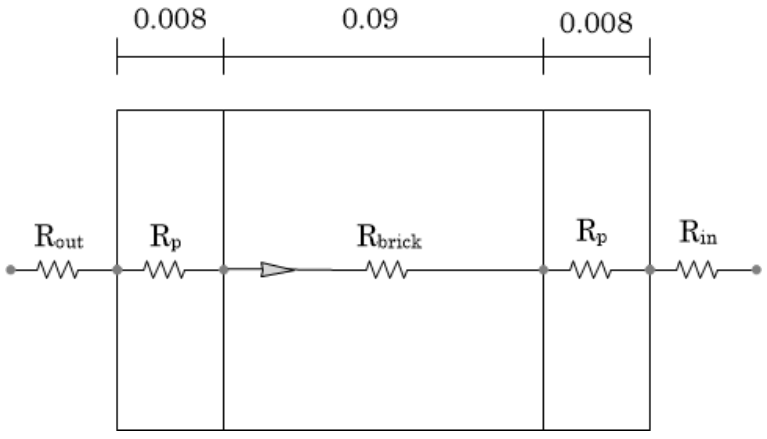

Figure B.1 Schematic diagram of wall

Rin	0.044
Rp	0.011
Rbrick	0.125
Rp	0.011
Rout	0.17
Rtot	0.361

With the resistance of the wall known, the load on each wall can be calculated and superimposed with

$\dot{Q}_{wall} = AT_{eq}/R_{tot}$ where A is the wall area, R_{tot} the wall resistance and T_{eq} the equivalent temperature difference. The equivalent temperature difference is selected from available tables.

The load due to radiation entering through the window also changes throughout the day. It is calculated by

$\dot{Q}_{window} = A\ SHGF_{max}CLF$ where A is the window area, $SHGF_{max}$ the maximum solar load and CLF the cooling load factor which changes throughout the day.

The load due to lighting and people stays constant throughout the day. It is assumed that the building uses 640 W florescent light bulbs. The load due to lighting is calculated by

$\dot{Q}_{light} = N_{bulbs}\dot{Q}_{bulp}CLF$, where N_{bulbs} is the number of bulbs, Q_{bulp} the rating of the bulb and CLF the cooling load factor influenced by the fixture of the light and the time of operation.

The number of occupants from 8:00 to 17:00 will be five and the load that needs to be removed by an occupant doing office work is 150 W (Stoecker and Jones). The load due to the occupants is calculated by

$\dot{Q}_{occupants} = N_{occupants}\dot{Q}_{occupants}CLF$ where $N_{occupants}$ is the number of occupants $Q_{occupants}$ the heat gained from the occupants and CLF the cooling load factor which is determined by the time of occupation.

The heat loads can now be superimposed, this leads to the total heat load the building is subjected to. This is the load that needs to be removed to keep the room at the designed inside temperature of 25 °C. The load for a work day in January is displayed in Figure B.2.

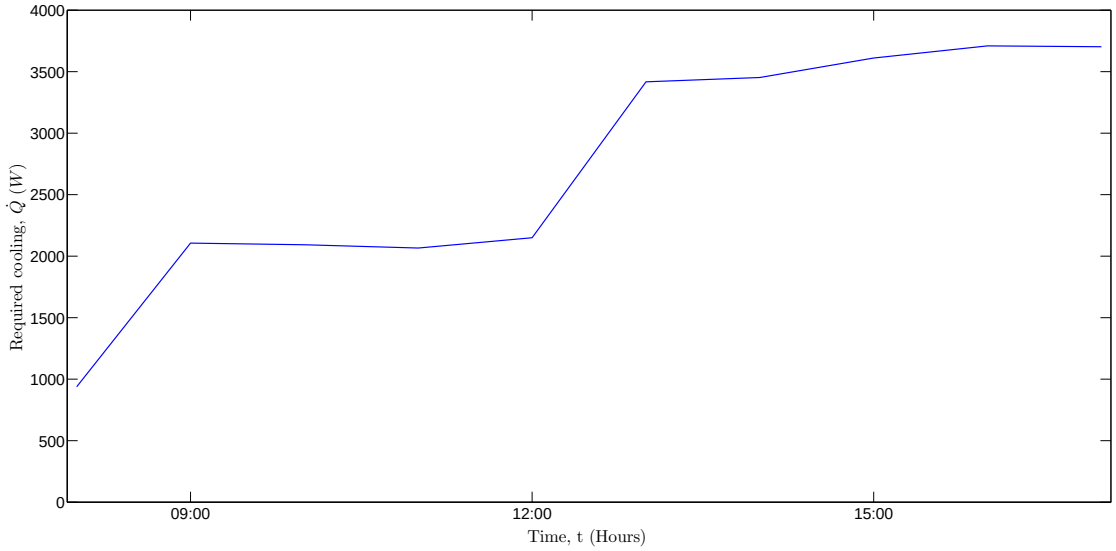

Figure B.2 Building heat load

The heat that has to be removed varies from 938 W at 8:00 to a maximum of 3611 W at 16:00 and total of 98.1 MJ for the day. The rate at which heat needs to be removed in kW at the maximum heat load is 3.71 kW. The experiment had a minimum average heat removal rate of 192 W and a maximum of 282 W. To compare the heat removed experimentally with that of the calculated required heat removal, the watts are divided by the volume of the room. This provides a value of 150 W/m^3 for the experiment while the calculated heat removal rate is 227 W/m^3. This comparison indicates that a night-sky radiation system has the potential to act as a room cooling system with the correct sizing.

B.2 Fin Spacing

For a rough calculation of the optimum fin spacing of the convector a room temperature of 30 °C and surface temperature of 20 °C is assumed. The constant surface temperature method of Cengel and Ghajar (2011) is used.

The film temperature is calculated by $T_{film} = 0.5 * (T_{surf} + T_{air})$, properties of the air at the film temperature are then used to calculate the Raleigh number.

$$Ra = \frac{g\beta(T_{air} - T_{surf})L^3\rho^2}{\mu^2}Pr$$

where $\beta = 1/T_{film}$, Pr the Prandtl number and μ the dynamic viscosity of the air. With the Raleigh number known, the optimum fin spacing can be calculated with

$S_{opt} = 2.715 * \frac{L}{Ra^{0.25}}$, where L is the length along the flow of the air.

The calculations suggest an optimum fin spacing of 7.45 mm for the specific case.

B.3 Cost

The cost of the system varies with the size of the radiator, convector and tank. The estimated price of the components is 1000 R/m^2 for the radiator, 1000 R/m for the convector and 3 R/l for the tank. Table B.1 shows the cost of the calculation for the original, the system optimized with one radiator and the system optimized with two radiators.

Table B.1 Calculated cost of base case and two optimized systems

		Optimized	
	Base Case (R)	One Radiator (R)	Two Radiators (R)
Convector	1 000	8 000	8 000
Radiator	3 600	3 600	7 200
Tank	450	1 484	3 016
Total	5 050	13 084	18 216

The cost doubles from the original to the system optimized with one radiator. This behaviour is ascribed to the maximum size of the convector. The optimized system with two radiators is even more expensive, the comfort gained by this system does not justify the additional cost.

The heat that has to be removed varies from 938 W at 8:00 to a maximum of 3611 W at 16:00 and total of 98.1 MJ for the nine hour period. The maximum rate at which heat needs to be removed from the building is 3.61 kW. The experiment had a minimum average heat removal rate of 192 W and a maximum of 282 W for the test period. To compare the heat removed experimentally with that of the calculated required heat removal, the watts are divided by the volume of the room. This provides a value of 150 W/m^3 for the experiment while the theoretical building has a calculated average heat removal rate of 22.7 W/m^3. This comparison indicates that a night-sky radiation system has the potential to act as a room cooling system with the correct sizing.

C Curve fits

The program requires the properties of the fluid at various temperatures to be known. To determine the properties of the fluid at these temperature data from Cengel and Ghajar (2011) and Stoecker and Jones are used. Using Matlab, a curve can be fitted to the data, this equation will then be used in the program to determine the required properties of the fluid. The required fluid properties are those of water and air. The curve fits for water are displayed in Figures C.1 to C.4 while those for air are displayed in Figures C.5 to C.9.

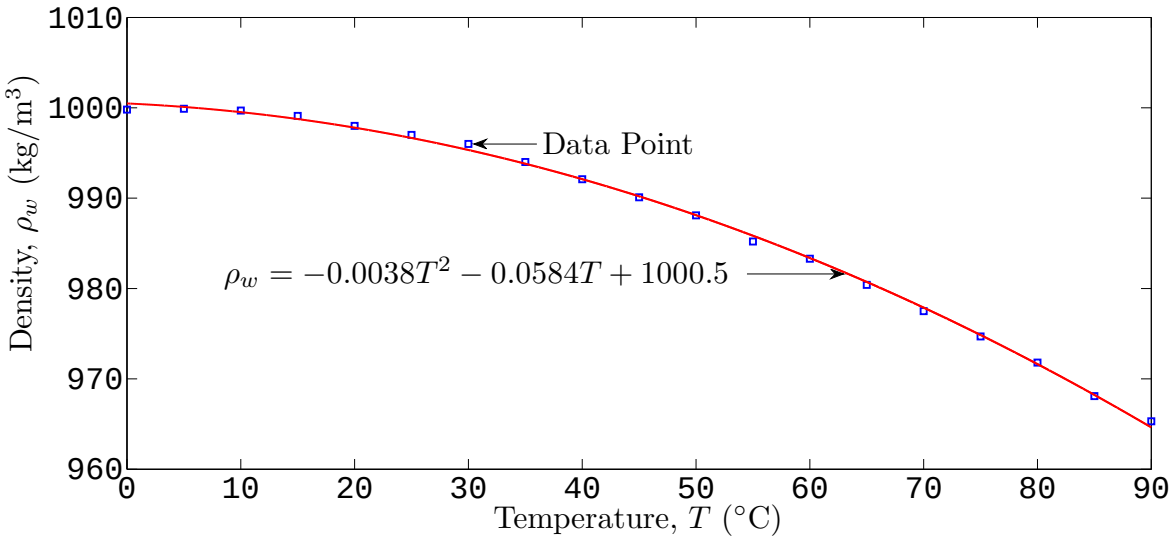

Figure C.1 Curve fit of the density of water as a function of temperature

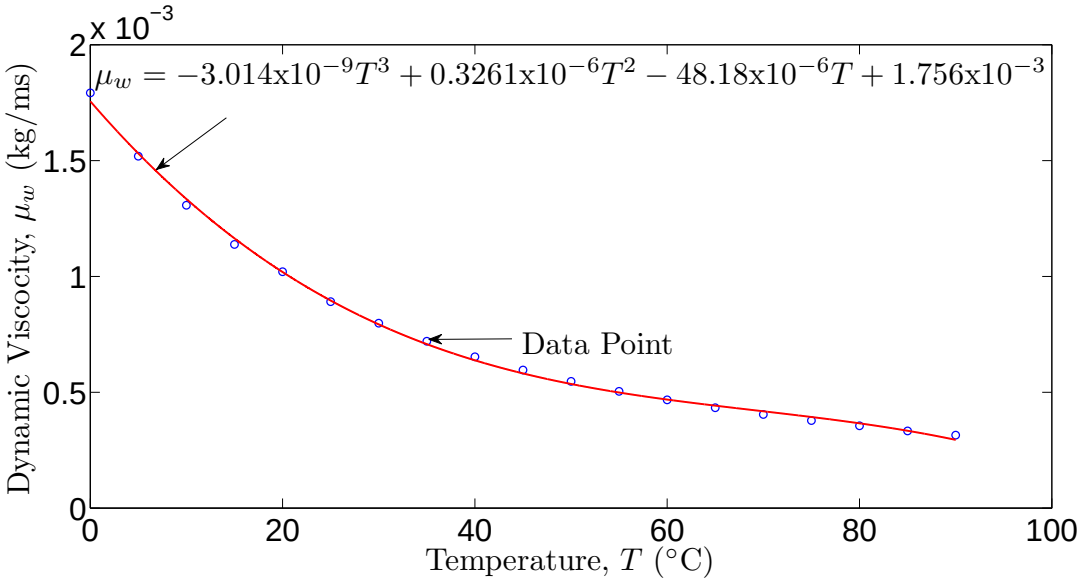

Figure C.2 Curve fit of the dynamic viscosity of water as a function of temperature

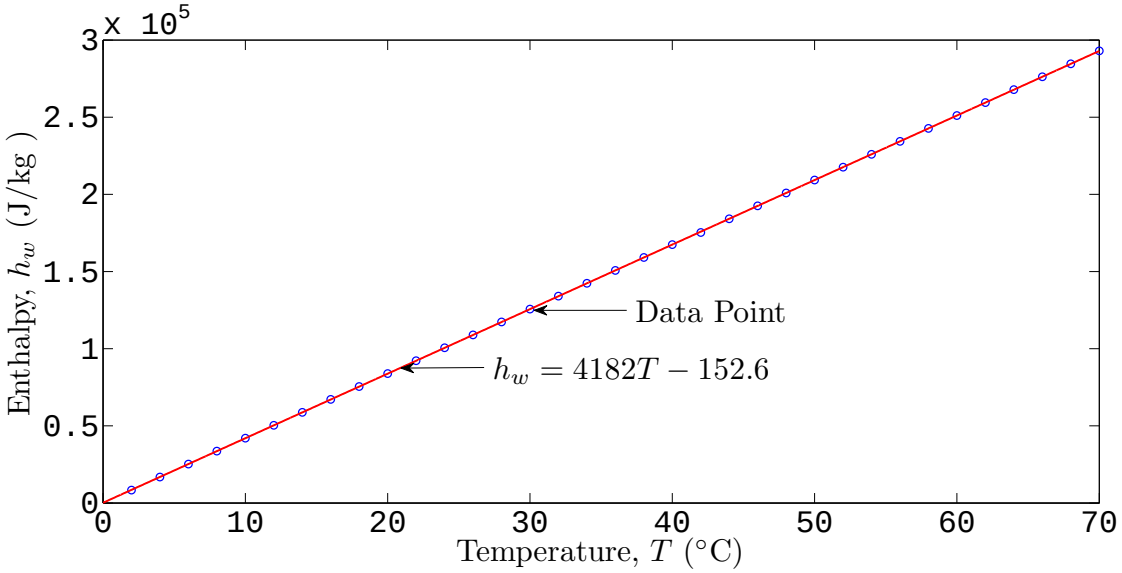

Figure C.3 Curve fit of the enthalpy of water as a function of temperature

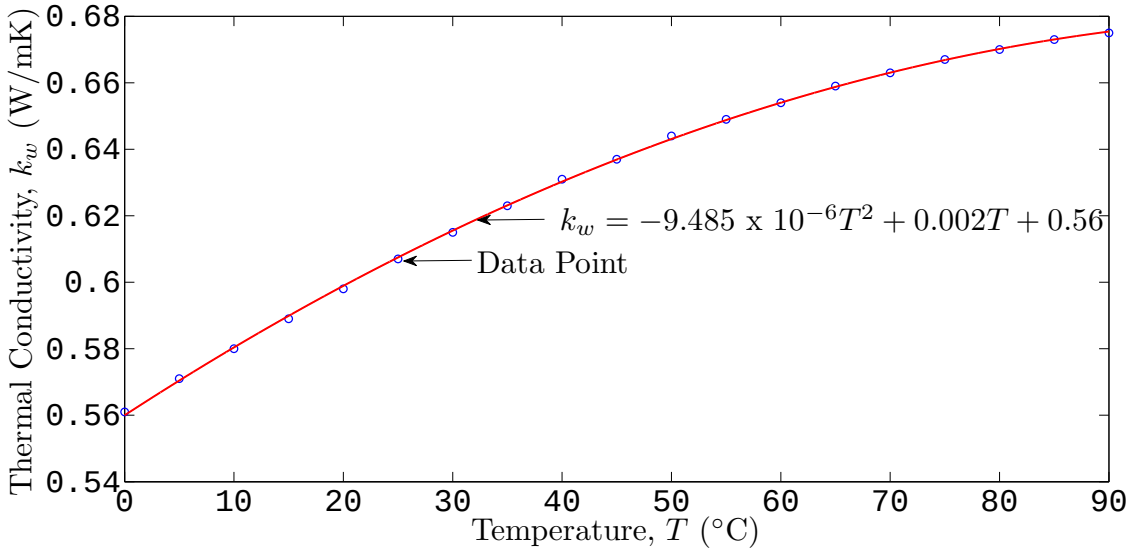

Figure C.4 Curve fit of thermal conductivity of water as a function of temperature

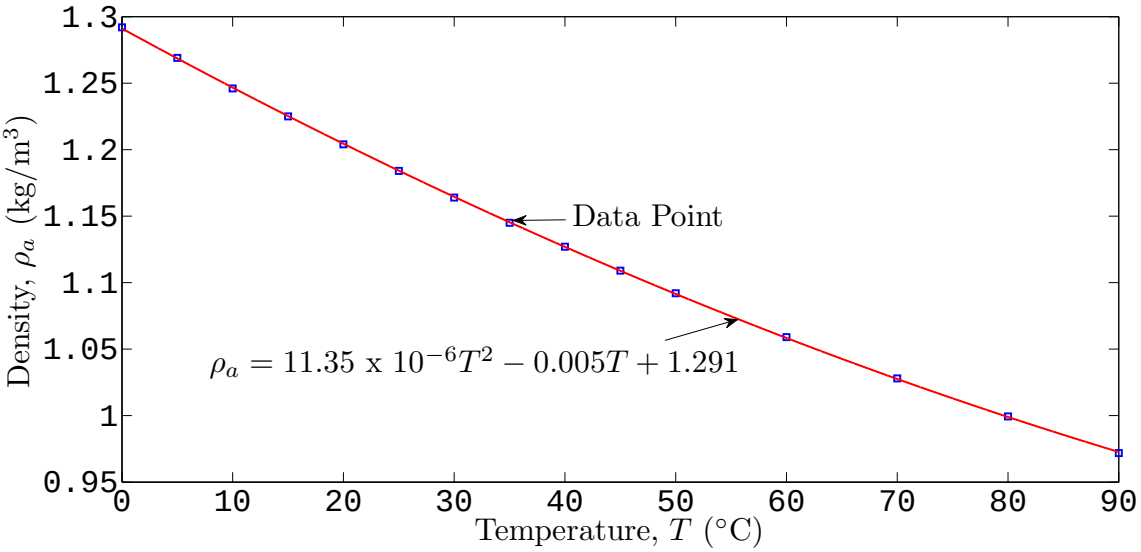

Figure C.5 Curve fit density of air as a function of temperature

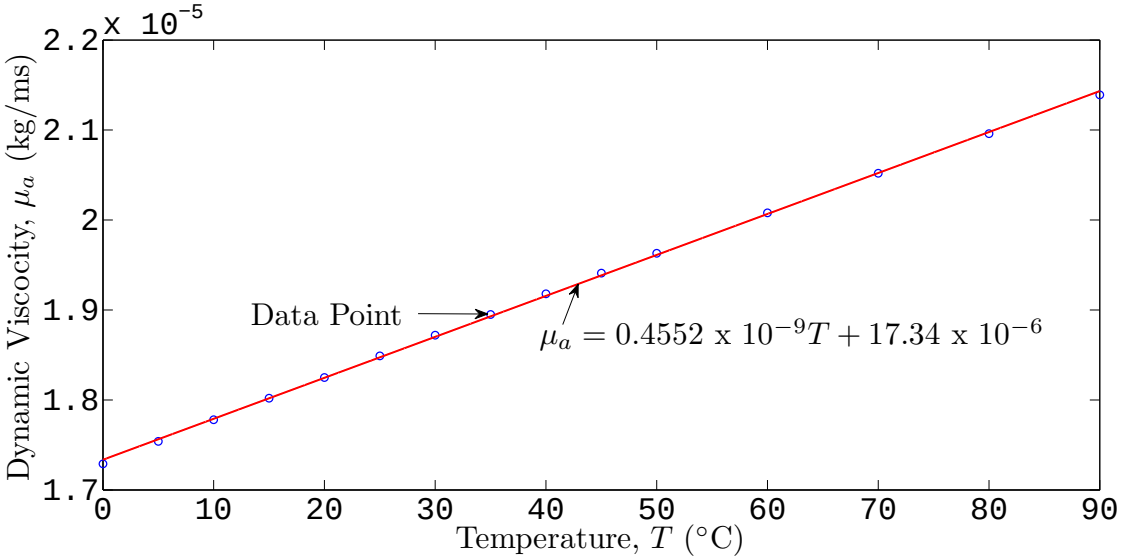

Figure C.6 Curve fit of dynamic viscosity of air as a function of temperature

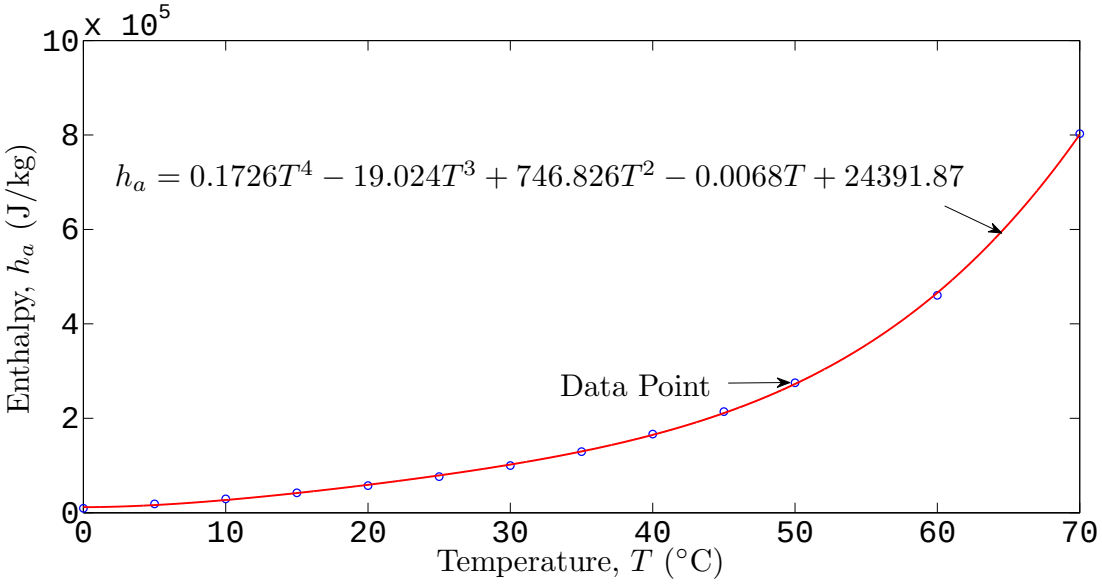

Figure C.7 Curve fit enthalpy of air as a function of temperature

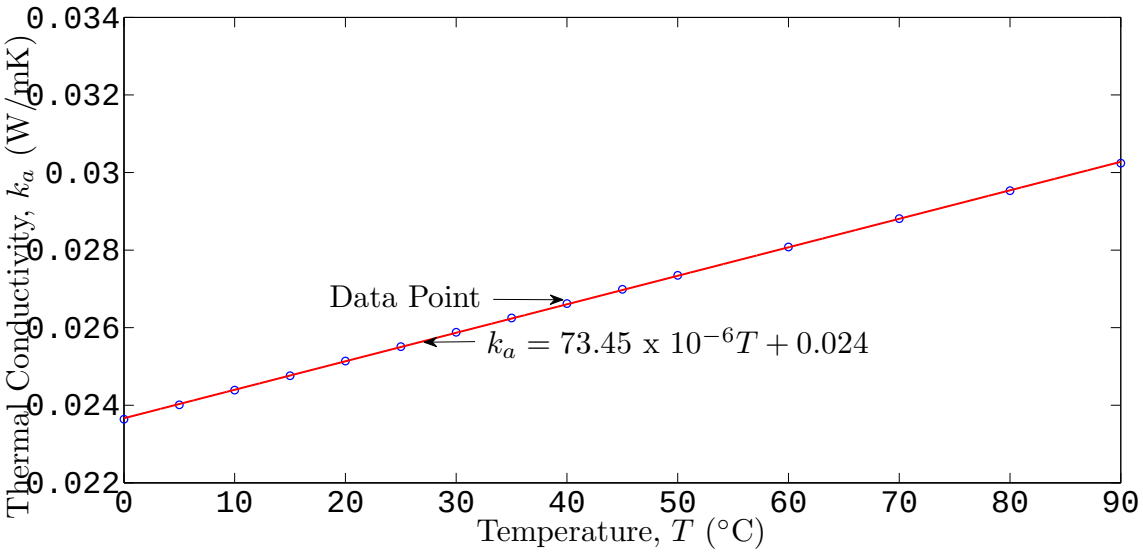

Figure C.8 Curve fit thermal conductivity of air's as a function of temperature

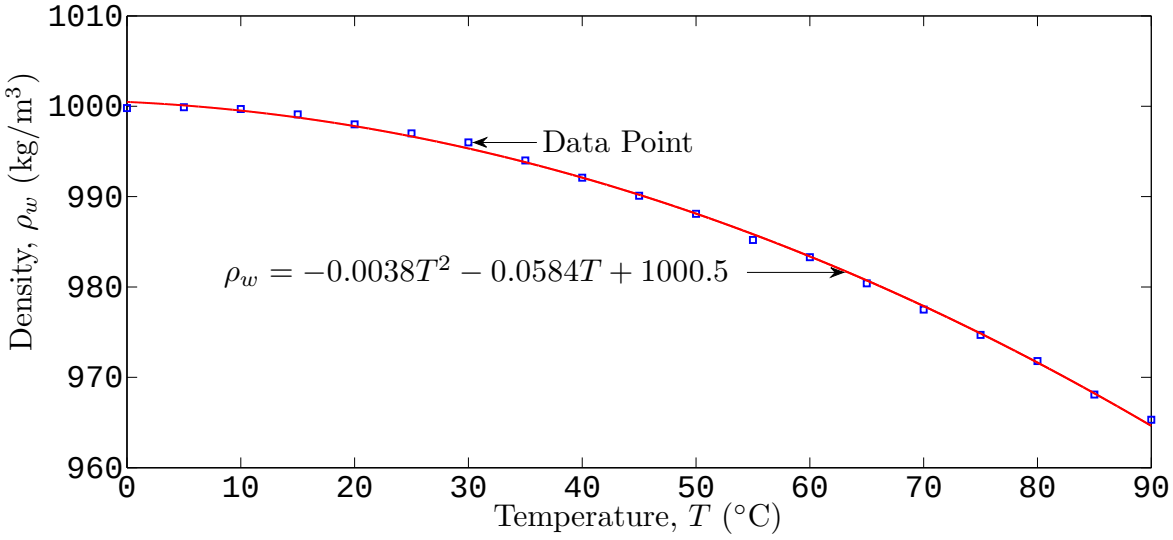

Figure C.9 Curve fit Prandtl number of air as a function of temperature